


12-2016

# Role of the Inner Shell Architecture on the Various Blinking States and Decay Dynamics of Core-Shell and Core-Multishell Quantum Dots

Pooja Bajwa

*University of Arkansas, Fayetteville*

Follow this and additional works at: <http://scholarworks.uark.edu/etd>

 Part of the [Materials Chemistry Commons](#), and the [Semiconductor and Optical Materials Commons](#)

---

## Recommended Citation

Bajwa, Pooja, "Role of the Inner Shell Architecture on the Various Blinking States and Decay Dynamics of Core-Shell and Core-Multishell Quantum Dots" (2016). *Theses and Dissertations*. 1799.  
<http://scholarworks.uark.edu/etd/1799>

This Dissertation is brought to you for free and open access by ScholarWorks@UARK. It has been accepted for inclusion in Theses and Dissertations by an authorized administrator of ScholarWorks@UARK. For more information, please contact [scholar@uark.edu](mailto:scholar@uark.edu), [ccmiddle@uark.edu](mailto:ccmiddle@uark.edu).

Role of the Inner Shell Architecture on the Various Blinking States and Decay Dynamics of Core-Shell and Core-Multishell Quantum Dots

A dissertation submitted in partial fulfillment  
of the requirements for the degree of  
Doctor of Philosophy in Chemistry

by

Pooja Bajwa  
Guru Nanak Dev University  
Master of Science in Chemistry, 2003  
Jammu University  
Bachelors of Education (Science and English), 2004

December 2016  
University of Arkansas

This dissertation is approved for recommendation to the Graduate Council.

---

Dr. Colin Heyes  
Dissertation Director

---

Dr. Neil Allison  
Committee Member

---

Dr. Jingyi Chen  
Committee Member

---

Dr. Nan Zheng  
Committee Member

---

Dr. Feng Wang  
Committee Member

## ABSTRACT

Colloidal semiconductor nanocrystals (quantum dots, QDs) have received much attention in recent years due to their uniquely size-tunable properties leading to a number of promising applications. Some of their most popular applications include their use as fluorescent probes in biology, as electro-optical components and in photovoltaic devices. CdSe-based QDs are particularly important because of their ease of synthesis, high photoluminescence quantum yields (PL QYs) across the whole visible spectrum and their photostability. Shelling of core QDs is usually carried out to improve their optical properties, minimize outer environmental effects on their properties, and avoid toxic element exposure to the environment. However, choosing the shell composition is not trivial, since the band-edge energy offset, interfacial lattice mismatch, shell thickness and chemical stability all play roles in influencing the optical properties. Interfacial lattice strain can be alleviated by either forming multi-shells or gradient-alloyed shells, but this comes at the expense of reducing charge carrier confinement. However, a comprehensive model to decide which shell configuration is best is not yet available. In this dissertation, a systematic comprehensive study of CdSe-based core/multi-shells and core/gradient-alloyed-shells is carried out in terms of their PL QYs, various blinking states and multiple radiative and non-radiative exciton decay rates. The experimental results for the ensemble and single particle optical properties for the different core-multishell QDs proves that the ensemble quantum yield is not a good indicator for single QD blinking. The exciton decay pathways in terms of radiative and non-radiative decay for different core-multishell architectures are shown to be strongly influenced by the lattice strain and band edge confinement. These studies were then extended to the study of multiple fluorescence intensity levels in single QDs as a function of the various shells using a range of time-resolved fluorescence spectroscopies. From this data, a mechanistic model showing various physical

transitions was proposed. Through a systematic, quantitative study, this dissertation highlights the factors of both lattice strain and band edge confinement potential in controlling exciton decay that is needed to design and synthesize QDs to reach their full potential in a range of future applications.

## ACKNOWLEDGEMENTS

Working as a Ph.D. student at University of Arkansas was a magnificent as well as challenging experience for me. In all these years, I have worked with a number of people whose contribution to my research work and framing of my doctoral dissertation deserved special attention. It is a pleasure to convey my gratitude to all of them in my humble dissertation.

First of all, I would like to thank the Almighty God for His blessings throughout these years. I am most privileged to have Dr. Colin D. Heyes as my current research advisor who enlightened every important step of my professional career. He has been a mentor whom I have always been able to count on for advice and support. He always had an open door policy, so I could approach him anytime for his guidance and opinions on my work. His keen scientific observation, sharp judgment and understanding have been pivotal in shaping this dissertation work. My special thanks also goes to my ex-research advisor late Dr. Robert E. Gawley for accepting me in his research group and for helping me initiate my research career. He left us so early but always remained as an inspiration in my heart; may he rest in peace.

I express my sincere thanks to my current committee members: Dr. Neil Alison, Dr. Nan Zheng, Dr. Jingyi Chen and Dr. Feng Wang. Their continued guidance and extensive discussions always challenged me to do more. I remain grateful to Ms. Liz Williams, Ms. Heather Jorgensen, and Ms. Leslie Johnson for their continuous administrative support, as well as the rest of Chemistry department faculty, staff and students that I was fortunate to meet and work with. I would like to convey my heartfelt thanks to all my lab group members; their friendship quickly turned the lab into a home like atmosphere.

I convey my special acknowledgement to Dr. Benard Omogo, who gave me the initial hands on training with making these nanoparticles. My special acknowledgement also goes to Dr. Feng Gao for the training on single molecule experiments and data analysis, and his helpful discussions. Thanks to Anh Nguyen for getting me TEM data whenever required. Finally, my deepest acknowledgement goes to all my friends who have been part of my life over this time and to every member of department of chemistry and biochemistry for contributing to the successful completion of my dissertation.

## **DEDICATION**

*I dedicate this dissertation to my family.*

I dedicate my dissertation first of all to my mother late Mrs. Shakuntla Gupta, who left me in the midway of my journey with an irreparable loss. I miss you a lot Mom, I would like to die if it could be possible to meet you in this way. Please shower me with your blessings as your wish to see Dr. with my name has been fulfilled. I owe my every achievement to my father Mr. Puran Chand Gupta, my brother Varun Gupta, my sister Jyoti Gupta, my brother-in-law Raman Mahajan, and kids Muskaan Mahajan and Paras Mahajan. I have no words to convey my thanks to them who shared all of ups and downs of my research. It would not be possible to achieve this work without their encouragement and motivation.

# TABLE OF CONTENTS

## CHAPTERS

1. Introduction	
1.1. Basics of Quantum Dots.....	1
1.2. Technical Background of Quantum Dots.....	2
1.2.1. Semiconductors.....	2
1.2.2. Quantum Confinement.....	4
1.3. Optical properties of QDs.....	7
1.4. Structural properties of QDs.....	12
1.5. Blinking in quantum dots.....	13
1.6. Synthesis of QDs.....	17
1.6.1. Core synthesis.....	17
1.6.2. Core/shell and core/shell/shell synthesis.....	19
1.7. Objectives and overview of the dissertation.....	21
2. Role of the Inner Shell Architecture on Quantum Yield and Blinking Dynamics in Core/Multi-Shell Quantum Dots	
2.1. Abstract.....	31
2.2. Introduction.....	32
2.3. Experimental Section.....	34
2.3.1. Chemicals.....	34
2.3.2. CdSe core synthesis.....	35
2.3.3. Core/shell/shell synthesis.....	35
2.3.4. Core/gradient-alloyed shell synthesis.....	36
2.4. Instrumentation and measurements.....	36
2.4.1. Fluorescence and Absorption Spectroscopy.....	36
2.4.2. Transmission Electron Microscopy.....	37
2.4.3. Blinking.....	37
2.5. Results and discussion.....	38
2.6. Summary and Conclusions.....	55
2.7. Acknowledgements.....	56
2.8. References.....	58
3. Radiative and Non-Radiative Decay Dynamics in Core-Multishell Quantum Dots: Role of Inner Shell Architecture	
3.1. Abstract.....	61
3.2. Introduction.....	62
3.3. Materials and Methods.....	64
3.3.1. Chemicals.....	64
3.3.2. CdSe core synthesis.....	64



3.3.3. Core/shell/shell synthesis.....	64
3.3.4. Core/gradient-alloyed shell/shell synthesis.....	65
3.3.5. Fluorescence and absorption spectroscopy.....	65
3.3.6. Fluorescence microscopy.....	65
3.3.7. Transmission electron microscopy.....	66
3.4.Results and discussion.....	66
3.5.Conclusions.....	82
3.6.References.....	85

#### 4. Reducing Blinking in Small Core-Multishell Quantum Dots by Carefully Balancing Confinement Potential and Induced Lattice Strain: The “Goldilocks” Effect

4.1.Abstract.....	90
4.2.Introduction.....	91
4.3.Results and Discussion.....	93
4.4.Conclusion.....	107
4.5.Methods.....	108
4.5.1. Chemicals.....	108
4.5.2. CdSe core synthesis.....	108
4.5.3. Shelling.....	109
4.5.4. Fluorescence and Absorption Spectroscopy.....	109
4.5.5. Transmission Electron Microscopy.....	109
4.5.6. Fluorescence Microscopy.....	105
4.6.Acknowledgements.....	110
4.7.Supporting information.....	111
4.8.References.....	111

#### 5. Shell-Dependent Photoluminescence Studies Provide Mechanistic Insights into the Off-Grey-On Transitions of Blinking Quantum Dots

5.1.Abstract.....	124
5.2.Introduction.....	125
5.3.Results.....	127
5.4.Discussion.....	137
5.5.Summary and conclusions.....	145
5.6.Materials and methods.....	146
5.6.1.Chemicals.....	146
5.6.2. CdSe core synthesis.....	146
5.6.3. Core/shell/shell synthesis.....	147
5.6.4. Fluorescence and absorption spectroscopy.....	147
5.6.5. Transition electron microscopy.....	147
5.6.6. Fluorescence microscopy.....	148
5.7.Acknowledgememnts.....	149

5.8.References.....	150
5.9.Supporting Information.....	154
6. Conclusions and Outlook.....	156
6.1.References.....	162

## LIST OF TABLES

<b>Table 1.1.</b>	Lattice mismatch for hexagonal lattices. Values quoted as % difference from core, and are the average of $a_0$ and $c_0$ axes mismatches.....	11
<b>Table 2.1:</b>	Relative goodness of fit tests to power law and multi-exponential models for the data in figure 5 (on times) and figure 6 (off times).....	55

## LIST OF FIGURES

<b>Figure 1.1.</b>	The wavelength of light emitted by quantum dots is tunable by changing the particle size. In this image, all of the quantum dot particles are excited by same UV wavelength, but emit different visible wavelengths depending upon particle size.....	2
<b>Figure 1.2.</b>	Energy barriers to conduction for metals, semiconductors and insulators.....	3
<b>Figure 1.3a.</b>	Schematic of photoexcitation of electron to create an electrostatically bound pair of excited electron and positive hole, called as <b>1.3b:</b> exciton (Image from Justin Galloway power point).....	3
<b>Figure 1.4.</b>	A quantum dot exhibits bandgap tunability because it is smaller than the spatial separation between the electron and its hole, known as the exciton Bohr radius.....	4
<b>Figure 1.5.</b>	Energy bands of bulk semiconductors, quantum dots and molecules.....	6
<b>Figure 1.6.</b>	Band (valence and conduction bands) alignment of core-shell systems.....	9
<b>Figure 1.7.</b>	Schematic of core-shell quantum dot .....	10
<b>Figure 1.8.</b>	2 <sup>nd</sup> -order relationship between ZnS shell thickness and quantum yield, with fluorescence quantum yield maximized between one and two monolayers.....	11
<b>Figure 1.9.</b>	Schematic showing radiative and non-radiative recombination of photo excited charge carriers.....	14
<b>Figure 1.10.</b>	Anatomy of a core-shell QD and relationship to the electron and hole trap states...	15
<b>Figure 2.1.</b>	a) Schematic of band gap offset and lattice mismatch values of semiconductor materials specific to our work. b) Schematic highlighting difference in band-edge offsets between core/shell/shell (left) and core/gradient-alloyed shell/shell (right) architectures.....	39
<b>Figure 2.2:</b>	a) PL peak maximum and b) photoluminescence quantum yield as a function of shell composition and thickness. Red: CdSe/CdS/ZnS; Green: CdSe/Cd <sub>(1-x)</sub> Zn <sub>x</sub> S/ZnS; Blue: CdSe/ZnSe/ZnS; Magenta: CdSe/ZnSe <sub>(1-x)</sub> S <sub>x</sub> /ZnS. Points are average values of 2 samples and the error bars are 1 standard deviation wide to show the reproducibility.....	40
<b>Figure 2.3.</b>	TEM Images and size distributions of core/multi-shell samples.....	41
<b>Figure 2.4.</b>	(a) A 60-second section of a typical fluorescence trace highlighting blinking behavior (b) 5-second section of the trace showing well-resolved on and off events using a threshold. Log-log plots of P <sub>on</sub> (c) and P <sub>off</sub> (d) distributions for CdSe cores (black) CdSe/CdS/3ZnS (red) and CdSe/5Cd <sub>(1-x)</sub> Zn <sub>x</sub> S/3ZnS (green) and CdSe/5ZnSe/3ZnS (blue) and CdSe/5ZnSe <sub>(1-x)</sub> S <sub>x</sub> /3ZnS (magenta). (e) Fraction of time a QD spends in the on state as a function of the shell architecture (the gradient alloy shells are labeled as CdZnS and ZnSeS rather than Cd <sub>(1-x)</sub> Zn <sub>x</sub> S and ZnSe <sub>(1-x)</sub> S <sub>x</sub> due to space limitations).....	45

<b>Figure 2.5.</b>	(a-c) Power law fitting of on-times and extracted parameters plotted as a function of shell architecture. (d-f) Multi-exponential fitting of on-times and extracted parameters plotted as a function of shell architecture. Color scheme is the same as for Figure 4. In (b, c, e, f), the gradient alloy shells are labeled as CdZnS and ZnSeS rather than $Cd_{(1-x)}Zn_xS$ and $ZnSe_{(1-x)}S_x$ due to space limitations.....	48
<b>Figure 2.6.</b>	(a-c) Power law fitting of off-times and extracted parameters plotted as a function of shell architecture. (d-f) Multi-exponential fitting of on-times and extracted parameters plotted as a function of shell architecture. Color scheme is the same as for Figure 4. In (b, c, e, f), the gradient alloy shells are labeled as CdZnS and ZnSeS rather than $Cd_{(1-x)}Zn_xS$ and $ZnSe_{(1-x)}S_x$ due to space limitations.....	49
<b>Figure 2.7.</b>	Overlay of on-times distributions (circles) and off-times distributions (triangles) from 1-ms binned data (open symbols) and 20-ms binned data (filled symbols) for each shell architecture. On and off data are offset relative to each other on the y-axis for visualization, so the y-axis has been relabeled as relative occurrence to reflect this fact.....	51
<b>Figure 3.1.</b>	Schematic of a typical wave function overlap influenced by band gap offset and interfacial trap states (created due to lattice mismatch) of semiconductor materials specific to our work.....	67
<b>Figure 3.2.</b>	PL peak maximum of a) QDs with CdS inner shell and b) QDs with ZnSe inner shell as a function of shell composition and thickness.....	69
<b>Figure 3.3.</b>	FWHM (full width at half maximum) of a) QDs with CdS inner shell and b) QDs with ZnSe inner shell as a function of shell composition and thickness.....	69
<b>Figure 3.4:</b>	b/a (red shift vs. blue shift in PL wavelength) of a) QDs with CdS inner shell and b) QDs with ZnSe inner shell.....	70
<b>Figure 3.5.</b>	TEM images of a) core b) core-shell c) core-shell-shell QDs for QDs with CdS inner shell.....	71
<b>Figure 3.6.</b>	TEM images of a) core b) core-shell c) core-shell-shell QDs for QDs with ZnSe inner shell.....	72
<b>Figure 3.7.</b>	Photoluminescence quantum yield of a) QDs with CdS inner shell and b) QDs with ZnSe inner shell as a function of shell composition and thickness.....	74
<b>Figure 3.8.</b>	Fitted fluorescence lifetime components for a) CdS inner shell (empty circles for 3CdS/5ZnS, crossed circles for 5CdS/3ZnS full solid circles for 5CdZnS/3ZnS) QDs b) ZnSe inner shell (empty triangles for 3ZnSe/5ZnS, crossed triangles for 5ZnSe/3ZnS and solid triangles for 5ZnSeS/3ZnS) QDs .....	75
<b>Figure 3.9.</b>	Component amplitudes as a function of shell thickness for (a-c) CdS inner shell and (d-f) ZnSe inner shell QDs.....	78

<b>Figure 3.10.</b>	a) Average fluorescence lifetime for CdS inner shell QDs and b) Average fluorescence lifetime for ZnSe inner shell QDs.....	79
<b>Figure 3.11.</b>	Radiative rate constant ( $k_r$ ) of a) QDs with CdS inner shell and b) QDs with ZnSe inner shell as a function of shell composition and thickness.....	81
<b>Figure 3.12.</b>	Average Non-radiative rate constant ( $\langle k_{nr} \rangle$ ) of a) QDs with CdS inner shell and b) QDs with ZnSe inner shell as a function of shell composition and thickness.....	81
<b>Figure 4.1.</b>	(A) PL quantum yields of CdSe/CdS core/shell QDs (red) and CdSe/CdS/ZnS core/shell/shell QDs (black) as a function of shell thickness. (B) Fluorescence lifetime decay curves of CdSe, CdSe/CdS core/shell and CdSe/CdS/ZnS core/shell/shell QDs with different shell thicknesses. (C) Relative amplitudes of decay components extracted from global fits to the set of decay curves for CdSe/CdS core/shell QDs. (D) Relative amplitudes of decay components extracted from global fits to the set of decay curves for CdSe/CdS/ZnS core/shell/shell QDs. (E) Relative amplitudes of decay components for CdSe/3ML CdS/3ML ZnS QDs as a function of power to support the assignments of each component to trion, band-edge and trap state emission, respectively. (F) Average radiative rate ( $\langle k_r \rangle$ ) for CdSe/CdS core/shell (red) and CdSe/CdS/ZnS core/shell/shell (black) QDs as a function of shell thickness. (G) Average non-radiative rate ( $\langle k_{nr} \rangle$ ) for CdSe/CdS core/shell (red) and CdSe/CdS/ZnS core/shell/shell (black) QDs as a function of shell thickness.....	116
<b>Figure 4.2.</b>	(A) TEM images of the selected samples together with their respective size distribution histogram (B). (C and D) Annular dark field (ADF)-STEM images of the CdSe/3CdS/5ZnS core/shell/shell sample. (E and F) are the electron energy loss spectra (EELS) of Cd and Zn signals, respectively, collected at positions indicated in figure D. (G and H) are the integrated area histograms calculated from the spectra in figures E (for Cd) and F (for Zn), respectively.....	117
<b>Figure 4.3.</b>	(A) Schematic structures of CdSe/CdS/ZnS core/shell/shell QDs with 0, 1, 3, and 5 ML ZnS outer shell. (B) The corresponding 300-s fluorescence traces of the synthesized CdSe/CdS/ZnS under cw laser excitation. (C) Photon counting histograms (PCHs) for the fluorescence traces shown in (B). (D) Zoomed in 20-s fluorescence traces showing the details of the fluorescence blinking behaviors of the QDs.....	118
<b>Figure 4.4.</b>	Log-log plots of $P_{on}$ (A) and $P_{off}$ (B) distributions for CdSe/CdS (red, orange) and CdSe/CdS/ZnS (blue, green, magenta) as a function of ZnS shell thickness under continuous wave laser excitation (pulsed laser excitation data is shown in supporting information). (C) Distributions of time spent by QDs in the on state (Fraction-on) for CdSe/CdS/ZnS QDs having 3 monolayers of CdS and different thickness of ZnS outer-shell under cw laser excitation. (D) Distributions of on state intensities for	

CdSe/CdS/ZnS QDs having 3 monolayers of CdS and different thickness of ZnS outer-shell under cw laser excitation.....119

**Figure 4.5.** A) Relationship between QD fluorescence lifetime decay components of single CdSe/3ML CdS/3ML ZnS Core/Shell/Shell QDs and the fraction of time the QD spends in the “On” state during the blinking trace without applying threshold so that all on and off events are included. Linear fits to the fast lifetime (trion) component as a function of fraction-on in the low fraction-on and high fraction-on regions are overlaid B) Relationship between QD fluorescence lifetime decay components of single CdSe/3ML CdS/3ML ZnS Core/Shell/Shell QDs and the fraction of time the QD spends in the “On” state during the blinking trace after applying threshold to remove all off events. A linear fit to the fast lifetime (trion) component as a function of fraction-on is overlaid C) Probability distribution of on-times at low power and high power indicating that the on times are reduced at higher power. D) the change in the amplitude of fluorescence lifetime components of the *same* QD at high power – low power plotted as a function of that QDs Fraction-On at the lower power to support the assignment that the fast component observed in single QDs is the result of trion state formation.....120

**Figure 4.6.** Proposed blinking model showing the conduction and valence bands of A) Core, B) CdSe/CdS core/shell and C) CdSe/CdS/ZnS core/shell/shell QDs, together with trap states at the surface and at the CdS/ZnS shell/shell interfaces. The black curves show the approximate wavefunctions of the delocalized electrons and holes. The red shaded area depicts the relative probability for charge carriers to be localized in these trap states based on both the relative number and accessibility. The green double-headed arrows represent fast trapping-detrapping processes at the interfacial trap states. The blue arrows represent possible transfer processes between the interfacial and long-lived surface trap states. The number of trap states at the CdSe/CdS interface is proposed to be negligible due to the much small lattice mismatch between CdSe and CdS (~3.8%).....121

**Figure 4.7.** A) On-times probability distribution and B) Off-times probability distribution when the inner CdS is increased from 3ML to 5ML without changing the thickness of the outer shell. As predicted by the model shown in figure 6, QD blinking is slightly reduced when the inner CdS shell thickness is increased from 3ML to 5ML.....122

**Figure 4.8.** TOC Graphic.....123

**Figure 5.1.** A) blinking trace of a single CdSe/5 ML CdS core/shell QD, highlighting the well-separated off, grey and on states. B) photon counting histograms (PCHs) of core/shell QDs of CdSe with either 5ML CdS (red), ZnSe (blue) or ZnS (green). The thresholds used to select the different states are highlighted.....128

- Figure 5.2.** Probability distributions of A) Off, B) Grey and C) On dwell times (number of events normalized to the first time point to enable easy comparison). D) average intensity of the grey (blue) and on (red) states as a function of CdS shell thickness. The error bars represent the standard deviation of the average intensity from QD-to-QD. E) The fraction of time a QD spends in the off (black), grey (blue) and on (red) states. The error bars represent the standard deviation of the average fraction of time from QD-to-QD.....130
- Figure 5.3.** Ratio of transitions between the various states. Black - the ratio of times that, if the QD is in the off state, it will transition to the grey state rather than directly to the on state. Red - the ratio of times that, if the QD is in the on state, it will transition to the grey state rather than directly to the off state. Blue - the ratio of times that, if the QD is in the grey state, it will transition to the off state compared to the on state.....131
- Figure 5.4.** A) fitted fluorescence lifetime components from a multiexponential fitting of single QDs as a function of shell thickness. The thin lines only include photons between 8 and 30 counts/ms in the blinking trace, medium lines only include photons between 30 and 150 counts/ms and thick lines include only photons above 150 counts/ms. The fitted lifetime components are independent of both shell thickness and intensity level, suggesting that changes in intensity level are only due to differences in their relative amplitudes. Fitted fluorescence lifetime components and amplitudes as a function of laser excitation power at the ensemble (B, D) and single QD (C, E) level. For the single QD level, error bars represent the QD-to-QD standard deviation....134
- Figure 5.5.** Fitted component amplitudes (same color scheme as in figure 4) for single QDs in the grey (A, C) and on (B, D) state as a function of the state intensity (A, B) and average state dwell time (C, D). Each colored dot represents the relative amplitude of that component in a single QD.....136
- Figure 5.6.** Relationship between the average on intensity and the average on time of single QDs. Each dot represents a different QD.....136
- Figure 5.7.** Model used to explain the blinking data. Black dots represent electrons and white circles represent holes. When the charge carrier is delocalized, the approximate wavefunction is shown in red above the electron or below the hole. The bright on state is proposed to be short lived, as represented by a fast-changing equilibrium while the normal on state is not as bright but longer lived, as represented by a more slowly hanging equilibrium. Proposed decay lifetimes for each state are given in blue with a description of the rationale in red.....139
- Figure 5.8.** Redrawing of the model in figure 7 for thinner shells used to explain the faster blinking and the reduced grey state formation. A direct transition between off and on is now seen via a rapid trapping-detrapping of the electron at the shell surface facilitated by the thinner shell.....143



## LIST OF PUBLICATIONS

**Chapter 2. Published:** Bajwa, P., Gao, F., Nguyen, A., Omogo, B., Heyes, C. D. Role of the Inner Shell Architecture on Quantum Yield and Blinking Dynamics in Core/Multi-Shell Quantum Dots. *ChemPhysChem*, 2016. 17(5): p. 731-740

**Chapter 3. To Be Submitted:** Bajwa, P., Nguyen, A., Gao, F., Heyes, C. D. Radiative and Non-Radiative Decay Dynamics in Core-Multishell Quantum Dots: Role of Inner Shell Architecture.

**Chapter 4. Published:** Omogo, B., Gao, F., Bajwa P., Kanekko, M., Heyes, C. D. Reducing Blinking in Small Core-Multishell Quantum Dots by Carefully Balancing Confinement Potential and Induced Lattice Strain: The “Goldilocks” Effect. *ACS Nano*, 2016. 10 (4): p. 4072-4082

**Chapter 5. Under review for ACS Nano journal:** Gao, F., Bajwa, P., Nguyen, A., Heyes, C. D. Shell-Dependent Photoluminescence Studies Provide Mechanistic Insights into the Off-Grey-On Transitions of Blinking Quantum Dots

## Chapter 1. Introduction

### 1.1. Basics of Quantum Dots

Quantum dots (QD's) are colloidal, nanocrystalline semiconductors that are often, but not always, spherical in shape and have a size that is equal to or less than the Bohr excitons diameter of the material, ~12 nm for the prototypical CdSe. This size regime puts them in a special size range that retains some properties of bulk materials, some properties of individual atoms and molecules and produces some additional unique properties. As semiconductors, quantum dots have certain associated optical and electronic properties. For bulk semiconductors (i.e. those that are larger than the Bohr excitons diameter), there is a set energy difference between the valence and conduction bands, called the band gap, and is dictated only by the composition of the material. Unlike bulk semiconductors, the band gap of a quantum dot is also influenced by its size. When this small size is close to or smaller than Bohr's bulk exciton radius, these QD's vary in properties compared to bulk solids due to the quantum confinement effect.<sup>1, 2, 3, 4, 5, 6, 7, 8</sup> Small quantum dots emit higher energy light than larger quantum dots, which allows the wavelength of light emitted by the particles to be tunable. Small particles of CdSe emit blue light and larger CdSe particles emit red light (figure 1.1). As such, the quantum dots become very unique in the sense that their optical and electronic properties can be tuned according to their sizes.



**Figure 1.1.** The wavelength of light emitted by quantum dots is tunable by changing the particle size. In this image, all of the quantum dot particles are excited by same UV wavelength, but emit different visible wavelengths depending upon particle size.

## 1.2. Technical Background of Quantum Dots

### 1.2.1. Semiconductors

To understand quantum dots, it is first necessary to discuss the general properties of semiconductors. Semiconductors are a class of materials defined primarily by their electronic properties. In metals and other conductors, the conduction and valence bands overlap, without a significant energy barrier for promoting electrons from the valence to the conduction band. In insulators, there is a large energy barrier for promoting electrons from valence to the conduction band, thus eliminating conduction under all but the most extreme conditions. In semiconductors, however, the energy barrier for conduction is intermediate between insulators and conductors (figure 1.2). Due to this intermediate energy barrier, semiconductors can be modified in numerous ways to make them highly useful for a wide range of applications such as transistors, LEDs and photovoltaics. For instance, the electrical properties of semiconductors can be modified by controlled addition of impurities or by the application of electrical fields or light and thereby devices made from semiconductors can be used for amplification, switching and energy conversion.

Typically, the bandgaps ( $E_g$ ) for metals, semiconductors and insulators are less than 0.1 eV, between 0.5 and 3.5 eV, and greater than 4 eV, respectively.<sup>9</sup>

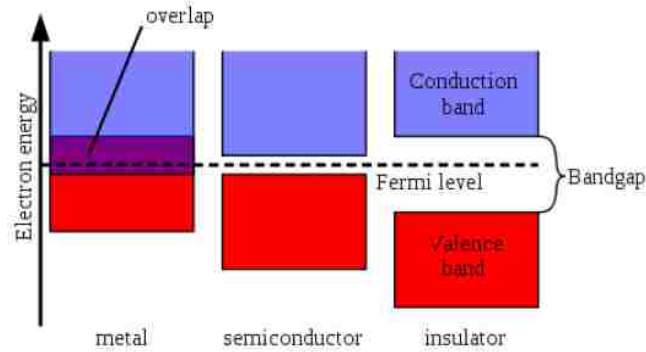


**Figure 1.2.** Energy barriers to conduction for metals, semiconductors and insulators (<https://bsclarified.wordpress.com>)

Furthermore, in semiconductors, excitation with energy equal to or greater than their band gap energy ( $E_g$ ) leads to the excitation of an electron from valence band to the conduction band, leaving behind a positive hole in the valence band (figure 1.3a). This gives rise to generation of an electrostatically bound pair of electron and hole, called an exciton (figure 1.3b).

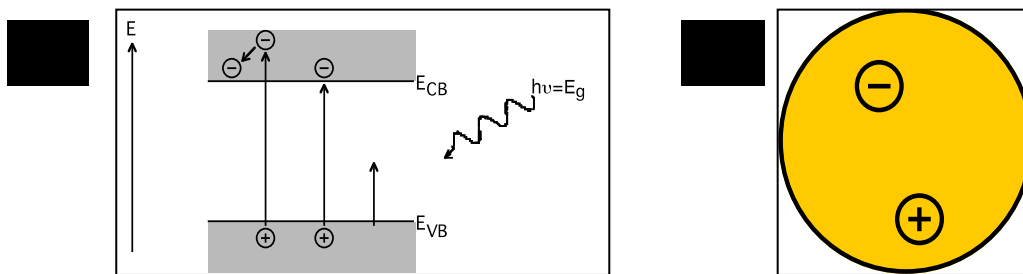


**Figure 1.3a:** Schematic of photoexcitation of electron to create an electrostatically bound pair of excited electron and positive hole, called as **1.3b:** exciton (Image from Justin Galloway power point)

### 1.2.2. Quantum confinement

A particle behaves as a bulk particle when the confining dimension of the material is large compared to Bohr exciton diameter. However, as the confining dimension of the particle decreases and reaches the Bohr exciton limit, which is usually at the nanometer scale, the energy levels close to the valence and conduction band edges become discrete, and the energy gap between the lowest conduction band energy level and the highest valence band energy level increases. As a result of this quantum confinement, the bandgap becomes size dependent, resulting in a blue shift in absorbance as the size of particle decreases. Thus, when particles are this small, their electronic and optical properties deviate substantially from those of bulk materials. When the nanoparticles are spherical in shape, the confinement effect is in all three dimensions, leading to the term “quantum dot”. When confinement is only in 2 dimensions, the nanomaterial is called a quantum wire, and when the confinement is only in 1 dimension, it is called a quantum well. These different shapes (confinement regimes) result in very different optical and electronic properties, which have been extensively studied.<sup>10</sup> Since these shape effects are not the focus of this dissertation, they will not be discussed further at this point.



**Figure 1.4.** A quantum dot exhibits bandgap tunability because it is smaller than the spatial separation between the electron and its hole, known as the exciton Bohr radius. (<http://janosh.myweb.usf.edu/QDs.html>)

To understand quantum confinement effect, there is a need to examine how energy bands contribute from atoms up to bulk scale. Atoms or molecules have discrete, degenerate energy levels in which electrons can reside, with no more than two electrons allowed to reside in a single energy level (according to the Pauli exclusion principle). As a crystal lattice forms, their electronic states interact and with each other and the degenerate states are split into discrete, non-degenerate energy levels. States formed from the bonding electronic orbitals lie below the Fermi level and is called the valence band, while the states formed from antibonding electronic orbitals lie above the Fermi level and is called the conduction band.

The wavefunctions of the electronic states and their energy levels can be modeled as a particle in a box, which leads to the energy level of quantum dots being dependent on its size. The quantum dots that have radii slightly larger than Exciton Bohr radius are said to be in the ‘weak confinement regime’ and the ones that have radii smaller than the Exciton Bohr radius are said to be in the ‘strong confinement regime’. Thus, if the size of quantum dot is small enough that the quantum confinement effects dominate (typically less than 10 nm for cadmium and zinc chalcogenides), the electronic properties change, and are determined by the size.

Once the number of interacting atoms reaches the bulk level, the states are split into so many energy levels that the states can be considered as continuous because the energy spacing between the many energy levels is infinitesimally small (figure 1.5).<sup>4</sup>

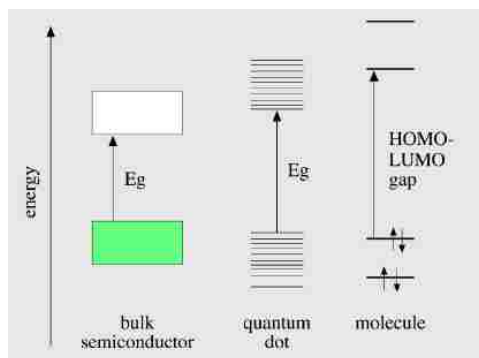


**Figure 1.5.** Energy bands of bulk semiconductors, quantum dots and molecules<sup>4</sup>

Brus developed an approximate relationship between the particle size of the quantum dot and its resultant bandgap, based on the material being used and its bulk bandgap (Equation 1.1).<sup>11</sup> In the equation,  $E_g^{QD}$  is the theoretical bandgap of quantum dot,  $E_g^{bulk}$  is the bandgap of the bulk material,  $h$  is Planck's constant,  $r$  is the radius of nanoparticle,  $m_0$  is the mass of an electron,  $m_e^*$  is the effective mass of the electron for the material,  $m_h^*$  is the effective mass of hole for the material,  $e$  is the charge of electron,  $\epsilon_0$  is the permittivity of free space,  $\epsilon$  is the permittivity of the material.

$$E_g^{QD} = E_g^{bulk} + \frac{h^2}{8m_0r^2} \left( \frac{1}{m_e^*} + \frac{1}{m_h^*} \right) - \frac{1.8e^2}{4\pi\epsilon_0\epsilon r}$$

**Equation 1.1.** Change in bandgap due to quantum confinement in a spherical nanoparticle

The first term is based on the properties of the bulk material, the second term is based on the particle-in-a-box confinement of the exciton, and the third term is based on the Coulombic attraction between the electron and the hole. While it is not a perfect fit to experimental values, the equation still qualitatively describes the bandgap as a function of radius, and therefore the wavelength of light absorbed/emitted.

### 1.3. Optical Properties of QDs

When an incoming photon of sufficient energy, equal to or greater than the bandgap of the material, is absorbed by the material, an electron is excited from the valence band to the conduction band, leaving behind a hole in the valence band. These charge carriers then drop to the band edge states by vibrational relaxation (phonon coupling). When the electron relaxes back down to valence band, recombining with the hole left behind by its absence, a photon is emitted, with energy equal to the bandgap of the material (figure 1.7). This mechanism is why a quantum dot can absorb all wavelengths of light greater than its bandgap and down-convert it to a specific emission wavelength.

These absorbance and emission spectra can be tuned based upon the quantum confinement effects in different materials. For instance, CdSe (the ones which we are used for all chapters in this dissertation) quantum dot materials<sup>12</sup> can be tuned to emit light from blue to red as the size becomes bigger. This dissertation was mainly focused on CdSe quantum dots because of their unique narrow photoluminescence spectra, good photostability and high photoluminescence quantum yields. Such properties make them highly promising for ultrasensitive bioimaging applications, which is one of our main motivations for the synthesis of high photoluminescence quantum yield and low-blinking quantum dots that this dissertation is focused towards. Furthermore, since it is known that a typical quantum dot consists of about  $10^2 - 10^5$  atoms<sup>13</sup>, resulting in a high surface-to-volume ratio, this means that surface effects also play a major role in optical properties of quantum dots. Therefore, to achieve high quality of the optical properties described above, both quantum confinement and surface effects need to be optimized.

QD synthesis is usually engineered to specific requirements, with the core, shell and coating characteristics all influencing their chemical and photochemical properties. QD's can be



synthesized in sizes ranging within a few nanometers and size distribution can be controlled within 2%<sup>14</sup> by some specific growth techniques which involve high nucleation and annealing temperatures.<sup>15</sup> Shelling (by inorganic materials) and coating (with organic materials) are also of great importance because the shell stabilizes the nanocrystal and, to some extent, improves the photophysical properties such as providing higher photostability and higher quantum yield.<sup>16</sup>

Uncapped core nanocrystals have been proven to be less applicable for two main reasons. First, the uncapped core nanocrystal surface has imperfections due to the available dangling bonds from the ligands and atoms at the surface, which require passivation to increase radiative pathways. Otherwise these trap states behave as non-radiative pathways, through which excited electrons and holes decay thereby reducing their photoluminescence quantum yield. Therefore, capping with an inorganic shell material is usually performed to lessen these surface trap states of crystals, resulting in a core/shell system. These core/shell systems result in improved luminescence. The improved luminescence by shelling is due to the reduction of surface-related trap states and also, passivation by the shell keeps the electron in lower energy core orbitals and hence, keeps the excited electron away from the outside reacting environment possible. Thus, the shelling helps in protecting the core. Nevertheless, capping with an inorganic shell can also introduce crystalline imperfections at the interface. For instance, Burda et al in 2003<sup>17</sup> explained that if CdSe core is capped with a thin layer of CdS, the CdS adopts the lattice parameters of CdSe core. Therefore, the thin CdS capping layer removes the original surface defects of CdSe without introducing many crystalline imperfections. However, with a continuous growth of a thicker shell on the CdSe core, the shell readjusts to the lattice parameters of bulk and induces lattice dislocation at the core-shell interface. This dislocation allows for the relief of some of the accumulated strain, but results into structural defects at the interface that may act as interfacial trap states. Later it was found that these interfacial

trap states give rise to some emission imperfections such as blinking.<sup>18</sup> This is because of the lattice mismatch and strain developed by the epitaxial growth of multilayers of shells on the core. Second, the large surface area/volume ratio makes cores very reactive and so, more prone to photochemical degradation. Hence, the core nanocrystals capped with ZnS shell have been proven to be more photochemically stable and with higher quantum yields at room temp.<sup>19,20</sup>

Choosing the shell material depends upon the properties of the material that are required after coating. There are three main types of core-shell systems, characterized by the alignment of valence and conduction bands between the core and shell (figure 1.6).<sup>21</sup>

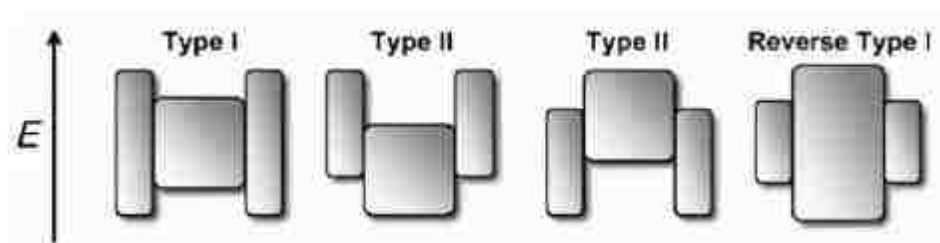


**Figure 1.6.** Band (valence and conduction bands) alignment of core-shell systems

The first and most common core shell system is type-I in which a higher bandgap shell is formed on the core, confining both the electron and hole to the core. One of the first core-shell systems of type-I architecture was CdSe-ZnS<sup>1</sup>. The primary purpose of type-I core-shell systems is to increase fluorescence quantum yield by forcing the electron and hole wavefunctions to overlap in the core while passivating non-radiative pathways at the core's surface. In type-I systems, there is slight red shift upon adding a shell, of the fluorescence due to some leakage of the exciton wave function from the core into the shell via quantum mechanical tunneling. In type-II systems, such as, CdTe/CdSe, either the conduction or valence band edge of the shell is lower in energy than the core, resulting into two possibilities where either the electron or the hole (but not both) is localized in the

shell, leading to charge separation, and is particularly used in systems where extraction of the charge carriers is required. In reverse type-I systems, a narrower bandgap semiconductor is grown onto a higher bandgap core, localizing both of the charge carriers from the core to the shell. Reverse type-I core shell quantum dots are used when there is need of control over the red shifting of the fluorescence spectrum, as the shift can be controlled by changing the coating thickness. The most common reverse type-I systems are CdS-CdSe and ZnSe-CdSe. These systems are used as NIR emitters, since the recombination energy is significantly reduced compared to the absorption energy.

As already stated above, the CdSe/ZnS core-shell system was one of the first type-I systems studied, and has been studied the most extensively (figure 1.7).<sup>1</sup> Due to the large difference in bandgap (as given in table 1.1) between the CdSe core (1.74 eV) and the ZnS shell (3.61 eV), the exciton is well confined to the core. The ZnS shell also passivates surface defects very well, greatly increasing the fluorescence quantum yield.

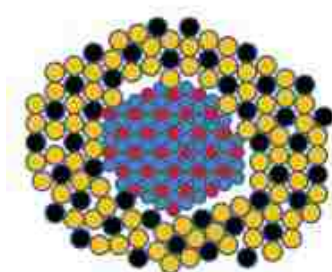


**Figure 1.7.** Schematic of core-shell quantum dot

In addition, on its own ZnS will crystallize into the zinc blende structure, but wurtzite is also thermodynamically stable at room temperature and atmospheric pressure, allowing epitaxial growth of wurtzite ZnS on CdSe cores. There is however ~12% lattice mismatch between the CdSe and

ZnS, so coatings thicker than 2-3 monolayers (MLs) tend to have decreased quantum yield due to the formation of new defects at the interface (figure 1.8).<sup>1</sup>

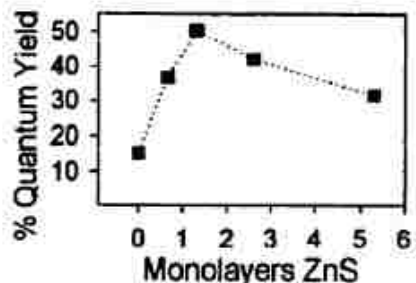


**Figure 1.8.** 2<sup>nd</sup>-order relationship between ZnS shell thickness and quantum yield, with fluorescence quantum yield maximized between one and two monolayers<sup>1</sup>

In addition to band gap energy offset, another very challenging parameter to be considered while tuning the optical properties of quantum dots is lattice mismatch between core and shell materials. Table 1.1 shows some of the lattice mismatch % values for some hexagonal lattices (% values given in red are type I and in blue are type II QDs), that we are particularly interested in.

Core\Shell→ ↓	CdS	CdSe	CdTe	ZnS	ZnSe	ZnTe
CdS		3.95%	10.67%	7.78%	3.55%	3.36%
CdSe	3.80%		6.47%	11.28%	7.21%	0.56%
CdTe	9.64%	6.07%		16.54%	12.64%	6.25%
ZnS	8.44%	12.72%	20.01%		4.59%	12.09%
ZnSe	3.68%	7.77%	14.74%	4.39%		7.17%
ZnTe	3.25%	0.57%	7.07%	10.78%	6.69%	

**Table 1.1.** Lattice mismatch for hexagonal lattices. Values quoted as % difference from core, and are the average of  $a_0$  and  $c_0$  axes mismatches.

#### 1.4. Structural Properties of QDs

QD synthesis was first described in 1982 by Efros and Ekimov.<sup>22,23</sup> Since their work, numerous synthetic methods have been developed for QD synthesis. Further, since the size-dependent properties of QDs depend upon the monodispersion of nanoparticles, there has been a drive to produce QD's with narrow size distributions. A significant step towards this goal was achieved by the Bawendi group in 1993 with the introduction of a hot injection pyrolysis method to synthesize colloidal monodispersed QDs of CdS, CdSe or CdTe that can be size-tuned by reaction conditions (temperature and time). Because of their size-tunable optical properties in the whole visible region, high fluorescence brightness, and photostability,<sup>13,24,25,26</sup> CdSe is most widely used for QD synthesis, and particularly used in biological imaging applications.<sup>27</sup>

As stated above, shelling helps to improve the optical properties of quantum dots, specifically photoluminescence quantum yield, however the quality of shell also plays an important role in the final optical properties.<sup>10, 12, 28</sup> For instance, although the passivation of surface defects of CdSe by ZnS diminishes the surface trap states, enhances the photoluminescence quantum yield (QY) and protects them from external environmental factors as well,<sup>21, 29, 30</sup> there have been reports<sup>1, 29-31</sup> on the imperfections for this material combination due to the large lattice mismatch (12%) between CdSe and ZnS crystal structure. This leads to deformation of CdSe/ZnS QDs shape in addition to dropping their photoluminescence QY by the lattice strain creating interfacial defects. According to another study,<sup>32</sup> the growth of ZnS on CdSe is not sufficient for improvement of properties since it leads to non-uniform spherical shells. In other words, there is a limitation in how much ZnS can improve them, which is proposed to be related to the non-spherical nature of the shell. The major reason as they explained for this anisotropic distribution in CdSe/ZnS core shell is the large difference in lattice constants ( $a = 3.81 \text{ \AA}$  and  $c = 6.26 \text{ \AA}$  for ZnS compared to  $a = 4.30 \text{ \AA}$  and  $c =$

7.01 Å for CdSe) for the two materials. Therefore, CdS and ZnSe shell materials are getting attention because of their lower lattice mismatch values, which are ~ 4% for CdS and ~ 7% for ZnSe crystal types. However, the problem with CdS or ZnSe as a shell for CdSe is that these are not as effective in confining the excitons as ZnS. The reason is the band gap energy offset, which is smaller for CdS or ZnSe as compared to ZnS.<sup>33,34</sup>

In addition to lattice mismatch, several other factors such as reaction conditions, reactivity of crystal planes can also be responsible for the uncontrollable shell distributions. It has also been found that the proper choice of inner shell layer, whether anionic or cationic, defines the overall quality of quantum dots.<sup>35</sup>

### **1.5. Blinking in quantum dots**

Blinking is the phenomenon of intermittence between fluorescent and dark states of single fluorescent probes, which includes organic dye molecules,<sup>36</sup> fluorescent proteins,<sup>37</sup> and nanoparticles.<sup>38,18,39</sup> Blinking behavior was first observed in QDs by Nirmal and coworkers in 1996.<sup>38</sup> Due to the phenomenon of blinking, the applications of QDs become limited for example, in bio-molecule imaging, optical storage and as a single photon source among others. The exact origin behind blinking of QDs had been ambiguous for several years, but it is generally agreed that charge carrier trap states (defects) either internal to or external to the QD are responsible for it as shown in figure 1.9.

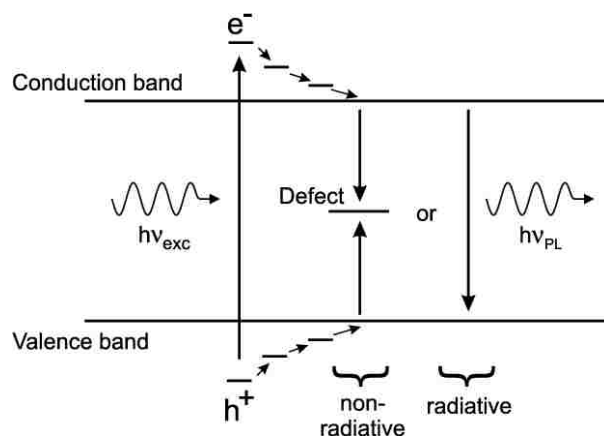


**Figure 1.9.** Schematic showing radiative and non-radiative recombination of photo excited charge carriers<sup>40</sup>

Several models have been proposed to explain the mechanism underlying blinking in QDs. One of the first and most commonly used models for blinking involves Auger-assisted processes,<sup>38,41</sup> According to this model, the fluorescent or “on” state results from the charge-neutral QD, while dark or “off” state is due to a charged state of QD. The extra charge in these charged QDs arises when either of the charge carriers of the photoexcited electron-hole pair is trapped in a localized, long-lived trap-state.<sup>42</sup> Once this occurs, a subsequent exciton that is formed can rapidly recombine non-radiatively by transferring its excess energy to the extra counter charge carrier leading to low fluorescence quantum yield event – the “off” state. This “off” state will persist until the QD is neutralized by recapture (i.e. re-delocalization) of the trapped charge carrier.

The study of trap states has been found to be extremely important to understand their origin and location in QDs. Two kinds of trap states can be explained on the basis of their location on QDs: trap states, which are external to the QDs, (shown in figure 1.10) and trap states in the interface of core-shell or shell-shell of QDs, called interfacial trap states (as shown in figure 1.10). The interplay between these proposed trap states, significantly how they relate to exciton decay dynamics and blinking is still unknown and will be a major focus of this dissertation.

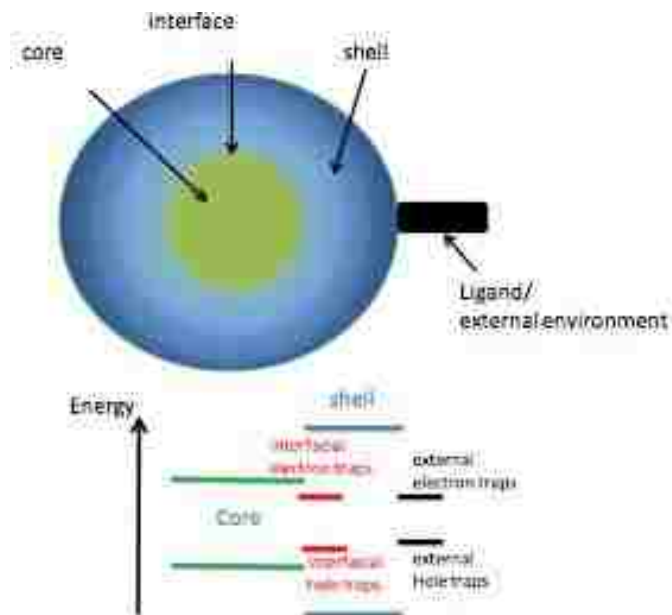


**Figure 1.10.** Anatomy of a core-shell QD and relationship to the electron and hole trap states

Surface trap states have been tremendously studied in literature and several methods have been proposed to reduce blinking by eliminating surface trap states through capping. One of the ways to suppress blinking in QDs was reported by Mahler et al,<sup>28</sup> in which they obtained about 68% non-blinking QDs by growing a ~14 ML thick shell of CdS around the CdSe core QDs. Since there is a small lattice mismatch (~4%) between CdSe and CdS, a thick shell of CdS can be epitaxially grown. A similar effort, by the growth of giant 19 ML shell of CdS around CdSe core by Klimov group was reported in 2008.<sup>43</sup> They also proposed a reduction in the number of interfacial trap states and lattice strain by the growth of thick shell around core, by which the blinking is minimized.

In 2007, Heyes et al<sup>30</sup> reported that blinking statistics do not depend upon shell thickness when up to 7 monolayers of the most common material, ZnS, were added onto CdSe cores. The later studies by Mahler et al,<sup>28</sup> and Klimov et al<sup>43</sup> used thick CdS shells on CdSe cores, so clearly the choice of shell material plays an important role. Since the growth of the ZnS shell effectively



prevents tunneling of the electron and hole wave functions to external trap states, there should be suppression of blinking if only external trap states were responsible for blinking. However, since this was not observed for ZnS shell growth, it was suggested that another source of trap states could be responsible in addition to or instead of external trap states. Therefore, this raised further questions as to where the charge carriers reside. One postulation is that they become trapped at the interfaces of the core and shell. This assumption was based on the fact that, due to large lattice mismatch (~12%) between CdSe and ZnS at the interface, the coating of ZnS shell on CdSe core does not result in good crystallinity of QD material. Therefore, the charge carriers might be trapped at interfaces, which are internal to QDs and more accessible giving rise to blinking in QDs.

For analysis of blinking data, Cordones and Leone<sup>44</sup> recently summarized three different methods: change point detection, autocorrelation, and bin-and-threshold methods. The first one, change point detection, was originally used for QDs by Watkins and Yang<sup>45</sup> and this method uses Bayesian information criterion (without thresholding). In this method, each duration at a given intensity is allocated to an emissive state determined from the statistically relevant change points from individual photon arrival times (without binning). The second method, autocorrelation makes use of photon autocorrelation function, and is more commonly used when shorter timescale dynamics are of more interest. The last method of bin-and-threshold is the most widely used method in blinking analysis and also, the method used in this dissertation in chapters 2 to 4. In this method, blinking traces are obtained by integrating the fluorescence counts into 1 – 100 ms time bins. Specifically, a blinking trace is obtained in such a way that the signal to noise ratio is high, followed by setting a threshold which separates the *on* and *off* events. A probability distribution is then determined by quantifying dwell times above or below the threshold, which is then plotted in terms of a probability distribution function (or probability density).<sup>44</sup> In this analysis method, the off-state

events are generally found to follow an inverse power law distribution while the on-states are generally found to be inverse power law with an exponential decay cut-off at longer timescales (usually several seconds), as described by the equations 1.2 and 1.3, respectively,

$$P_{off}(\tau) \propto \tau^{-\alpha} \quad \mathbf{1.2}$$

$$P_{on}(\tau) \propto \tau^{-\alpha} e^{-\tau/\tau_c} \quad \mathbf{1.3}$$

where  $\alpha$  is the power law exponent with typical values between 1 and 2.  $\tau_c$  is the cross-over time, that shows the characteristic time of the exponential cut off.

## **1.6. Synthesis of QDs**

The two major methods for the synthesis of QDs, which have been used in the literature since the discovery of QDs, involve either deposition on a substrate (e.g. chemical vapor deposition, CVD) or dispersion in a solution. The latter, which is more commonly known as colloidal synthesis is the most popular among chemists because this method provides relatively large amounts of material and meticulous processibility for a wide range of applications. This method involves the chemical reaction between salt precursors in a coordinating ligand solution to make the inorganic crystal with nanometer scales. The ligand solution is heated until the temperature specific to the material being synthesized, is achieved. At this temperature, the precursors are injected and nucleate, forming a seed material on which continuous deposition of solid products results in an increase in the size and control over the shape of the quantum dots.

### 1.6.1. Core Synthesis

As also discussed above, the colloidal synthesis of semiconductor quantum dots generally involves the nucleation of anionic and cationic precursors. This happens in the presence of coordinating and non-coordinating solvents to form an inorganic material surrounded by organic ligands. Actually, the process initiates with the rapid chemical disintegration of the precursors when heated to a specific temperature where multiple nuclei are rapidly formed from the supersaturated solution. Once the concentration of precursors drops below the supersaturation condition, the precursors then start to slowly deposit on the already-formed nuclei until the size of the particles approaches the desired size and at that point, the temperature is quenched. Further details of their synthesis are given in chapters 2 to 4.

The major sources used for cadmium precursors are dimethyl cadmium and CdO/oleic acid (to form Cd-oleate). Before the introduction of the CdO precursor by Peng in 2001,<sup>24</sup> the main precursor of cadmium used was dimethyl cadmium.<sup>8, 25</sup> In addition to high cost, the dimethyl cadmium is more toxic and more sensitive to air (necessitating the use of a glove box) compared to the CdO. Despite such limitations, dimethyl cadmium is still used as cadmium precursor by some groups because this precursor is known to produce high quality quantum dots with narrow size distribution.<sup>46</sup> Nowadays, the easier to use CdO has mostly replaced dimethylcadmium, since this has also proved to produce very high quality and reproducible quantum dots.<sup>46-48</sup> For Se precursor, Se powder is dissolved in either tributylphosphine (TBP) or trioctylphosphine (TOP) or directly in octadecene (ODE). The reaction solvent, trioctylphosphine oxide (TOPO) is heated up to 300°C in an oxygen free environment followed by rapid injection of the precursors into the reaction flask.<sup>8</sup> As discussed earlier, CdSe quantum dots start nucleating immediately and grow to the desired size

that can be easily monitored by gradual change in the solution color or with UV-Vis light or spectrophotometer.

### 1.6.2. Core/shell and core/shell/shell Synthesis

The two main approaches used are the two-step and one-pot synthesis.<sup>21</sup> In two-step method, the core quantum dots are purified followed by their synthesis, before adding shelling precursors to grow the shell. While in the one-pot synthesis method, the continuous injection of shell precursors is done in the same pot after the core formation. Whatever method is used, but there are two criteria that should be taken into account for proper control of shell growth. First, the shelling temperature should be lower than that used during core formation to avoid nucleation of the shell material and uncontrolled ripening. Second, the addition of shell precursors should be done slowly (dropwise) to allow uniform deposition onto the core in order to achieve uniform size-distribution.

Further, for the growth of a given shell thickness, it is required to calculate the correct precursor amounts, and for that, it is necessary to know about the concentration of core material being used. This is done by measuring first excitonic absorption peak of quantum dots using UV-Vis spectroscopy, that can be related to several parameters that leads to the concentration calculation. By using the first excitonic peak wavelength, the size of quantum dots in diameter ( $D$ ) is calculated with the empirically-derived equation 1.4 and then the molar extinction coefficient is calculated by applying to the equation 1.5. The example for CdSe is provided here since the dissertation is focused on CdSe based nanoparticles, but similar equations for other materials are also provided in the same paper.<sup>48</sup>

$$D = (1.6122 \times 10^{-9})\lambda^4 - (2.6575 \times 10^{-6})\lambda^3 + (1.6242 \times 10^{-3})\lambda^2 - (0.4277)\lambda + (41.57) \quad \mathbf{1.4}$$

$$\varepsilon = 5857(D)^{2.65} \quad \mathbf{1.5}$$

Finally, the concentration of the quantum dots is calculated by applying  $\epsilon$  to the Beer-Lambert law (equation 1.6) by which allows the shell precursor amounts were accurately calculated.

$$A = cl\epsilon \qquad \qquad \qquad \mathbf{1.6}$$

Where  $A$  is the absorbance,  $\epsilon$  is the molar extinction coefficient ( $\text{L mol cm}^{-1}$ ),  $c$  is the molar concentration ( $\text{mol L}^{-1}$ ) and  $l$  is the cuvette path length (cm). The earlier method used for several years<sup>1, 8, 20</sup> was the injection of both precursors simultaneously. However, successive ion layer absorption and reaction (SILAR) and Thermal Cycling, was introduced by Peng in 2003<sup>47</sup> and 2007<sup>49</sup> respectively. Both SILAR and TC methods are particularly useful techniques to optimize the quality of core/shell quantum dots. SILAR requires that an exactly-calculated amount of shell precursors is added in a manner that one monolayer of shell is grown at a time, with anionic and cationic precursors added alternately in a sequential manner to ensure the adsorption of one of precursor to the core surface before adding the second one. Thermal Cycling (TC) was also proven to be successful when it was found that injection of precursors at a lower temperature followed by growth of the shell monolayer at higher temperature (usually 20-40°C higher) enables better diffusion of shell precursors to the particle surface at the lower temperature before actual growth at higher temperature.

Therefore, in this dissertation, we followed SILAR (successive ion layer absorption and reaction) and TC (thermal cycling) methods along with a slow, dropwise injection of precursors for the shelling to ensure as uniform a shell distribution around the core quantum dots as possible. As guided from the literature, we also used anionic shell layer first and then cationic for the efficient shelling. For the structural characterization of the QDs regarding size and shape, further characterization tools such as TEM (Transition Electron Microscopy) and HRTEM (High Resolution Transmission Electron Microscopy) are used.

## 1.7. Objectives and overview of the dissertation

This dissertation was categorized into four main parts; with each part presenting the findings in the form of published or to-be-published manuscripts. The first part (chapter 2) concerns how the inner shell architecture of core/multishell QDs influences the ensemble quantum yield and blinking behavior. Specifically, this study involves the monolayer by monolayer (by using modified SILAR and TC) synthesis of four different architectures of QDs. These four different kinds of QDs were synthesized by taking their lattice mismatch and band edge offset parameters into consideration. The synthesis in each case starts with a high quality CdSe core (QY = 30-50 %) and the inner shell is varied up to 5 ML of CdS, ZnSe or their gradient alloy analogs ( $\text{Cd}_{(1-x)}\text{Zn}_x\text{S}$  and  $\text{ZnSe}_{(1-x)}\text{S}_x$ , respectively, with x increasing by 0.2 per ML and will be referred to more simply as CdZnS and ZnSeS from now on), followed by up to 3 ML of ZnS. It was found that CdSe/CdS/ZnS result in the lowest-blinking QDs but also have a lower ensemble photoluminescence quantum yield (PL QY ~20 %) while CdSe/ZnSe/ZnS had about 3 times higher ensemble PL QY (~60 %) but more blinking, although still less blinking than CdSe core QDs. Gradient-alloys of ZnSeS resulted in higher ensemble PL QY as compared to ZnSe (up to 80 %), although blinking didn't show much of a difference compared to ZnSe. However gradient alloys of CdZnS were generally worse than using CdS alone. Therefore, another interesting finding in this project was that ensemble QY is not necessarily a good indicator of blinking behavior. Furthermore, the on and off time distributions were explained by two different mathematical models – the more common truncated power-law model and the more recent multi-exponential model. By binning the same blinking data with 1 ms and 20 ms resolution, it was found that on-times can be better explained by multi-exponential model while off-times can be better explained by truncated power-law model.

The second part (chapter 3) of the dissertation is an extension of chapter 2 in the sense that, the study focuses upon the influence of inner shell architecture and thickness on the exciton decay dynamics of core/multishell quantum dots by using time-resolved fluorescence spectroscopy. It is already known that core/multishell quantum dots (QDs) are becoming a popular alternative to simple core/shell QDs since it allows for more control over the competing effects of exciton wavefunction confinement and interfacial lattice strain. However, introducing a second (*i.e.* shell/shell) interface complicates prediction of the final optical properties of the QD due to a lack of systematic, quantitative studies on such systems. So, here we reported on the influence of the interfacial lattice strain on the structural and optical properties of CdSe/XX/ZnS core/multishell QDs in which we varied the thickness and composition of XX to be CdS, ZnSe,  $\text{Cd}_{(1-x)}\text{Zn}_x\text{S}$  or  $\text{ZnSe}_{(1-x)}\text{S}_x$ , where x increased from 0 to 1 by 0.2 increments in each sequential monolayer. We studied how these shell composition and thickness variations affects the steady-state and time-resolved photoluminescence (PL) properties. The same modified SILAR (successive ion layer and absorption) and TC (thermal cycling) methods were used as in chapter 2 to synthesize a wider range of QD core/multishell architectures (six in total). Similar to chapter 2, the synthesis started with high quality CdSe cores (PL QY = 30-50 %) and then the inner shell thickness or architecture was varied. In one variant, an inner shell of either 3 or 5 ML of CdS or ZnSe was used with an outer shell of 5 or 3 ML of ZnS to investigate the effect of inner shell thickness on the radiative and non-radiative decay pathways of quantum dots. In another variation, 5 ML of gradient alloy analogs ( $\text{Cd}_{(1-x)}\text{Zn}_x\text{S}$  and  $\text{ZnSe}_{(1-x)}\text{S}_x$ , respectively, with x increasing by 0.2 per ML) of CdS or ZnS, followed by 3 ML of ZnS were used to study the effect of architecture variations on the radiative/non-radiative rate constants. In this work, it was shown that the lattice strain (due to lattice mismatch) and the excitons confinement (due to band gap energy offset) not only affects the PL QY

and blinking in QDs, but also contributes towards controlling the exciton decay dynamics of the QDs. Here, we found the quantum yield and fluorescence decay components strongly depend on both the inner shell material and the relative thickness of each shell in complex, but reproducible ways. The growth of QDs was monitored by measuring wavelength red shift in PL spectra and verified by TEM analysis.

The third part (chapter 4) describes a “Goldilocks” effect to reduce blinking in core/multishell QDs by carefully varying the thickness of shells to balance the competing effects of induced lattice strain and confinement potential. We found that blinking can be reduced in small sized core/multishell QDs (~7 nm in total size), smaller than those that are currently available. The QDs used in this project were CdSe/CdS/ZnS core-multi shell QDs with inner shell of 3 ML of CdS and outer shell of 5 ML of ZnS. These QDs were again synthesized by SILAR (successive ion layer and absorption) and TC (thermal cyclic) methods as in chapter 2. The only difference in synthesis of QDs here is in the quality of core QD (PL QY= ~10%) and the ratio of Cd:Se atoms, which is 1:1 in this chapter compared to 1:5 in chapters 2 and 3. Furthermore, by correlating the fluorescence lifetime components of single QDs as a function of fraction of time that they spend in the on-state, both with and without applying a threshold, two types of blinking were found that separately affect the average fluorescence lifetime of a single QD. A physical model was proposed on the basis of thorough characterization of the time-resolved fluorescence at the ensemble and single-particle level and this model involves both short-lived interfacial trap states and long-lived surface trap states that are coupled. This project (chapter 4) is a collaborative project with contribution from my work as highlighted in figures 4.5 and 4.7. In this work, for CdSe/3 ML CdS/3 ML ZnS QDs, which showed widest distribution of fraction-on, the fluorescence lifetime decay was measured for the single QDs using time-correlated single photon counting (TCSPC) with pulsed laser illumination and the



power-dependence experiments were conducted for single QDs to provide an evidence about the contribution of trap-state and band-edge emissions in blinking.

The fourth part (chapter 5) is the study of mechanistic insights into the blinking dynamics of core/shell QDs in terms of off-grey-on transitions in the blinking of these QDs. Here, we have done the systematic study of how the multiple state blinking behaviors of CdSe/CdS core/shell QDs evolve with increasing CdS shell thickness and so, thereby give much reduced blinking QDs. Specifically, a distinct low-intensity level has been identified in these QDs and in several reports already in the literature. This low-intensity state is usually referred as “grey” or “dim” state. In this project, we have synthesized CdSe/CdS QDs with different CdS shell thicknesses to study the dependence of multiple state blinking behaviors on CdS shell thickness. Our results show that the QD blinking occurs in a stepwise manner with the intermediate grey state linking between the off and on states. We here proposed this stepwise transition between on and off states to be due to the stepwise charge or discharge of QDs between multiple charged excitons, trion, and neutral excitons or biexciton states, that all have their individual fluorescence quantum yield and fluorescence lifetime. Therefore, in addition to shell-dependent blinking analysis, we also did intensity-resolved fluorescence lifetime analysis, which gave three distinct fluorescence decay components. The fastest ( $\sim 0.2$  ns) component is present in significant amplitudes in both the on and grey states. The medium component ( $\sim 1-4$  ns) is present mostly in the grey state, while the slowest component ( $\sim 15-30$  ns) is present in the on state only. So, from the intensity-resolved fluorescence lifetime analysis, we observed a very bright but short-lived on-state in our CdSe/CdS QDs. A similar observation was also reported recently for CdSe/ZnS QDs in literature. In our analysis of this state, we observed a correlation of the amplitude of a fast lifetime component with on-state intensity and anti-correlation with on-state time. This implies that there is a high quantum yield state with a very fast lifetime that

can be accessed from the grey state but that this pathway is only available for a relatively short time. On the basis of these results, we proposed a model to explain the rationale behind it. If our hypothesis of bright on state is correct, this state is more likely to come from the negative trion grey state rather than the positive trion (usually positive trion is assigned to grey state in literature). However, technically, both possibilities are possible and more work is still needed to unambiguously make this assignment. We also compared these multiple-state blinking analysis results with other common core/shell combinations of CdSe/ZnSe and CdSe/ZnS QDs. From comparing the blinking analysis results of all these core/shell combinations of CdSe/CdS, CdSe/ZnSe and CdSe/ZnS QDs, we found that the grey state formation has a strong dependence on the lattice strain between core and shell interface. Since the lattice strain in these core/shell combinations is in the order of CdS < ZnSe < ZnS, so our experimental results suggested that grey state formation is very obvious in QDs with CdS shell and this is present to a very small extent (and not well resolved) in ZnSe shell QDs and not at all in ZnS shell QDs. Therefore, our results suggest that minimizing structural defects in QDs is one of the important factor in reducing QD blinking and achieving non-blinking QDs.

## 1.8. References

1. Dabbousi, B. O.; RodriguezViejo, J.; Mikulec, F. V.; Heine, J. R.; Mattoussi, H.; Ober, R.; Jensen, K. F.; Bawendi, M. G., (CdSe)ZnS core-shell quantum dots: Synthesis and characterization of a size series of highly luminescent nanocrystallites. *Journal of Physical Chemistry B* **1997**, *101* (46), 9463-9475.
2. Alivisatos, A. P., Semiconductor clusters, nanocrystals, and quantum dots. *Science* **1996**, *271* (5251), 933-937.
3. Weller, H., COLLOIDAL SEMICONDUCTOR Q-PARTICLES - CHEMISTRY IN THE TRANSITION REGION BETWEEN SOLID-STATE AND MOLECULES. *Angewandte Chemie-International Edition in English* **1993**, *32* (1), 41-53.
4. Murphy, C. J.; Coffey, J. L., Quantum dots: A primer. *Applied Spectroscopy* **2002**, *56* (1), 16A-27A.
5. Brus, L. E., A SIMPLE-MODEL FOR THE IONIZATION-POTENTIAL, ELECTRON-AFFINITY, AND AQUEOUS REDOX POTENTIALS OF SMALL SEMICONDUCTOR CRYSTALLITES. *Journal of Chemical Physics* **1983**, *79* (11), 5566-5571.
6. Brus, L. E., ELECTRON ELECTRON AND ELECTRON-HOLE INTERACTIONS IN SMALL SEMICONDUCTOR CRYSTALLITES - THE SIZE DEPENDENCE OF THE LOWEST EXCITED ELECTRONIC STATE. *Journal of Chemical Physics* **1984**, *80* (9), 4403-4409.
7. Spanhel, L.; Haase, M.; Weller, H.; Henglein, A., PHOTOCHEMISTRY OF COLLOIDAL SEMICONDUCTORS .20. SURFACE MODIFICATION AND STABILITY OF STRONG LUMINESCING CDS PARTICLES. *Journal of the American Chemical Society* **1987**, *109* (19), 5649-5655.
8. Murray, C. B.; Norris, D. J.; Bawendi, M. G., SYNTHESIS AND CHARACTERIZATION OF NEARLY MONODISPERSE CDE (E = S, SE, TE) SEMICONDUCTOR NANOCRYSTALLITES. *Journal of the American Chemical Society* **1993**, *115* (19), 8706-8715.
9. Grabolle, M.; Ziegler, J.; Merkulov, A.; Nann, T.; Resch-Genger, U., Stability and fluorescence quantum yield of CdSe-ZnS quantum dots - Influence of the thickness of the ZnS shell. *Fluorescence Methods and Applications: Spectroscopy, Imaging, and Probes* **2008**, *1130*, 235-241.
10. Chen, O.; Zhao, J.; Chauhan, V. P.; Cui, J.; Wong, C.; Harris, D. K.; Wei, H.; Han, H. S.; Fukumura, D.; Jain, R. K.; Bawendi, M. G., Compact high-quality CdSe-CdS core-shell nanocrystals with narrow emission linewidths and suppressed blinking. *Nature Materials* **2013**, *12* (5), 445-451.
11. Brus, L., ELECTRONIC WAVE-FUNCTIONS IN SEMICONDUCTOR CLUSTERS - EXPERIMENT AND THEORY. *Journal of Physical Chemistry* **1986**, *90* (12), 2555-2560.

12. Smith, A. M.; Mohs, A. M.; Nie, S., Tuning the optical and electronic properties of colloidal nanocrystals by lattice strain. *Nature Nanotechnology* **2009**, *4* (1), 56-63.
13. Omogo, B.; Aldana, J. F.; Heyes, C. D., Radiative and Nonradiative Lifetime Engineering of Quantum Dots in Multiple Solvents by Surface Atom Stoichiometry and Ligands. *Journal of Physical Chemistry C* **2013**, *117* (5), 2317-2327.
14. Santra, S.; Wang, K. M.; Tapecc, R.; Tan, W. H., Development of novel dye-doped silica nanoparticles for biomarker application. *Journal of Biomedical Optics* **2001**, *6* (2), 160-166.
15. Raab, R. M.; Stephanopoulos, G., Dynamics of gene silencing by RNA interference. *Biotechnology and Bioengineering* **2004**, *88* (1), 121-132.
16. Jamieson, T.; Bakhshi, R.; Petrova, D.; Pocock, R.; Imani, M.; Seifalian, A. M., Biological applications of quantum dots. *Biomaterials* **2007**, *28* (31), 4717-4732.
17. Chen, X. B.; Lou, Y. B.; Samia, A. C.; Burda, C., Coherency strain effects on the optical response of core/shell heteronanostructures. *Nano Lett.* **2003**, *3* (6), 799-803.
18. Kuno, M.; Fromm, D. P.; Johnson, S. T.; Gallagher, A.; Nesbitt, D. J., Modeling distributed kinetics in isolated semiconductor quantum dots. *Phys. Rev. B* **2003**, *67* (12), 15.
19. Manna, L.; Scher, E. C.; Li, L. S.; Alivisatos, A. P., Epitaxial growth and photochemical annealing of graded CdS/ZnS shells on colloidal CdSe nanorods. *Journal of the American Chemical Society* **2002**, *124* (24), 7136-7145.
20. Hines, M. A.; Guyot-Sionnest, P., Synthesis and characterization of strongly luminescing ZnS-Capped CdSe nanocrystals. *Journal of Physical Chemistry* **1996**, *100* (2), 468-471.
21. Reiss, P.; Protiere, M.; Li, L., Core/Shell Semiconductor Nanocrystals. *Small* **2009**, *5* (2), 154-168.
22. Efros, A. L., INTERBAND ABSORPTION OF LIGHT IN A SEMICONDUCTOR SPHERE. *Soviet Physics Semiconductors-Ussr* **1982**, *16* (7), 772-775.
23. Ekimov, A. I.; Onushchenko, A. A., QUANTUM SIZE EFFECT IN THE OPTICAL-SPECTRA OF SEMICONDUCTOR MICRO-CRYSTALS. *Soviet Physics Semiconductors-Ussr* **1982**, *16* (7), 775-778.
24. Peng, Z. A.; Peng, X. G., Nearly monodisperse and shape-controlled CdSe nanocrystals via alternative routes: Nucleation and growth. *J. Am. Chem. Soc.* **2002**, *124* (13), 3343-3353.
25. Peng, X. G.; Schlamp, M. C.; Kadavanich, A. V.; Alivisatos, A. P., Epitaxial growth of highly luminescent CdSe/CdS core/shell nanocrystals with photostability and electronic accessibility. *J. Am. Chem. Soc.* **1997**, *119* (30), 7019-7029.

26. Breus, V. V.; Heyes, C. D.; Nienhaus, G. U., Quenching of CdSe-ZnS core-shell quantum dot luminescence by water-soluble thiolated ligands. *J. Phys. Chem. C* **2007**, *111* (50), 18589-18594.
27. Smith, A. M.; Ruan, G.; Rhyner, M. N.; Nie, S. M., Engineering luminescent quantum dots for In vivo molecular and cellular imaging. *Annals of Biomedical Engineering* **2006**, *34* (1), 3-14.
28. Mahler, B.; Spinicelli, P.; Buil, S.; Quelin, X.; Hermier, J. P.; Dubertret, B., Towards non-blinking colloidal quantum dots. *Nat. Mater.* **2008**, *7* (8), 659-664.
29. Talapin, D. V.; Rogach, A. L.; Kornowski, A.; Haase, M.; Weller, H., Highly luminescent monodisperse CdSe and CdSe/ZnS nanocrystals synthesized in a hexadecylamine-trioctylphosphine oxide-trioctylphosphine mixture. *Nano Letters* **2001**, *1* (4), 207-211.
30. Heyes, C. D.; Kobitski, A. Y.; Breus, V. V.; Nienhaus, G. U., Effect of the shell on the blinking statistics of core-shell quantum dots: A single-particle fluorescence study. *Phys. Rev. B* **2007**, *75* (12), 8.
31. Spinicelli, P.; Mahler, B.; Buil, S.; Quelin, X.; Dubertret, B.; Hermier, J. P., Non-Blinking Semiconductor Colloidal Quantum Dots for Biology, Optoelectronics and Quantum Optics. *Chemphyschem* **2009**, *10* (6), 879-882.
32. Yu, Z. H.; Guo, L.; Du, H.; Krauss, T.; Silcox, J., Shell distribution on colloidal CdSe/ZnS quantum dots. *Nano Letters* **2005**, *5* (4), 565-570.
33. Zhu, H. M.; Song, N. H.; Lian, T. Q., Controlling Charge Separation and Recombination Rates in CdSe/ZnS Type I Core-Shell Quantum Dots by Shell Thicknesses. *Journal of the American Chemical Society* **2010**, *132* (42), 15038-15045.
34. Scotognella, F.; Miszta, K.; Dorfs, D.; Zavelani-Rossi, M.; Brescia, R.; Marras, S.; Manna, L.; Lanzani, G.; Tassone, F., Ultrafast Exciton Dynamics in Colloidal CdSe/CdS Octapod Shaped Nanocrystals. *Journal of Physical Chemistry C* **2011**, *115* (18), 9005-9011.
35. Soni, U.; Sapra, S., The Importance of Surface in Core-Shell Semiconductor Nanocrystals. *Journal of Physical Chemistry C* **2010**, *114* (51), 22514-22518.
36. Hoogenboom, J. P.; Hernando, J.; van Dijk, E.; van Hulst, N. F.; Garcia-Parajo, M. F., Power-law blinking in the fluorescence of single organic molecules. *ChemPhysChem* **2007**, *8* (6), 823-833.
37. Dickson, R. M.; Cubitt, A. B.; Tsien, R. Y.; Moerner, W. E., On/off blinking and switching behaviour of single molecules of green fluorescent protein. *Nature* **1997**, *388* (6640), 355-358.
38. Nirmal, M.; Dabbousi, B. O.; Bawendi, M. G.; Macklin, J. J.; Trautman, J. K.; Harris, T. D.; Brus, L. E., Fluorescence intermittency in single cadmium selenide nanocrystals. *Nature* **1996**, *383* (6603), 802-804.

39. Kuno, M.; Fromm, D. P.; Gallagher, A.; Nesbitt, D. J.; Micic, O. I.; Nozik, A. J., Fluorescence intermittency in single InP quantum dots. *Nano Lett.* **2001**, *1* (10), 557-564.
40. Ledoux, G.; Guillois, O.; Huisken, F.; Kohn, B.; Porterat, D.; Reynaud, C., Crystalline silicon nanoparticles as carriers for the Extended Red Emission. *Astron. Astrophys.* **2001**, *377* (2), 707-720.
41. Efros, A. L.; Rosen, M., Random telegraph signal in the photoluminescence intensity of a single quantum dot. *Phys. Rev. Lett.* **1997**, *78* (6), 1110-1113.
42. Wang, X. Y.; Ren, X. F.; Kahen, K.; Hahn, M. A.; Rajeswaran, M.; Maccagnano-Zacher, S.; Silcox, J.; Cragg, G. E.; Efros, A. L.; Krauss, T. D., Non-blinking semiconductor nanocrystals. *Nature* **2009**, *459* (7247), 686-689.
43. Chen, Y.; Vela, J.; Htoon, H.; Casson, J. L.; Werder, D. J.; Bussian, D. A.; Klimov, V. I.; Hollingsworth, J. A., "Giant" multishell CdSe nanocrystal quantum dots with suppressed blinking. *J. Am. Chem. Soc.* **2008**, *130* (15), 5026-+.
44. Cordones, A. A.; Leone, S. R., Mechanisms for charge trapping in single semiconductor nanocrystals probed by fluorescence blinking. *Chemical Society Reviews* **2013**, *42* (8), 3209-3221.
45. Watkins, L. P.; Yang, H., Detection of intensity change points in time-resolved single-molecule measurements. *Journal of Physical Chemistry B* **2005**, *109* (1), 617-628.
46. Wang, Q. A.; Pan, D. C.; Jiang, S. C.; Ji, X. L.; An, L. J.; Jiang, B. Z., Luminescent CdSe and CdSe/CdS core-shell nanocrystals synthesized via a combination of solvothermal and two-phase thermal routes. *Journal of Luminescence* **2006**, *118* (1), 91-98.
47. Li, J. J.; Wang, Y. A.; Guo, W. Z.; Keay, J. C.; Mishima, T. D.; Johnson, M. B.; Peng, X. G., Large-scale synthesis of nearly monodisperse CdSe/CdS core/shell nanocrystals using air-stable reagents via successive ion layer adsorption and reaction. *Journal of the American Chemical Society* **2003**, *125* (41), 12567-12575.
48. Yu, W. W.; Qu, L. H.; Guo, W. Z.; Peng, X. G., Experimental determination of the extinction coefficient of CdTe, CdSe and CdS nanocrystals (vol 15, pg 2854, 2003). *Chemistry of Materials* **2004**, *16* (3), 560-560.
49. Blackman, B.; Battaglia, D. M.; Mishima, T. D.; Johnson, M. B.; Peng, X. G., Control of the morphology of complex semiconductor nanocrystals with a type II heterojunction, dots vs peanuts, by thermal cycling. *Chemistry of Materials* **2007**, *19* (15), 3815-3821.

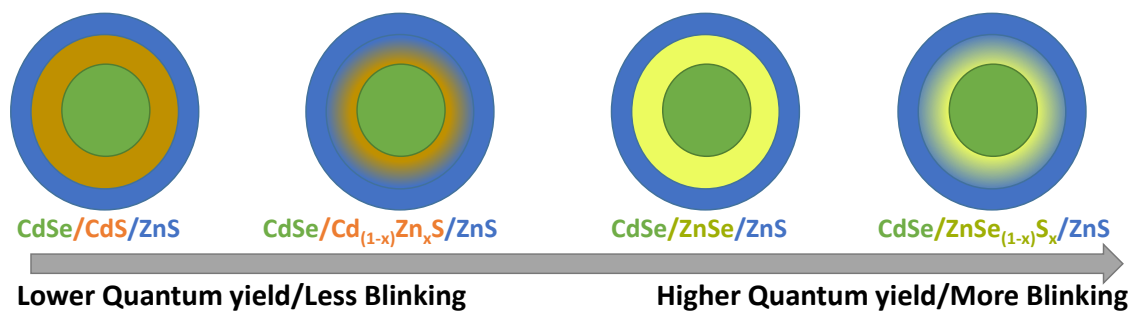
## Chapter 2. Role of the Inner Shell Architecture on Quantum Yield and Blinking Dynamics in Core/Multi-Shell Quantum Dots

*Pooja Bajwa, Feng Gao, Anh Nguyen, Benard Omogo and Colin D. Heyes\**

*Department of Chemistry and Biochemistry, University of Arkansas, 345 N. Campus Drive,  
Fayetteville, AR 72701*

*\*To whom correspondence should be addressed*

**TOC graphic:**



**What the Shell?** Here we show that choosing the correct shell architecture is a complex problem, especially for multi-shell quantum dots. Different shell combinations, and whether they are alloyed or not, lead to different properties at the ensemble level (quantum yield) and the single particle level (blinking).

## 2.1. Abstract

Choosing the composition of the shell for QDs is not trivial, since both the band-edge energy offset and interfacial lattice mismatch play roles in influencing the final optical properties. One way to balance these competing effects is by forming multi-shells and/or gradient-alloyed shells. However, this introduces multiple interfaces and their relative effects on quantum yield and blinking are not yet fully understood. Here we undertake a systematic, comparative study of adding inner shells of single composition vs gradient-alloyed shells of cadmium/zinc chalcogenides onto CdSe cores, and then capping with a thin ZnS outer shell to form various core/multi-shell configurations. We show that the inner shell architecture between the CdSe core and the outer ZnS shell plays a significant role in both quantum yield and blinking dynamics but that these effects are not correlated – a high ensemble quantum yield doesn't necessarily equate to reduced blinking. Two mathematical models have been proposed to describe the blinking dynamics – the more common power-law model and a more recent multi-exponential model. By binning the same data with 1 ms and 20 ms resolution, we show that the on-times can be better described by the multi-exponential model while the off-times can be better described by the power-law model. We discuss physical mechanisms that might explain this behavior and how it can be affected by the inner shell architecture.



## 2.2. Introduction

It is well known that adding a wide band-gap shell onto colloidal core CdSe quantum dots (QDs) significantly improves their photoluminescence quantum yield.<sup>[1, 2]</sup> The subsequent modification of the shelling procedure to a stepwise monolayer-by-monolayer growth of shell material, termed SILAR, has led to more accurate control and higher reproducibility of the shell thickness and size distribution.<sup>[3]</sup> Moreover, this advance allows for multiple shell materials to be easily grown leading to more advanced tailoring of QDs for wide-ranging applications in LEDs,<sup>[4]</sup> photovoltaics,<sup>[5]</sup> optoelectronics<sup>[6]</sup> and chemical/biochemical sensors.<sup>[7-9]</sup> In particular, QDs have certain advantages over molecular fluorophores for bioimaging applications due to their broad absorption spectra, narrow emission spectra, long fluorescence lifetime and their high photostability under real operating conditions.<sup>[10-14]</sup>

CdSe/ZnS nanostructures were the first studied core/shell system<sup>[1, 2]</sup> because ZnS offers the widest band gap energy that is compatible with CdSe, leading to the photoexcited charge carriers to better be confined inside the core materials. It was considered that reducing the accessibility of the exciton to surface states decreases non-radiative recombination pathways. However, a major limitation with this core/shell combination is that the large lattice mismatch (~12%) between CdSe and ZnS may lead to dislocations/defects at the core/shell interface if the shell is too thick that creates new non-radiative recombination pathways and limits the maximum QY.<sup>[15]</sup> Other core/shell combinations have been investigated, such as the very low lattice mismatched CdSe/CdS (~4%)<sup>[16]</sup> and the moderately mismatched CdSe/ZnSe (~8%).<sup>[17]</sup> However, these combinations suffer from the fact that they do not confine the exciton to the core as well as ZnS, leading to the fact that the external environment can affect the QY if the shell is too thin and reducing wavefunction overlap and thus QY if the shell is too thick. It was then shown that using multi-shells of a lower lattice

mismatch material as a thin inner shell with a higher bandgap ZnS as a thin outer shell led to higher QYs than using only single shell materials. <sup>[15, 18]</sup>

The choice of shell material also has an effect on single QD blinking. Blinking is the phenomenon of intermittence between fluorescent and dark states of single fluorescence probes under continuous excitation and occurs in organic dye molecules,<sup>[19, 20]</sup> fluorescent proteins,<sup>[21, 22]</sup> or nanoparticles.<sup>[19, 23]</sup> Blinking severely limits the applications of fluorophores, especially in bioimaging, optical storage and as single photon sources. Although blinking in organic dyes and fluorescent proteins is generally understood, the underlying mechanism behind blinking in QDs has remained elusive. It is generally agreed upon that trapping of charge carriers is responsible for blinking, but microscopic details as to which charge carriers are trapped and where the trap states are is still under intense investigation. It was found that adding a ZnS shell up to ~7 monolayers (ML) thick onto CdSe does not reduce blinking, although it does increase the ensemble quantum yield.<sup>[24]</sup> Adding CdS shells to CdSe does allow blinking to be significantly reduced, but the shell must either be very thick (~15ML)<sup>[25]</sup> or be grown at a slow rate but at high temperature to give near-perfect crystallinity.<sup>[26]</sup> It appears that the lattice mismatch creates interfacial trap states at the core/shell interface which are involved in blinking, but mechanistic details are still lacking. Furthermore, for biological applications, it is less than ideal to have the outer shell containing toxic cadmium. Chen *et al.* reported that Multishell QDs of CdSe/CdS/ZnS could also reduce blinking but, again, it was required to make the shells thick, producing what they called “Giant” multishell QDs.<sup>[27]</sup> While this approach is suitable for many applications, their large size does not make them well-suited for applications where a small size is needed, such as for labeling small biomolecules or when they need to be optically coupled.

A major question that remains is whether the choice of inner shell material and whether it is alloyed or not can be systematically chosen to reduce blinking and increase QY without the detrimental side effects of too large a size or using CdS as the outer shell. To reach this goal it is necessary to more thoroughly understand the role of the inner shell architecture on such properties. In this work, we have synthesized four different QD architectures on the basis of their lattice mismatch and band gap energy offset parameters. We started with a high quality CdSe core (QY = 30-50%) and varied the inner shell material up to 5ML of CdS, ZnSe or their gradient alloy analogs ( $\text{Cd}_{(1-x)}\text{Zn}_x\text{S}$  and  $\text{ZnSe}_{(1-x)}\text{S}_x$ , respectively, with x increasing by 0.2 per ML), followed by up to 3 ML of ZnS. We found that CdSe/CdS/ZnS showed lower blinking QDs but also had a lower ensemble QY (~20%) while CdSe/ZnSe/ZnS had a 3-fold higher ensemble QY (~60%) but more blinking, although still blinking less than the core-only CdSe. Gradient alloys of CdZnS were generally worse than just using CdS, but gradient alloys of ZnSeS led to higher QYs than ZnSe (up to 80%), although blinking remained the same as when using ZnSe. While these are among the highest QY reported for core/shell/shell QDs, it is interesting to find that ensemble QY isn't necessarily a good indicator of the blinking behavior. We fit the distribution of on and off times to two models – a truncated power-law and a multi-exponential model – and discuss the relative merits of current blinking models to explain our data.

## 2.3. Experimental Section

**2.3.1. Chemicals:** Cadmium oxide (CdO, 90%, Sigma-Aldrich), selenium powder (Se, 99.99%, Alfa Aesar), zinc oxide (ZnO, 99%, Sigma-Aldrich), sulfur powder (S, 99.9%, Alfa Aesar), oleic acid (OA, tech. grade, Alfa Aesar), 1-octadecene (ODE, 90%, Alfa Aesar), octadecylamine (ODA, 95%, Acros Organics), tri-butylphosphine (TBP, 95%, Alfa Aesar), Sulforhodamine 101 dye (S

101 dye Invitrogen), poly(methyl methacrylate) (PMMA, Sigma Aldrich) and tri-octylphosphine oxide (TOPO, Sigma-Aldrich) were used as prepared without further purification. Solvents: All solvents were purchased from VWR international. Methanol, hexane and acetone were of pure grade. Toluene was of high purity HPLC grade.

**2.3.2. CdSe Core Synthesis:** CdSe core samples were synthesized by modification of the literature methods.<sup>[28]</sup> Briefly, 0.04 M cadmium (Cd) precursor was prepared by degassing under vacuum and then heating a mixture of 0.02565 g CdO, 0.4452 g OA and 2 g ODE to 200°C under argon flow until the solution became clear. The temperature was then reduced to 50°C and then 1.5092 g ODA and 0.5026 g of TOPO was added. The reaction mixture was degassed again and heated to 300°C under argon flow. Once at this temperature, 0.04 M Se precursor solution (made from 0.01579 g Se, 0.4653 g TBP and 1.37 g ODE) was rapidly injected and, within a few seconds, the heating mantle was removed and reaction was quenched by adding hexane to avoid further growth of particles. After cooling the solution to room temperature, it was purified by washing with approximately equal amounts of hexane and methanol. The mixture was centrifuged for about 5 minutes at 7K rpm and the process was repeated 2 more times.

**2.3.3. Core/shell/shell synthesis:** The shelling of CdSe core was accomplished by applying successive ion layer absorption and reaction (SILAR) with thermal cycling (TC).<sup>[3]</sup> Generally, 0.08 M Cd or Zn and 0.4 M S precursors (depending on the amount of precursor needed for each injection) were prepared by the same method as the Cd precursor while 0.08 M or 0.4 M S precursor was prepared in the same way as that of Se. The starting CdSe core solution for the shelling process was prepared by mixing together 3 mL of CdSe in hexane, 1.5 g ODA and 3 mL of ODE in a 3 necked reaction flask. Now, calculated amounts of Se or S and Zn or Cd were injected alternately one monolayer (ML) at a time at a temperature of 180°C, allowed to equilibrate for 5

minutes each, followed by crystallization of the shell by raising the temperature to 210°C for CdS or to 230°C for ZnSe or ZnS shell for 20 more minutes. The S or Se precursor was always injected first. Approximately 1 mL aliquots were taken out and dissolved in hexane after the growth of each ML before lowering the temperature and used for characterization. The first 5 ML injections were for either CdS or ZnSe shell while the last 3 ML injections were for the ZnS shell. All sample syntheses were performed twice to ensure reproducibility in the resulting optical and structural properties.

**2.3.4. Core/gradient-alloyed shell/shell synthesis:** The growth of 5 ML of alloyed  $\text{Cd}_{(1-x)}\text{Zn}_x\text{S}$  or  $\text{ZnSe}_{(1-x)}\text{S}_x$ , was carried out by varying the ratio of  $x$  from 0 to 1 in increments of 0.2 per ML. The synthesis is exactly similar to the core/shell/shell synthesis except 0.08 M Cd and Zn precursors or 0.08 M Se and S precursors, with exact volumes varying depending on the required alloy composition for that ML, were injected together at 180°C and heated at 220°C for CdZnS and at 230°C for ZnSeS. All sample syntheses were performed twice to ensure reproducibility in the resulting optical and structural properties.

## **2.4. Instrumentation and measurements**

**2.4.1. Fluorescence and Absorption Spectroscopy:** Photoluminescence (PL) and absorbance of the aliquots for different monolayers were measured with a Perkin Elmer LS 55 luminescence spectrometer and Hitachi U-3900H spectrophotometer, respectively. PL percentage quantum yields (PL QYs) were measured by comparing the integrated areas of the PL spectra of QDs dissolved in hexane to that of the dye standard, Sulforhodamine 101 in ethanol, with the same optical density of 0.05 at the excitation wavelength of 530 nm.

**2.4.2. Transmission Electron Microscopy:** Transmission electron microscopy (TEM) and high resolution TEM (HRTEM) were performed using a Tecnai G2 F20-TWIN (TF20, FEI, Hillsboro, OR). To prepare TEM samples, 200  $\mu$ L of thoroughly washed/purified samples were deposited on a thin film of carbon-coated grids. The QDs diameter was measured using the ImageJ software.

**2.4.3. Blinking:** A MicroTime 200 scanning confocal fluorescence microscope (PicoQuant GmbH, Berlin, Germany), which is based on Olympus IX71 equipped with PicoHarp 300 TCSPC controller, was used.<sup>[29]</sup> It utilizes a 485 nm laser (PDL 485, Picoquant) operating in continuous wave mode at a power of 10  $\mu$ W for excitation of QD samples. A dichroic mirror (500dextr, Chroma, McHenry, IL) sends the light through a water immersion objective (Olympus, Apochromat 60x, NA 1.3) to a diffraction-limited laser focus. The same objective collects the fluorescence and sends it through the same dichroic mirror and a 100  $\mu$ m pinhole. To reject background fluorescence and scattered laser light, a fluorescence filter that best matches the emission wavelength of the QDs (HQ560/40M for CdSe cores, HQ620/60M for CdSe/CdS/ZnS and CdSe/CdS<sub>(1-x)</sub>S<sub>x</sub>/ZnS, HQ585/65M for CdSe/ZnSe/ZnS and HQ605/55M for CdSe/ZnSe<sub>(1-x)</sub>S<sub>x</sub>/ZnS, Chroma) is placed in front of Single Photon Avalanche Diode Detector (SPAD, MPI, Microphotonic devices, Bolano, Italy). To perform blinking experiments, 50  $\mu$ l of a diluted quantum dot solution containing ~ 3% (W/V) Poly(methyl methacrylate) (PMMA) in toluene was spin coated onto a clean No. 1 glass coverslip to make a thin film of immobilized single QDs in a PMMA matrix. The objective is positioned on a sub-nanometer precision 3D piezo scanning stage (PI, Berlin, Germany) and fluorescence images of 20 x 20  $\mu$ m were recorded. Then, from the recorded fluorescence images, the diffraction-limited focus was focused onto the individually well-isolated bright spots to collect fluorescence time traces for up to 5 minutes. The collected photons were binned at 1 ms resolution or 20 ms resolution and the intensity-time data extracted for analysis of on and off time distributions

using homemade analysis software written in Igor. All blinking data is the average of two separate preparations for each sample to ensure that the observed differences were reproducible.

## **2.5. Results and discussion:**

Both the band-edge offsets and the lattice strain between the different materials are important contributors to the optical and structural properties of heteronanostructured QDs. A schematic showing the relative differences in these parameters for the material combinations used in this study is shown in figure 2.1a. The key difference between using CdS/ZnS and ZnSe/ZnS on CdSe cores is the relative degree of confinement and the lattice strain at each interface.

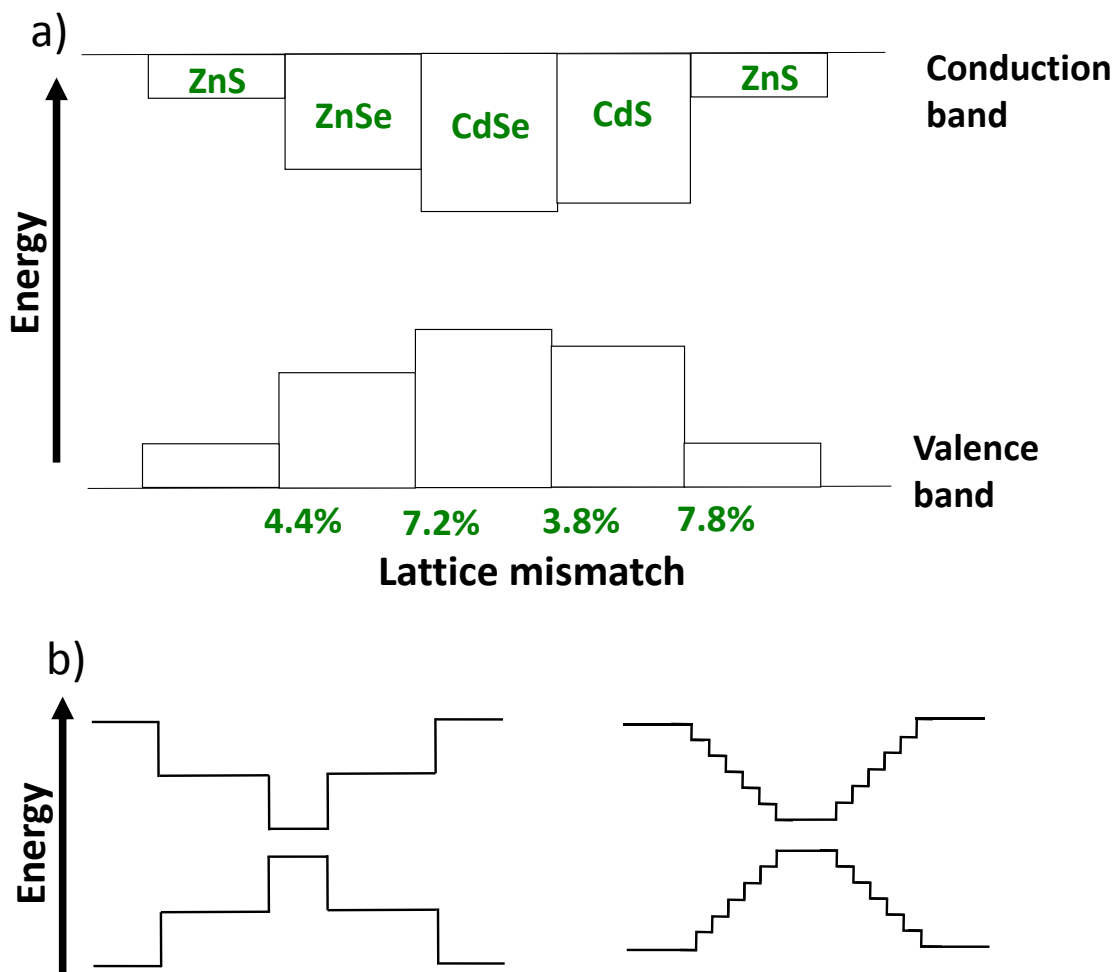


**Figure 2.1:** (a) Schematic of band gap offset and lattice mismatch values of semiconductor materials specific to our work. (b) Schematic highlighting difference in band-edge offsets between core/shell/shell (left) and core/gradient-alloyed shell/shell (right) architectures.

The conduction band offset for CdSe/CdS is very small, leading to a high probability for the electron to tunnel into the inner shell, but the lattice mismatch between these materials is also very small leading to fewer trap states closer to the core. When ZnS is then added to the CdS, a larger lattice mismatch at this interface is likely to cause trap states to form. For ZnSe, the opposite is true; the higher lattice strain is moved from the shell/shell interface to the core/shell interface, but the electron and hole wavefunctions have less penetration into the inner shell. When the inner shell is



changed from pure CdS or ZnSe to gradient-alloyed analogs that gradually change the composition to ZnS, the confinement potential changes from a step function at the interface to a more gradual change with each ML (Figure 2.1b). Furthermore, the lattice strain between the inner and outer shell is eliminated, but is instead spread out through the inner shell. The main goal of this study is to determine how these parameters affect the optical and structural properties.

The change in PL  $\lambda_{\max}$  and the PL QY upon shelling with each ML of each material combination is shown in figure 2.2.

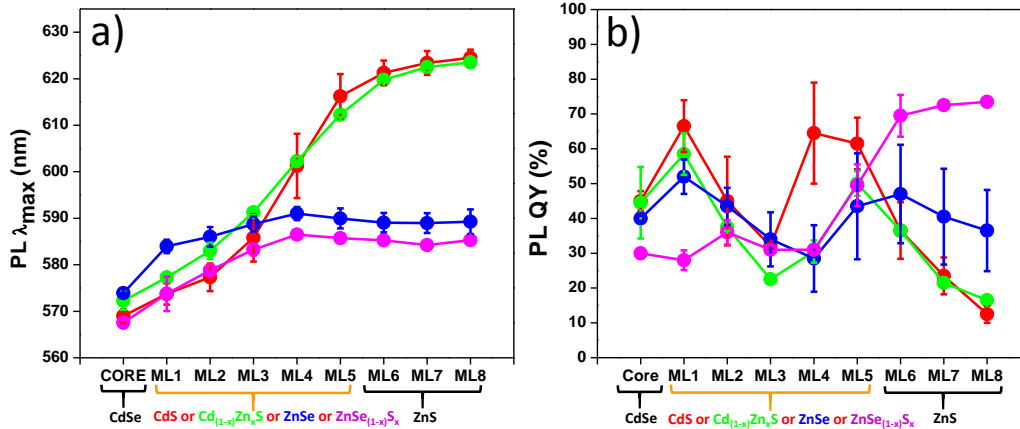


**Figure 2.2:** a) PL peak maximum and b) photoluminescence quantum yield as a function of shell composition and thickness. Red: CdSe/CdS/ZnS; Green: CdSe/Cd<sub>(1-x)</sub>Zn<sub>x</sub>S/ZnS; Blue: CdSe/ZnSe/ZnS; Magenta: CdSe/ZnSe<sub>(1-x)</sub>S<sub>x</sub>/ZnS. Points are average values of 2 samples and the error bars are 1 standard deviation wide to show the reproducibility.

The data is the average of 2 separate preparations of each sample. The error bars ( $1\sigma$  in width) show that the  $\lambda_{\max}$  shifts are highly reproducible. There is some variation in the exact PL QY values, but we found that the actual trends were very reproducible. As expected, upon shelling there is a red-shift in the  $\lambda_{\max}$ , with CdS showing a larger shift than ZnSe due to the smaller band-gap of CdS compared to ZnSe that results in weaker confinement of the exciton to the CdSe core. Once 5 ML of either shell is added, adding 3 ML ZnS causes very little change in the  $\lambda_{\max}$ . The PL QY

changes, however, are more complex. We start from a relatively high QY core then, for CdS, it increases with the first ML, then decreases between ML1 and ML3, and increases again up to 5 ML. Adding ZnS to this high QY CdSe/CdS then causes a significant decrease in the QY to eventually become lower than even the original core. Using a gradient-alloy  $\text{Cd}_{(1-x)}\text{Zn}_x\text{S}$ , where  $x$  changes by 0.2 per ML, shows the same trend, although the increase in QY is much less than using the pure CdS. On the other hand, shelling with ZnSe causes a slight decrease in QY until adding the 5<sup>th</sup> ML, at which point the rise is fairly large. For shelling with  $\text{ZnSe}_{(1-x)}\text{S}_x$  there is a slight increase in QY until the 5<sup>th</sup> ML at which the rise is, again, fairly large. Interestingly, when ZnS is added to CdSe/ZnSe, there is a decrease in QY, whereas when ZnS is added to CdSe/ $\text{ZnSe}_{(1-x)}\text{S}_x$  the QY continues to rise. It appears that the lattice strain at the ZnSe/ZnS shell/shell interface causes the introduction of additional non-radiative pathways, which is eliminated by forming the gradient from ZnSe to ZnS over the 5ML of inner shell. It is important to point out at this point that these trends and QY fluctuations are all reproducible at each ML using different CdSe core batches of about the same QY. It has been suggested that there is an inverse relationship between the core quality and the final maximal QY of the core/shell system,<sup>[30]</sup> although in that study the core QYs were much lower than those used in our study. The ability to grow good quality shells onto cores appeared to be facilitated by the presence of defects in the core. Our data suggests that this complex behavior may also extend to the quality of the inner shell architecture when using core/multi-shell systems. Still, using the gradient-alloyed inner shell of  $\text{ZnSe}_{(1-x)}\text{S}_x$ , we are able to synthesize QDs with a very high 80% QY and with a less toxic composition than using CdS, which are attractive for a number of applications where toxicity is important, such as for biological labeling or for use in consumer devices such as LEDs in TVs.

To ensure that the SILAR/thermal cycling process grows the shells as anticipated, TEM was used to monitor the increase in size of QDs after shelling with each material combination, as shown in figure 2.3. For CdSe cores, the average size was  $4.6 \pm 0.6$  nm. Upon shelling with CdS/ZnS or ZnSe/ZnS, the average size was  $12.7 \pm 1.4$  nm and  $12.4 \pm 1.6$  nm, respectively. When gradient-alloyed inner shells were used, the increase in size was about 1.5 - 2 nm less in both cases,  $11.3 \pm 1.4$  nm and  $10.4 \pm 1.0$  nm respectively. It is interesting to note that using  $\text{Cd}_{(1-x)}\text{Zn}_x\text{S}$  caused the final shape to be less spherical than just CdS while using  $\text{ZnSe}_{(1-x)}\text{S}_x$  caused the final shape to be more spherical than using just ZnSe.

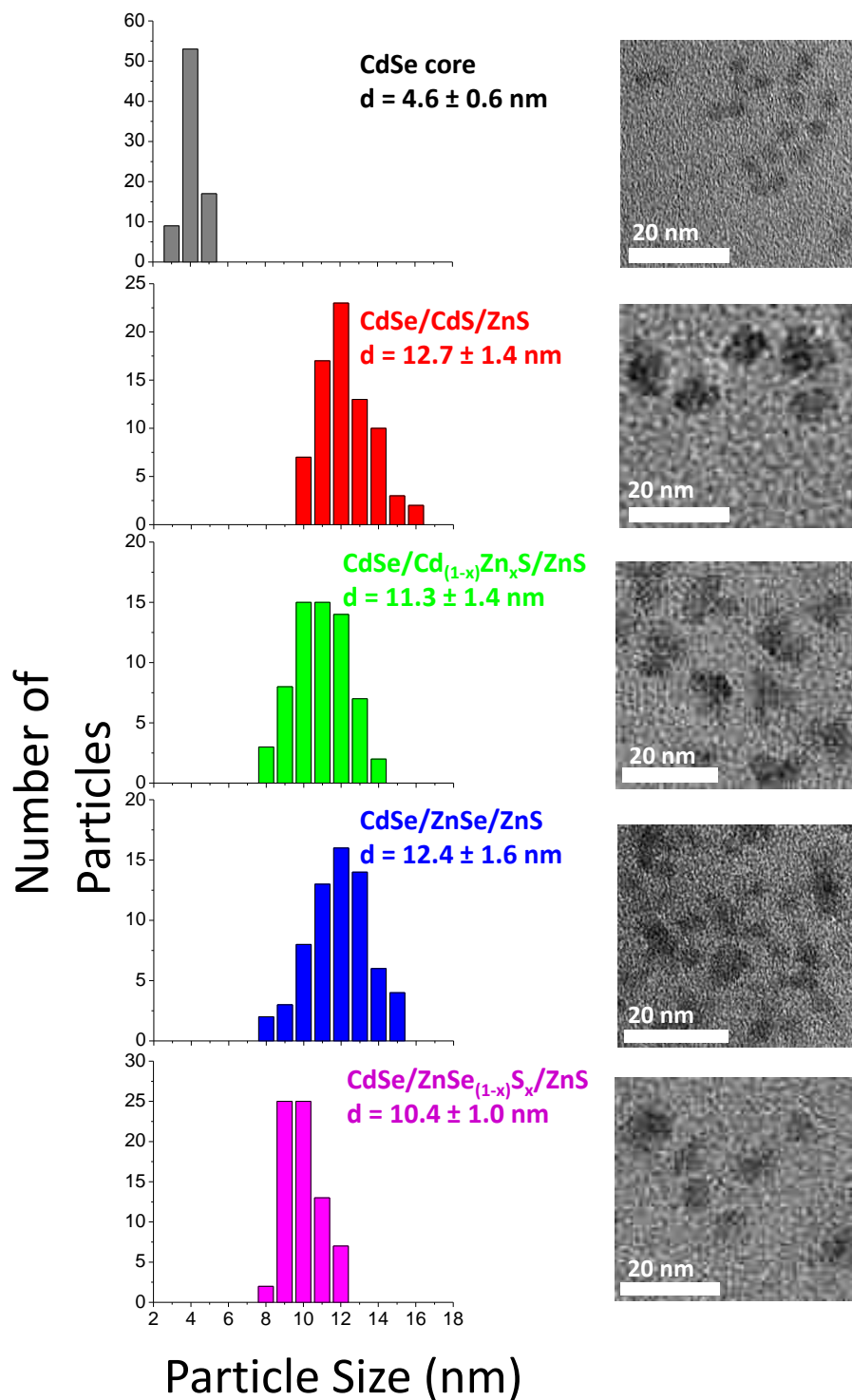


**Figure 2.3:** TEM Images and size distributions of core/multi-shell samples.

This could indicate that Cd and Zn are less amenable to alloying than S and Se, with Zn causing more lattice strain in the inner shell when it replaces Cd than when S replaces Se. This is in agreement with the QY results of figure 2.2, where adding ZnS to  $\text{ZnSe}_{(1-x)}\text{S}_x$  caused the QY to continue increasing, where adding ZnS to  $\text{Cd}_{(1-x)}\text{Zn}_x\text{S}$  caused the QY to decrease.

One potential application for QDs in biological labeling is for single molecule studies, due to their higher brightness and photostability over organic dyes.<sup>[31-33]</sup> However, a major hurdle for such studies is fluorescence blinking. As discussed in the introduction, several reports on suppressing blinking *via* the shell have been published, but none are yet ideal for biological imaging applications. Either they have a CdS outer shell, which leaves toxic Cd exposed to the biological system,<sup>[25, 26]</sup> and/or they are very large.<sup>[25, 27]</sup> Using multishells provides more flexibility over where the lattice strain is placed while reducing potential toxicity by using a ZnS outer shell. In order to investigate the role of where the lattice strain resides in these materials on blinking, we performed single particle fluorescence experiments. Fluorescence traces of single QDs embedded in a PMMA matrix were recorded of each different structure as shown in figure 2.4a and 2.4b, which gave a high signal to noise ratio (>80) with easily distinguishable on and off states. Therefore, we could directly apply a fluorescence threshold to the fluorescence traces to obtain on-time and off-time distributions as shown in figure 2.4c and 2.4d. Figure 2.4e shows how the fraction of time that a QD spends in the on state depends on the shell architecture. Overall, figure 2.4 shows that shelling with multi-shells significantly reduced the blinking of quantum dots, but that the inner shell architecture determines by how much.

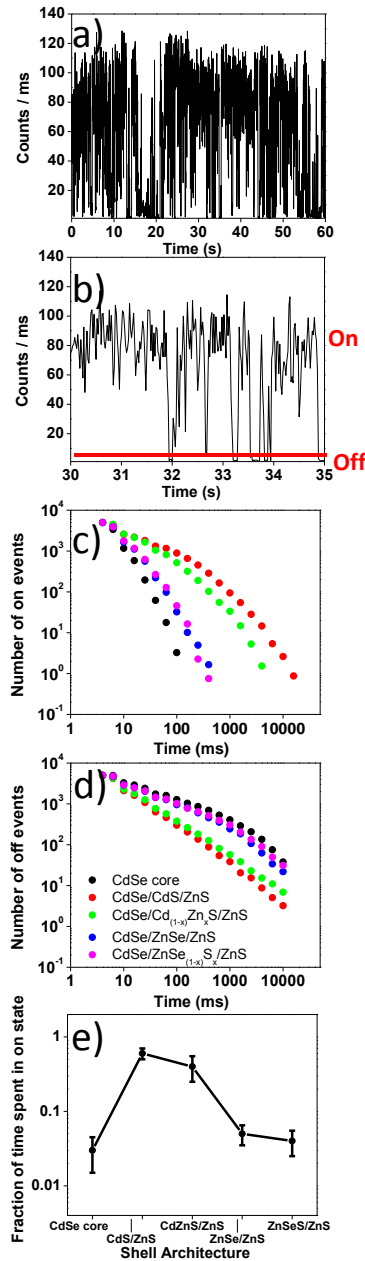


**Figure 2.4:** (a) A 60-second section of a typical fluorescence trace highlighting blinking behavior (b) 5-second section of the trace showing well-resolved on and off events using a threshold. Log-log plots of  $P_{on}$  (c) and  $P_{off}$  (d) distributions for CdSe cores (black) CdSe/CdS/3ZnS (red) and CdSe/5Cd<sub>(1-x)</sub>Zn<sub>x</sub>S/3ZnS (green) and CdSe/5ZnSe/3ZnS (blue) and CdSe/5ZnSe<sub>(1-x)</sub>S<sub>x</sub>/3ZnS (magenta). (e) Fraction of time a QD spends in the on state as a function of the shell architecture (the gradient alloy shells are labeled as CdZnS and ZnSeS rather than Cd<sub>(1-x)</sub>Zn<sub>x</sub>S and ZnSe<sub>(1-x)</sub>S<sub>x</sub> due to space limitations).

As was already mentioned, shelling helps to reduce the surface traps of core QDs but may also introduce new trap states due to induced lattice strain.<sup>[24]</sup> When CdS or Cd<sub>(1-x)</sub>Zn<sub>x</sub>S is used as the inner shell, blinking is reduced significantly more than with ZnSe or ZnSe<sub>(1-x)</sub>S<sub>x</sub>, even though the ensemble quantum yield of CdSe/ZnSe<sub>(1-x)</sub>S<sub>x</sub>/ZnS is by far the highest. In fact, although there is a significant difference in the quantum yield of CdSe/ZnSe<sub>(1-x)</sub>S<sub>x</sub>/ZnS and CdSe/ZnSe/ZnS, their blinking dynamics are similar. This result shows that a high ensemble QY is not necessarily a good indicator for reduced blinking. One reason for this is that the dark fraction plays a significant role in the ensemble QY and the fraction of QDs visible for blinking analysis, as we had previously identified.<sup>[29, 34]</sup> In those studies, we identified a relationship between increased blinking and dark fraction formation. One possibility that may explain this result is that the QDs that blink the most will become part of the dark fraction when using CdS or Cd<sub>(1-x)</sub>Zn<sub>x</sub>S as the inner shell, lowering QY, but allowing the QDs that blink the least to remain so. On the other hand, using ZnSe or ZnSe<sub>(1-x)</sub>S<sub>x</sub> will reduce blinking of all QDs (when compared to the core), but not switch the worse-blinking QDs into the dark fraction. In fact, using this shell may even switch some of the dark fraction back into on-but-blinking QDs, having the effect of increasing ensemble QY. The physical reasons for this behavior at this point would be somewhat speculative, but is likely affected by where the lattice strain is placed in the QD – at the core/shell interface vs the shell/shell interface. The dark fraction is likely only part of the explanation for the lack of correlation between ensemble QY and blinking. Changes in radiative and non-radiative recombination rates directly affect the ensemble QY but may not show up in the blinking statistics. Multiple on states have been observed in some QD reports, with each having a different QY.<sup>[35, 36]</sup> Differences in these states would not show up in the blinking statistics when analyzed using a threshold but will directly affect the ensemble QY. Quantifying the differences in various on states is beyond the scope of this

manuscript, but will be the subject of future studies. One other possible source for the lack of correlation between ensemble PL QY and blinking is the different environment of the QDs in the two experiments. For PL QY measurements, the QDs are dissolved in organic solvent and blinking is performed in PMMA film. Quantifying the ensemble PL QY of QDs in PMMA film is technically very difficult due to film inhomogeneity, although the PL QY of *single* QDs in such an environment has been previously measured.<sup>[37]</sup> While not an exact comparison, we did compare the ensemble PL QY of QDs in toluene to those in 12% (w/v) PMMA in toluene (we used toluene instead of hexane here due to the higher solubility of PMMA in toluene) and found no difference (results not shown), suggesting that PMMA quenching is not a major problem, although we cannot completely rule it out when QDs are cast in a film. At this point, we would like to note that the TEM images (figure 2.3) show that CdSe/ZnSe/ZnS particles are the least spherical and CdSe/ZnSe<sub>(1-x)</sub>S<sub>x</sub>/ZnS are the most spherical, although they show similar blinking statistics. This indicates that, when there is sufficient lattice strain at the core/inner-shell interface, the overall shape of the QD and the strain at the inner-shell/outer-shell interface play less important roles in blinking.

The majority of QD literature to date has analyzed the blinking dynamics as being power-law distributed in the duration of both the on and off events.<sup>[38-42]</sup> Some extensions have also been added to explain deviations in this behavior such as the exponential cutoff in observing long on times<sup>[24, 43, 44]</sup> and changes in the power-law slope at short time-scales.<sup>[34, 45]</sup> Further deviations from power-law behavior have been reported upon varying the QD local environment, such as changing the immobilization matrix and the proximity of silanol groups leading to exponential terms in the on-times distribution function.<sup>[46, 47]</sup> Recently, a multiple recombination centers model has been proposed<sup>[48]</sup> to describe blinking in which the on times can be fit to a multi-exponential decay



function rather than a (truncated) power law.<sup>[35]</sup> These recent studies have brought into question whether the blinking dynamics are indeed power-law distributed, as was generally thought.

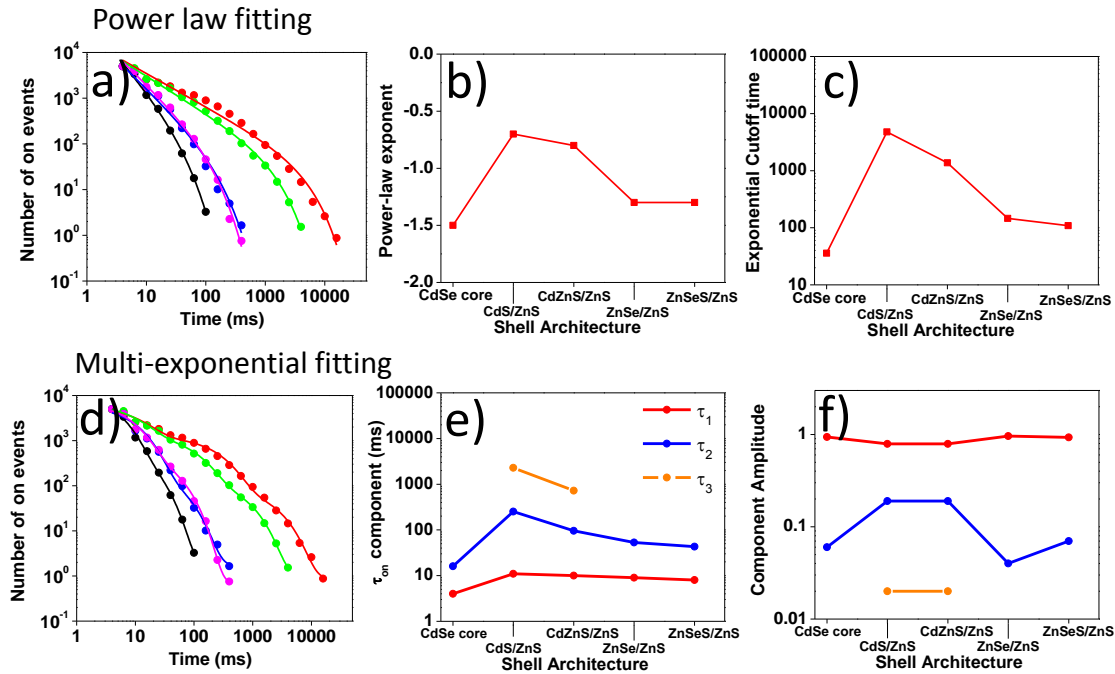


**Figure 2.5:** (a-c) Power law fitting of on-times and extracted parameters plotted as a function of shell architecture. (d-f) Multi-exponential fitting of on-times and extracted parameters plotted as a function of shell architecture. Color scheme is the same as for Figure 4. In (b, c, e, f), the gradient alloy shells are labeled as CdZnS and ZnSeS rather than Cd<sub>(1-x)</sub>Zn<sub>x</sub>S and ZnSe<sub>(1-x)</sub>S<sub>x</sub> due to space limitations.

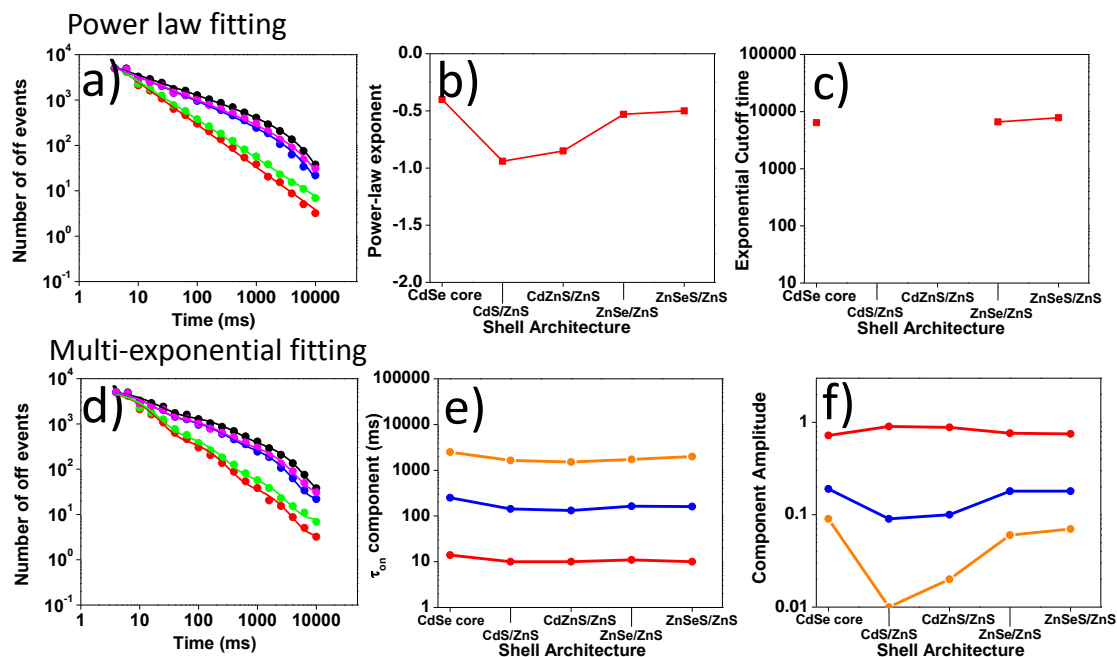


**Figure 2.6:** (a-c) Power law fitting of off-times and extracted parameters plotted as a function of shell architecture. (d-f) Multi-exponential fitting of on-times and extracted parameters plotted as a function of shell architecture. Color scheme is the same as for Figure 4. In (b, c, e, f), the gradient alloy shells are labeled as CdZnS and ZnSeS rather than  $Cd_{(1-x)}Zn_xS$  and  $ZnSe_{(1-x)}S_x$  due to space limitations.

In light of this new debate, we decided to examine our blinking dynamics in more detail to ascertain if the shell architecture affects which model best describes blinking. We fitted our blinking data to each of the two general models (truncated power law vs. multi-exponential) in figure 2.5 for the on-times distributions and in figure 2.6 for the off-times distributions. For the on times, fitting CdSe cores, CdSe/ZnSe/ZnS and CdSe/ZnSe<sub>(1-x)</sub>S<sub>x</sub>/ZnS to the multi-exponential model required only 2 exponentials while CdSe/CdS/ZnS and CdSe/Cd<sub>(1-x)</sub>Zn<sub>x</sub>S/ZnS required 3 exponentials. Fitting the on times to a power law required an exponential cutoff time for all samples. Fitting the distributions of off times to a multi-exponential model required 3 exponentials to reasonably fit the data for all samples. For the power-law fit to off times, CdSe cores and the Zn-based inner shells,

CdSe/ZnSe/ZnS and CdSe/ZnSe<sub>(1-x)</sub>S<sub>x</sub>/ZnS, show an exponential cutoff time. A cutoff time for the off states was proposed from ensemble experiments to exist at much longer timescales than the on states,<sup>[44]</sup> and our data provides additional evidence for this. On the other hand, the Cd-based inner shells, CdSe/CdS/ZnS and CdSe/Cd<sub>(1-x)</sub>Zn<sub>x</sub>S/ZnS, did not require an exponential cutoff time, probably a result of shifting to even longer timescales, outside of our analysis window. Clearly, for either model, the fit parameters are highly dependent on the inner shell architecture.

Schmidt *et al.* recently used a change-point analysis method to resolve the various exponential dwell time components based on their varying on intensity.<sup>[35]</sup> In their case, they uncovered up to 5 exponentials for CdSe/ZnS core/shell particles, with their longest on-state dwell time of ~120 ms. For CdSe cores, CdSe/ZnSe/ZnS and CdSe/ZnSe<sub>(1-x)</sub>S<sub>x</sub>/ZnS, our timescales are in general agreement with Schmidt *et al.*,<sup>[35]</sup> although we do not recover as many exponentials due to using a threshold rather than change-point analysis algorithm. However for CdSe/CdS/ZnS and CdSe/Cd<sub>(1-x)</sub>Zn<sub>x</sub>S/ZnS, the longest component is an order of magnitude longer than the CdSe/ZnS particles of Schmidt *et al.*<sup>[35]</sup> Differences in the QD architecture (core/shell vs core/multi-shell) may be the reason for this variation, but differences in the excitation mode is also a possibility; Schmidt *et al.*<sup>[35]</sup> used a pulsed laser with an average power of 500 nW and a 100× 0.9 NA objective, while our setup used an average power of 10 μW with a 60× 1.2 NA objective.

From visual inspection of the data in figures 2.5 and 2.6, it appears that the multi-exponential model fits some of our on-times data better, although the difference is small, but that both models seem to fit the off-times equally well. Normally, the relative goodness of fit is quantified by calculating a reduced chi-squared value. However, this is difficult due to not knowing the exact uncertainty for each point in the distributions of number of events. The uncertainty in the number of events comes from two sources: incorrectly assigning an on (or off) state due to noise

crossing the on-off threshold and particle-to-particle variations. The first source of uncertainty is likely to be very small due to the high signal:noise ratio separating the on and off events (as shown in figure 2.4) and, even if it did occur, would not lead to a state of longer than just a few bins (i.e.  $< \sim 5$  ms). The second source of uncertainty is more difficult to estimate. We collected long traces from many QDs (at least 30 traces of 300 s each) to reduce the uncertainty as much as we could but there is still likely to be some. We can overcome this problem by using the Pearson chi-squared test in which we do not need to know the variance in the experimental value, but assume that the model (fit) value is the exact value and calculate the deviation of the experimental value from it. This data is reported in table 1 as a ratio, calculated as  $\chi^2_{\text{multi-exp}}/\chi^2_{\text{power-law}}$ . If this ratio is greater than 1 it suggests that power-law is a better fit, if it is less than 1 then a multi-exponential fit is better and, if it is close to 1 the two models cannot be easily distinguished. From the data in table 1, the ratio for the on times are consistently less than 1, although the cores are only slightly below 1. For the off times, the ratios are more variable, but are generally either above 1 or closer to 1 than are the on times. While this data is not conclusive, it does suggest that the on times might fit better to the multi-exponential model, while the off times are much more difficult to assign to a model.

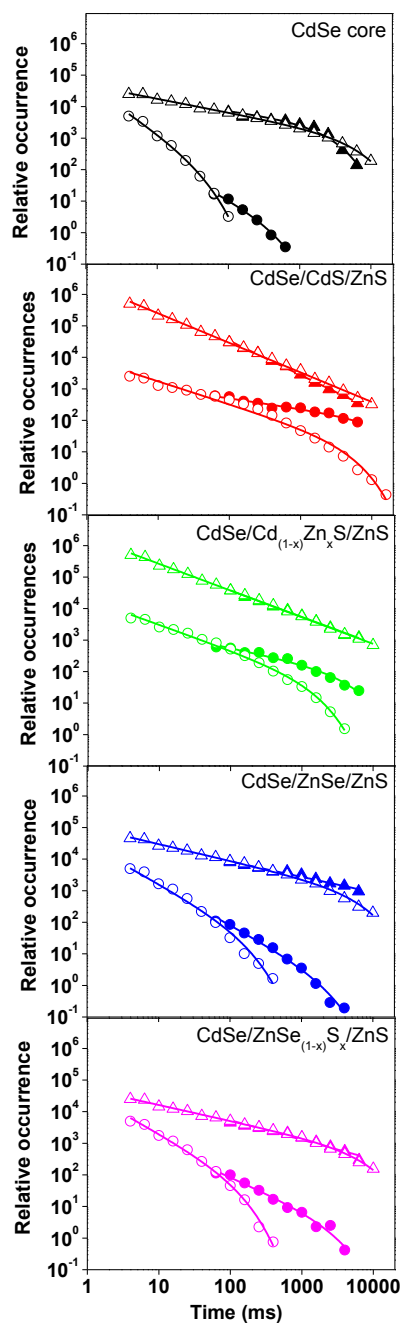


**Figure 2.7:** Overlay of on-times distributions (circles) and off-times distributions (triangles) from 1-ms binned data (open symbols) and 20-ms binned data (filled symbols) for each shell architecture. On and off data are offset relative to each other on the y-axis for visualization, so the y-axis has been relabeled as relative occurrence to reflect this fact.

Another way of distinguishing between the two mathematical models is to re-bin the blinking data at 20 ms resolution rather than 1 ms resolution. If the data are power-law distributed, the power law exponent and cutoff time (which are all longer than 20 ms) should not vary upon re-binning. If the data are indeed multi-exponential, one would expect re-binning to change the recovered fit parameters, since at least one of the exponential lifetimes is on this 1-20 ms timescale. Figure 2.7 shows the effect of re-binning the data for both on-times and off-times. The off times are generally unaffected by the re-binning whereas the on-times are significantly affected. One must be careful with this type of analysis, however, as was discussed by Crouch *et al.*<sup>[49]</sup> It is necessary that a large enough number of events are analyzed (at least 3000) and that there is a good separation of on and off intensities to avoid artefacts in the data analysis. In our data, we analyzed between 50,000 and 200,000 events for each sample (except for the cores, which had 10,000 - 30,000 events, still well in excess of the minimum criteria needed, as discussed by Crouch *et al.*). Most of our traces also showed excellent separation of on and off intensities, as highlighted in figure 2.4, with average on intensities higher and lower dark (off) noise than those in Crouch *et al.*<sup>[49]</sup>. While we cannot completely exclude the possibility, we feel that the data in figure 2.7 adequately avoids the pitfalls discussed by Crouch *et al.*<sup>[49]</sup> Figure 2.7 thus indicates that re-binning at 20 ms causes very short off events to be missed, leading to a shift to longer on-times. This is not true for short on events. In other words, if the particle is on, it is possible for the particle to quickly turn off and back on again whereas if the particle is off, the recovery on the on state is more long-lived (at least longer than 20 ms). This observation indicates that the mechanisms underlying switching on and switching off behaviors are different in origin. The change in behavior upon re-binning, taken together with the goodness of fit data from table 2.1, supports the conclusion that the off-times are best fit to a power law distribution while the on-times are best fit to a multi-exponential model that underlies a

multiple recombination centers explanation for blinking. In this case, the recovered exponentials will depend on the binning time, and this must be taken into account when comparing different blinking reports. Importantly, our data further suggests that switching from the high-to-low quantum yield recombination centers (that determines the on-time distributions) is influenced strongly by lattice strain at the core/shell interface, but that moving the lattice strain to the shell/shell interface in core/multi-shell quantum dots reduces the high-to-low switching probability. Switching from the low-to-high quantum yield recombination centers (that determines the off-time distributions) is also affected by the shell architecture, but to a lesser extent, and is likely to be influenced by random processes that underlie a power-law distribution. The exact mechanism(s) of these processes is still unclear but could be related to random static and/or dynamic heterogeneity in the environment of the quantum dot such as ligand dynamics, surface reorganization or fluctuations in the external, local environment. A recent report used a variable pulse rate approach to show that surface trap states can vary with light flux, which they postulated to be related to photoinduced ligand reorganization.<sup>[50]</sup> A subsequent paper used the slightly different approach of vary the number of pulses at a fixed repetition rate.<sup>[51]</sup> Together these studies showed that both fast and slow decay processes are affected via multiphoton absorption on varying timescales. Our continuous wave excitation at 10  $\mu$ W power can certainly lead to multiphoton processes, especially when long-lived trap states are involved to produce trion states that may be affected by both the interfacial trap states and the surface ligands. In this case, it is likely that trapping of the charge carrier to one of these surface traps depends on the number of traps at the core/shell interface and, to a lesser extent, at the shell/shell interface. Then, ligand re-reorganization back to an emitting state could be a more random process (i.e. resulting in power law behavior) that is not light-induced. This could allow for the ability for both slow recovery and fast recovery. The fast recovery processes leads to very short

off times being missed by binning at 20 ms rather than 1 ms, which, in turn, pushes the on-times distribution towards longer times (as figure 5.7 shows). More work on systematically changing the environment is needed to thoroughly evaluate this mechanism but, in any case, our results show that both of these processes – trapping and recovery – are affected by the inner shell architecture.

	CdSe	CdSe/CdS	CdSe/CdZnS	CdSe/ZnSe	CdSe/ZnSeS/ ZnS
On times $\chi^2$ ratio	0.8863	0.6111	0.1603	0.1080	0.1205
Off-times $\chi^2$ ratio	1.1629	0.8229	2.5919	0.3206	0.8857

**Table 2.1:** Relative goodness of fit tests to power law and multi-exponential models for the data in figure 5 (on times) and figure 6 (off times). Data are reported as  $\chi^2$  ratios (multi-exponential/power-law) using the Pearson  $\chi^2$  test. A ratio less than 1 indicates that the multi-exponential model is a better fit and a ratio greater than 1 indicates that a power-law model is a better fit.

## 2.6. Summary and Conclusions

We systematically synthesized a range of multi-shell QDs containing CdSe cores, ZnS outer shells with various inner shells to determine the role of the inner shell architecture on the QY and blinking properties. For the inner shell, we used CdS, ZnSe and the gradient alloys  $\text{Cd}_{(1-x)}\text{Zn}_x\text{S}$  and  $\text{ZnSe}_{(1-x)}\text{S}_x$  where x changes by 0.2 per monolayer to slowly change the inner shell composition to ZnS. We



found that the QY depends strongly on the inner shell thickness and composition. Upon adding ZnS, the maximum QY of ~80% is reached when a gradient-alloy of  $\text{ZnSe}_{(1-x)}\text{S}_x$  is used as the inner shell. For all other inner shell architectures, adding ZnS reduces the QY. On the other hand, blinking is reduced more when CdS is used and using a gradient-alloy does not improve blinking over using just the single-component inner shell. This result highlights that a high QY is not necessarily a good indicator for reduced blinking. The connection between blinking and the dark fraction formation<sup>[29, 34]</sup> is one likely candidate for this lack of correlation between QY and blinking, and the inner shell architecture could play a role in whether the worse blinking QDs are turned off or not. Another possibility is that the inner shell architecture could lead to variations in radiative and non-radiative rates of the on state(s). Future work will further investigate the contributions from these possibilities.

We analyzed the blinking statistics according to 2 mathematical models: the more common truncated power-law and the more recent multi-exponential model. By comparing the fit qualities as well as how the blinking data changes with binning at 1ms vs. 20 ms, we proposed that the off-times are best described by the power law model while the on-times can be best described by the multi-exponential model. The key result from this work is that both are affected by the inner shell architecture.

## **2.7. Acknowledgements**

Generous financial support by the NSF (CHE-1255440), the NIH (COBRE P30 GM103450), and the Arkansas Biosciences Institute is gratefully acknowledged. TEM instrumentation access is

provided by the Arkansas Materials Characterization Facility (Funded in part by the NSF) and the Institute of Nanoscience and Engineering at the University of Arkansas.

## 2.8. References

- [1] M. A. Hines, P. Guyot-Sionnest *J. Phys. Chem.* **1996**, 100, 468-471.
- [2] B. O. Dabbousi, J. Rodriguez-Viejo, F. V. Mikulec, J. R. Heine, H. Mattoussi, R. Ober, K. F. Jensen, M. G. Bawendi *J. Phys. Chem. B.* **1997**, 101, 9463-9475.
- [3] J. J. Li, Y. A. Wang, W. Guo, J. C. Keay, T. D. Mishima, M. B. Johnson, X. Peng *J. Am. Chem. Soc.* **2003**, 125, 12567-12575.
- [4] P. Anikeeva, J. Halpert, M. Bawendi, V. Bulovic *Nano Lett.* **2009**, 9, 2532-2536.
- [5] P. V. Kamat *J. Phys. Chem. C.* **2008**, 112, 18737-18753.
- [6] V. I. Klimov, A. A. Mikhailovsky, S. Xu, A. Malko, J. A. Hollingsworth, C. A. Leatherdale, H. Eisler, M. G. Bawendi *Science.* **2000**, 290, 314-317.
- [7] A. Shamirian, A. Ghai, P. Snee *Sensors.* **2015**, 15, 13028-13051.
- [8] C. Wang, J. Zhao, Y. Wang, N. Lou, Q. Ma, X. Su *Sens. Act. B: Chem. Sens. Mater.* **2009**, B139, 476-482.
- [9] L.-X. Qin, W. Ma, D.-W. Li, Y. Li, X. Chen, H.-B. Kraatz, T. D. James, Y.-T. Long *Chem. Eur. J.* **2011**, 17, 5262-5271.
- [10] M. Bruchez, M. Moronne, P. Gin, S. Weiss, A. P. Alivisatos *Science.* **1998**, 281, 2013-2016.
- [11] W. C. Chan, S. Nie *Science.* **1998**, 281, 2016-2018.
- [12] A. P. Alivisatos *Nat. Biotechnol.* **2004**, 22, 47-52.
- [13] X. Michalet, F. Pinaud, L. Bentolila, J. Tsay, S. Doose, J. Li, G. Sundaresan, A. Wu, S. Gambhir, S. Weiss *Science.* **2005**, 307, 538-544.
- [14] G. Mandal, M. Darragh, Y. A. Wang, C. D. Heyes *Chem. Commun.* **2013**, 49, 624-626.
- [15] D. V. Talapin, I. Mekis, S. Götzinger, A. Kornowski, O. Benson, H. Weller *J. Phys. Chem. B.* **2004**, 108, 18826-18831.
- [16] X. Peng, M. C. Schlamp, A. V. Kadavanich, A. P. Alivisatos *J. Am. Chem. Soc.* **1997**, 119, 7019-7029.
- [17] P. Reiss, J. Bleuse, A. Pron *Nano Lett.* **2001**, 2, 781-784.

- [18] R. Xie, U. Kolb, J. Li, T. Basche, A. Mews *J. Am. Chem. Soc.* **2005**, 127, 7480-7488.
- [19] F. Cichos, C. von Borczyskowski, M. Orrit *Curr. Opin. Coll. Int. Sci.* **2010**, 12, 272-284.
- [20] T. Ha, A. Y. Ting, J. Liang, D. S. Chemla, P. G. Schultz, S. Weiss, A. A. Deniz *Chem. Phys.* **1999**, 247, 107-118.
- [21] R. M. Dickson, A. B. Cubitt, R. Y. Tsien, W. E. Moerner *Nature*. **1997**, 388, 3558-3358.
- [22] A. Schenk, S. Ivanchenko, C. Rocker, J. Wiedenmann, G. U. Nienhaus *Biophys. J.* **2004**, 86, 384-394.
- [23] M. Nirmal, B. O. Dabbousi, M. G. Bawendi, J. J. Maklin, J. K. Trautman, T. D. Harris, L. E. Brus *Nature*. **1996**, 383, 802-804.
- [24] C. D. Heyes, A. Y. Kobitski, V. V. Breus, G. U. Nienhaus *Phys. Rev. B.* **2007**, 75, 125431.
- [25] B. Mahler, P. Spinicelli, S. Buil, X. Quelin, J. P. Hermier, B. Dubertret *Nature Materials*. **2008**, 7, 659-664.
- [26] O. Chen, J. Zhao, V. P. Chauhan, J. Cui, C. Wong, D. K. Harris, H. Wei, H.-S. Han, D. Fukumura, R. K. Jain, M. G. Bawendi *Nat. Mater.* **2013**, 12, 445-451.
- [27] Y. Chen, J. Vela, H. Htoon, J. L. Casson, D. J. Werder, D. A. Bussian, V. I. Klimov, J. A. Hollingsworth *J. Am. Chem. Soc.* **2008**, 130, 5026-5027.
- [28] Z. A. Peng, X. Peng *J. Am. Chem. Soc.* **2001**, 123, 183-184.
- [29] N. Durisic, A. G. Godin, P. Grutter, P. W. Wiseman, C. D. Heyes *ACS Nano*. **2011**, 5, 9062-9073.
- [30] A. Saha, K. Chellappan, K. Narayan, J. Ghatak, R. Datta, R. Viswanatha *J. Phys. Chem. Lett.* **2013**, 4, 3544-3549.
- [31] M. Dahan, S. Lévi, C. Luccardini, P. Rostaing, B. Riveau, A. Triller *Science*. **2003**, 302, 442-445.
- [32] J. C. Chang, S. J. Rosenthal *Meth. Mol. Biol.* **2011**, 726, 51-62.
- [33] Q. Zhang, Y. Li, R. W. Tsien *Science*. **2009**, 323, 1448-1453.
- [34] N. Durisic, P. W. Wiseman, P. Grutter, C. D. Heyes *ACS Nano*. **2009**, 3, 1167-1175.

- [35] R. Schmidt, C. Krasselt, C. Gohler, C. von Borczyskowski *ACS Nano*. **2014**, 8, 3506-3521.
- [36] K. Zhang, H. Chang, A. Fu, A. P. Alivisatos, H. Yang *Nano Lett.* **2006**, 6, 843-847.
- [37] X. Brokmann, L. Coolen, M. Dahan, J. P. Hermier *Phys. Rev. Lett.* **2004**, 93.
- [38] A. L. Efros, M. Rosen *Physical Review Letters*. **1997**, 78, 1110-1113.
- [39] M. Kuno, D. P. Fromm, S. T. Johnson, A. Gallagher, D. J. Nesbitt *Phys. Rev. B*. **2003**, 67, 125304.
- [40] P. A. Frantsuzov, R. A. Marcus *Phys. Rev. B*. **2005**, 72, 155321.
- [41] J. Tang, R. A. Marcus *Phys. Rev. Lett.* **2005**, 95, 107401.
- [42] P. Frantsuzov, M. Kuno, B. Janko, R. A. Marcus *Nat. Phys.* **2008**, 4, 519-522.
- [43] K. T. Shimizu, R. G. Neuhauser, C. A. Leatherdale, S. A. Emedocles, W. K. Woo, M. G. Bawendi *Phys. Rev. B*. **2001**, 63, 205316.
- [44] I. Chung, M. G. Bawendi *Phys. Rev. B*. **2004**, 70, 165304.
- [45] M. Pelton, G. Smith, N. F. Scherer, R. A. Marcus *Proc. Natl. Acad. Sci. U.S.A.* **2007**, 104, 14249-14254.
- [46] R. Schmidt, C. Krasselt, C. von Borczyskowski *Chem. Phys.* **2012**, 406, 9-14.
- [47] C. Krasselt, J. Schuster, C. von Borczyskowski *Phys. Chem. Chem. Phys.* **2011**, 13, 17084-17092.
- [48] P. A. Frantsuzov, S. Volkan-Kacso, B. Janko *Phys. Rev. Lett.* **2009**, 103, 207402.
- [49] C. H. Crouch, O. Sauter, X. Wu, R. Purcell, C. Querner, M. Drndic, M. Pelton *Nano Lett.* **2010**, 10, 1692-1698.
- [50] M. Saba, M. Aresti, F. Quochi, M. Marceddu, M. Loi, J. Huang, D. Talapin, A. Mura, G. Bongiovanni *ACS Nano*. **2013**, 7, 229-238.
- [51] G. Singh, M. Guericke, Q. Song, M. Jones *J. Phys. Chem. C*. **2014**, 118, 14692-14702.

## **Chapter 3. Radiative and Non-Radiative Decay Dynamics in Core-Multishell Quantum Dots: Role of Inner Shell Architecture**

*Pooja Bajwa, Anh Nguyen, Feng Gao and Colin D. Heyes*

*Department of Chemistry and Biochemistry, University of Arkansas, 345 N. Campus Drive,  
Fayetteville, AR 72701*

### **3.1. Abstract**

Core-Multishell quantum dots (QDs) are becoming a popular alternative to simple core/shell QDs since it allows for more control over the competing effects of exciton wavefunction confinement and interfacial lattice strain. However, introducing a second (*i.e.* shell/shell) interface complicates prediction of the final optical properties of the QD due to a lack of systematic, quantitative studies on such systems. Here, we report on the influence of the interfacial lattice strain on the structural and optical properties of CdSe/XX/ZnS core-multishell QDs in which we varied the thickness and composition of XX to be CdS, ZnSe, Cd<sub>(1-x)</sub>Zn<sub>x</sub>S or ZnSe<sub>(1-x)</sub>S<sub>x</sub>, where x increased from 0 to 1 by 0.2 increments in each sequential monolayer. We studied how these shell composition and thickness variations affects the steady-state and time-resolved photoluminescence (PL) properties, which is used to determine the effect of the interfaces on the radiative and non-radiative exciton decay pathways.

### 3.2. Introduction:

Colloidal semiconductor nanocrystals, usually referred to as quantum dots (QDs) have attained a great deal of attention over recent decades due to their uniquely size-tunable optical and electronic properties.<sup>1</sup> CdSe-based semiconductor materials are the most widely studied QDs and used for photoluminescence-based applications, particularly for labelling of biomolecules<sup>2</sup> or in chemical/biochemical sensing assays.<sup>3</sup> However, to achieve their full potential in light emitting applications, it is advantageous to coat these semiconductor nanocrystals by adding a wider band-gap inorganic material onto the core, forming a core/shell structure. This shell layer performs a number of functions. First, it helps improve their luminescence quantum yield (QY) by reducing non-radiative decay through confining the excitons to the nanocrystal core and away from the surface.<sup>1, 4, 5</sup> Second, it helps to stabilize the QDs against photobleaching or other adverse environmental effects on their emission properties.<sup>1, 6, 7</sup> Third, and perhaps most importantly for biolabelling and environmental sensing applications, it provides a chemically-stable barrier to the dissolution of the toxic Cd material.<sup>8, 9</sup> The first developed and most extensively used shell for CdSe cores is ZnS due to this material fulfilling most of these requirements.<sup>1</sup>

Unfortunately, there have been a number of reports<sup>6</sup> on the limitations of using ZnS due to the large lattice mismatch (12%) between the CdSe and ZnS crystal lattices. The lattice constants for ZnS are  $a = 3.81 \text{ \AA}$ ,  $c = 6.26 \text{ \AA}$  for ZnS compared to  $a = 4.30 \text{ \AA}$  and  $c = 7.01 \text{ \AA}$  for CdSe. If the shell is made too thick, this leads to deformation of CdSe/ZnS QDs shape<sup>10</sup>, in addition to reducing their PL QY by lattice strain creating interfacial defects.<sup>1, 7, 11, 12</sup> CdS and ZnSe shell materials are also popular alternatives for capping CdSe because of their lower lattice mismatch values,  $\sim 4\%$  for CdS and  $\sim 7\%$  for ZnSe. However, CdS and ZnSe are not as effective in confining the excitons to the core as ZnS due to the lower band-gap offsets,<sup>13, 14</sup> allowing the wavefunction to leak into the

shell and thereby mitigating some of the advantages of the shell in improving the optical properties. Furthermore, CdS is not a good material to have exposed in biological/environmental applications due to the toxicity of Cd, and ZnSe is less chemically stable than ZnS, since Se has a lower oxidation potential than S.<sup>15, 16</sup>

In order to engineer the QDs with a uniform shell of spherical shape, high PL quantum yield, and high chemical stability with a non-toxic outer shell, a balance between all these competing properties must be found. Ideally, it is also preferable to maintain as small a total QD size as possible. Such a balance has been made possible by sandwiching either CdS or ZnSe in between the CdSe core and a ZnS outer shell.<sup>4, 16-21</sup> By doing so, the CdS or ZnSe inner shell reduces the interfacial strain at the core/shell interface and thus, the number of interfacial trap states, while the outer ZnS confines the exciton away from the surface trap states and provides a non-toxic material exposed to the environment. The use of such multishells introduces new interfaces, with different degrees of lattice strain between them, depending upon the materials used and their thickness. However, it is not clear which of the interfacial lattice strains (core/inner shell vs inner shell/outer shell) is the major contributor to the properties, making predicting the final shape and PL properties of the target QD difficult. Further control can be gained by gradient-alloying the inner shell to provide a smoother transition in lattice strain between the materials, although at the expense of the wavefunction confinement.<sup>22</sup> Again, determining the relative importance of these factors requires systematic study.

We recently published<sup>22</sup> that the choice of inner shell material significantly influences the PL QY and blinking of the QDs. Here, we extend the study to determine the role of the inner shell architecture (material and thickness) in determining the radiative and non-radiative decay dynamics of the exciton by using time-resolved fluorescence spectroscopy. We first synthesized a high-quality



CdSe core (QY = 30-50%) and then added inner shells of varying thickness and material before adding an outer shell of ZnS. For all combinations, the total number of shells added was 8 monolayers (ML) to enable meaningful comparisons to be made. Specifically, we synthesized CdSe/3MLXX/5MLZnS and CdSe/5MLXX/3MLZnS, where XX was CdS, ZnSe or their gradient-alloyed analogues ( $\text{Cd}_{(1-x)}\text{Zn}_x\text{S}$  and  $\text{ZnSe}_{(1-x)}\text{S}_x$ , with x increasing by 0.2 per ML, so only the CdSe/5MLXX/3MLZnS versions of these were made). We found that the quantum yield and fluorescence lifetime decay components depend strongly on both the inner shell material and the relative thickness of each shell in complex, but reproducible, ways.

### **3.3. Materials and Methods:**

**3.3.1. Chemicals:** Cadmium oxide (CdO, 90%, Sigma-Aldrich), selenium powder (Se, 99.99%, Alfa Aesar), zinc oxide (ZnO, 99%, Sigma-Aldrich), sulfur powder (S, 99.9%, Alfa Aesar), oleic acid (OA, tech. grade, Alfa Aesar), 1-octadecene (ODE, 90%, Alfa Aesar), octadecylamine (ODA, 95%, Acros Organics), tri-butylphosphine (TBP, 95%, Alfa Aesar), Sulforhodamine 101 dye (S 101 dye Invitrogen), poly(methyl methacrylate) (PMMA, Sigma Aldrich) and tri-octylphosphine oxide (TOPO, Sigma-Aldrich) were used as prepared without further purification. Solvents: All solvents were purchased from VWR international. Methanol, hexane and acetone were of pure grade. Toluene was of high purity HPLC grade.

**3.3.2. CdSe Core Synthesis:** CdSe core samples were synthesized by modification of the literature methods, as explained in our already published work.<sup>22</sup>

**3.3.3. Core/shell/shell synthesis:** The shelling of CdSe core was accomplished by applying successive ion layer absorption and reaction (SILAR) with thermal cycling (TC), with a few modifications, as was already discussed in our earlier work.<sup>22</sup> In addition to those QDs, here we

varied the inner shell with either 5 ML or 3 ML injections for either CdS or ZnSe shell while the last 3 or 5 ML injections were for the ZnS shell.

**3.3.4. Core/gradient-alloyed shell/shell synthesis:** The growth of 5 ML of alloyed  $\text{Cd}_{(1-x)}\text{Zn}_x\text{S}$  or  $\text{ZnSe}_{(1-x)}\text{S}_x$ , was carried out by varying the ratio of  $x$  from 0 to 1 in increments of 0.2 per ML. The synthesis protocol is as in our already published work.<sup>22</sup>

The reproducibility of the all structural and optical properties was confirmed by performing all the sample syntheses twice.

**3.3.5. Fluorescence and Absorption Spectroscopy:** Photoluminescence (PL) and absorbance of the aliquots for different monolayers were measured with a Perkin Elmer LS 55 luminescence spectrometer and Hitachi U-3900H spectrophotometer, respectively. PL percentage quantum yields (PL QYs) were measured by comparing the integrated areas of each ML PL spectra to that of S 101 dye dissolved in ethanol to the same optical density of 0.05 at the excitation wavelength of 530 nm.

**3.3.6. Fluorescence Microscopy:** Fluorescence lifetimes measurements were measured using a MicroTime 200 scanning confocal fluorescence microscope (PicoQuant GmbH, Berlin, Germany), which is based on Olympus IX71 equipped with PicoHarp 300 TCSPC controller, was used.<sup>23-25</sup> It utilizes a 485 nm laser (PDL 485, Picoquant) operating in pulsed wave mode at a power of 0.5  $\mu\text{W}$  and repetition rate of 8 MHz for excitation of QD samples. A dichroic mirror (500dcxr, Chroma, McHenry, IL) sends the light through a water immersion objective (Olympus, Apochromat 60x, NA 1.3) to a diffraction-limited laser focus into a  $\sim 10$  nm solution of QDs. The same objective collects the fluorescence and sends it through the same dichroic mirror and a 100  $\mu\text{m}$  pinhole. To reject background fluorescence and scattered laser light, a fluorescence filter that best matches the emission wavelength of the QDs is placed in front of a single photon avalanche diode detector

(SPAD, MPI, Microphonic devices, Bolano, Italy). Then the collected photons are binned according to their arrival time after the excitation pulse using a time-correlated single photon counting (TCSPC) card into 64ps channels and the fluorescence lifetime decay curves were then analyzed using the freely downloadable program DecayFit (Fluorescence Decay Analysis Software 1.3, FluorTools, [www.fluortools.com](http://www.fluortools.com)) using the instrument response function (IRF) for iterative reconvolution fitting.

**3.3.7. Transmission Electron Microscopy:** Transmission electron microscopy (TEM) and high resolution TEM (HRTEM) were performed using a Tecnai G2 F20-TWIN (TF20, FEI, Hillsboro, OR). To prepare TEM samples, 200  $\mu\text{L}$  of thoroughly washed/purified samples were deposited on a thin film of carbon-coated grids. The QDs diameter was measured using the ImageJ software.

### **3.4. Results and discussion**

The two major parameters that affect the optical properties while engineering core-multishell QDs are lattice mismatches and band-gap energy offsets between the materials. In general, a wider band-gap offset at the interface between the core and innermost shell helps confine the exciton wavefunctions within the core and keeps it away from the surface trap states. On the other hand, a large lattice mismatch is expected to give rise to a larger number of trap states at this interface. Unfortunately, these two parameters usually go hand-in-hand. The schematic of the influence of band-gap offset and lattice mismatch as relevant to the core-multishell QDs used in this work is shown in figure 3.1.

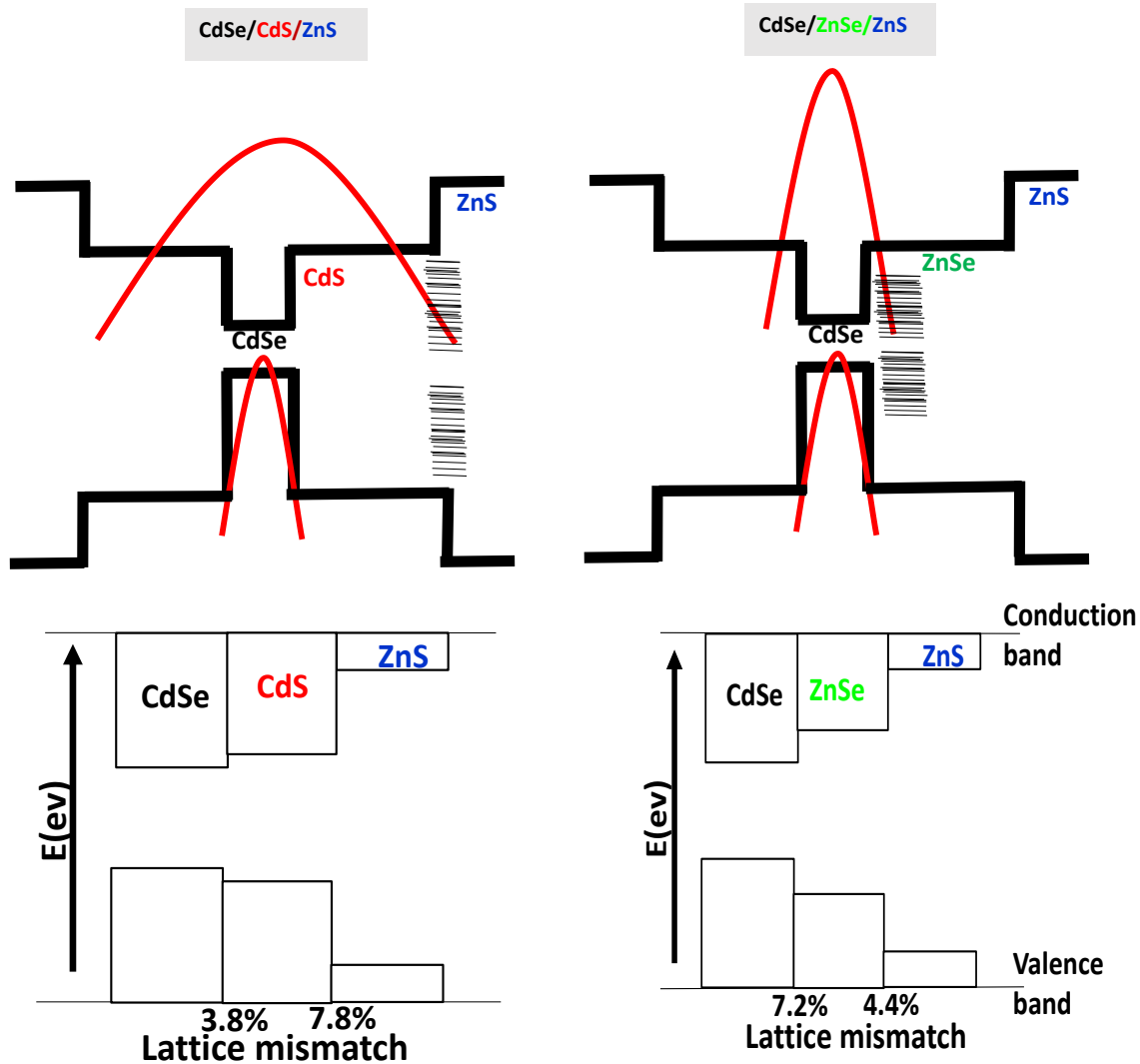


**Figure 3.1:** Schematic of a typical wave function overlap influenced by band gap offset and interfacial trap states (created due to lattice mismatch) of semiconductor materials specific to our work.

We used CdSe as the core material and CdS or ZnSe or their gradient-alloyed analogs as inner shell and ZnS as outer shell material. We also varied the relative thicknesses of the inner shell vs the outer shell, maintaining the same total size. The hypothesis is that, due to the lattice mismatch parameters, ZnSe will result in more traps formed at the core/inner shell interface than the inner shell/outer shell interface, while CdS will result in more traps formed at the inner shell/outer shell

interface than the core/inner shell interface. Thicker shells should result in higher strain and higher strain. For CdS shells, the conduction band (CB) offset is less than the valence band (VB) offset, resulting in less confining of the electron wavefunction compared to the hole wavefunction, while for ZnSe, the CB offsets is larger, resulting in better confining of both electron and hole.<sup>13, 14, 18</sup> Then, adding a ZnS outer shell is expected to result in the formation of more traps at the CdS/ZnS interface than in the ZnSe/ZnS interface.<sup>18</sup>

As expected from the wavefunction confinement effects shown in the schematic in figure 3.1, and in agreement with previous reports.<sup>13, 14</sup> we observed more of a red shift in the photoluminescence peak maximum position, (PL  $\lambda_{\max}$ ) for CdS shelling than ZnSe shelling. (figure 3.2) Using 3 ML CdS shifts the PL  $\lambda_{\max}$  by ~20 nm while using 5 ML CdS shifts the PL  $\lambda_{\max}$  by ~50 nm. If the 5 ML CdS inner shell is gradient-alloyed with ZnS,  $\text{Cd}_{(1-x)}\text{Zn}_x\text{S}$ , the shift is less than using pure CdS, since the more ZnS the shell contains, the higher its band gap and stronger the wavefunction confinement. In all cases, when adding the outer ZnS, much less red shift occurs, attributed to the stronger confinement of exciton due to larger band gap of ZnS. For ZnSe shelling, adding 3 ML ZnSe causes a shift of ~15 nm in the PL  $\lambda_{\max}$ , but adding 2 extra ML of ZnSe does not cause a significant further shift, nor does adding the outer ZnS shell. If the ZnSe is gradient-alloyed with ZnS,  $\text{ZnSe}_{(1-x)}\text{S}_x$ , the shift in PL  $\lambda_{\max}$  is lower, for the same reason as with CdS.

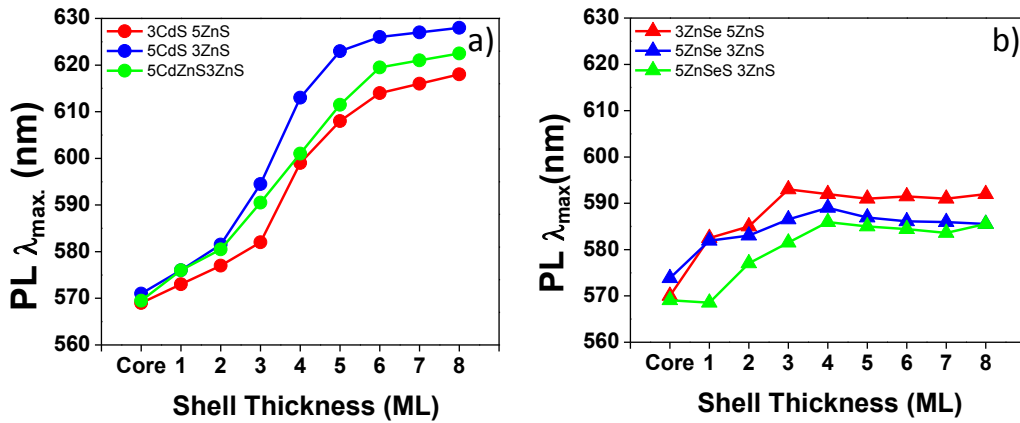


**Figure 3.2:** PL peak maximum of a) QDs with CdS inner shell and b) QDs with ZnSe inner shell as a function of shell composition and thickness.

Peng et al,<sup>26</sup> recommended a high SILAR growth temperature to be the key factor for shell growth of CdS on CdSe, although there have been reports about the effect of SILAR temperature on core-shell interdiffusion<sup>27, 28</sup> or polytypism<sup>29</sup> and alloying due to cation mixing.<sup>30</sup> However, most of the literature discussing the influence of shell-growth temperature on the structural properties of core/shell QDs is for the case of zinc-blende crystals, since zinc-blende structure is less stable at high temperature than wurtzite structure.

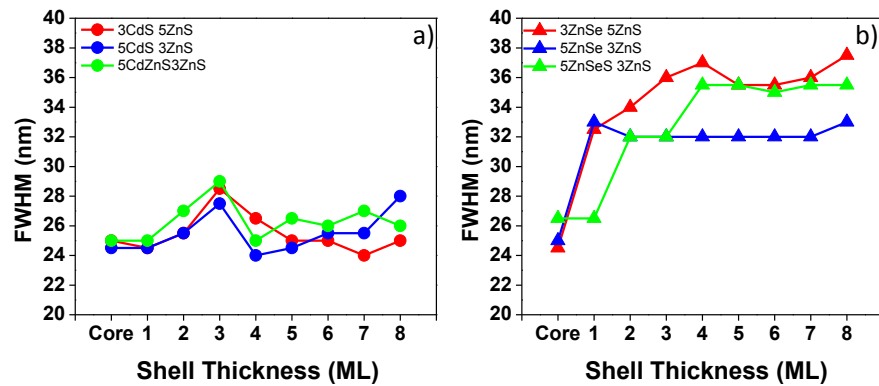


**Figure 3.3:** FWHM (full width at half maximum) of a) QDs with CdS inner shell and b) QDs with ZnSe inner shell as a function of shell composition and thickness.

The narrow range of FWHM (full width at half maximum) of the PL spectra shown in figure 3.3 (a) for QDs shelled with CdS or Cd<sub>(1-x)</sub>Zn<sub>x</sub>S (i.e. 26 ± 2 nm) suggests that all the three sets of core-multishell QDs have uniform shell-size distributions during shelling. On the other hand, the FWHM for QDs shelled with ZnSe or ZnSe<sub>(1-x)</sub>S<sub>x</sub> as in figure 3.3 (b) increases from ~26 nm (for CdSe core) to 34 ± 3 nm, although adding the outer ZnS shell did not increase it further. There are 3 main reasons for the widening of the PL FWHM: (i) trap states (ii) non-uniform shell growth or (iii) the homogeneous line-width increases due to a decrease in the lifetime of the excited state. These three possibilities will be addressed individually below.

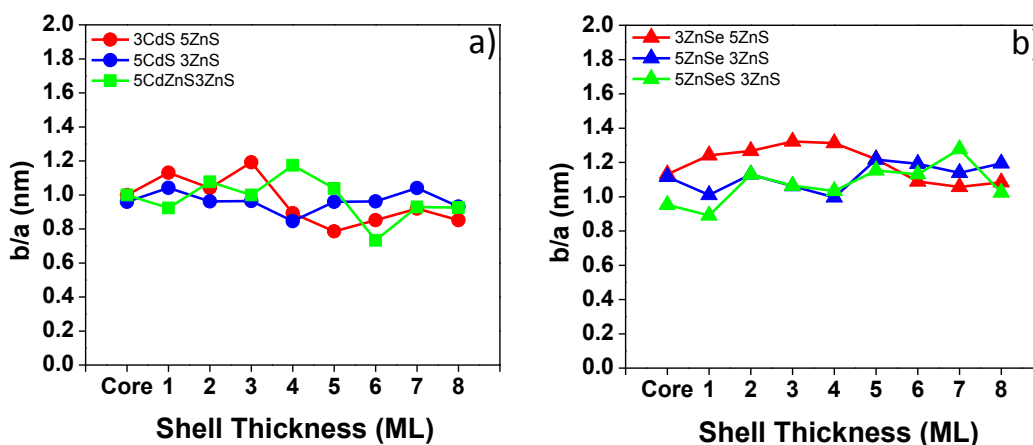


**Figure 3.4:** b/a (red shift vs. blue shift in PL wavelength) of a) QDs with CdS inner shell and b) QDs with ZnSe inner shell.

Figure 3.4 is a measure of the symmetry of the PL spectra. The parameter **a** measures the width from the center of the peak (PL  $\lambda_{\max}$ ) to the wavelength at which the PL intensity is half of the maximum on the blue side (higher energy), while the parameter **b** measures the width from the center of the peak (PL  $\lambda_{\max}$ ) to the wavelength at which the PL intensity is half of the maximum on the red side (lower energy). Thus, b/a measures if there is a higher probability of lower energy emission compared to higher energy emission compared to the PL  $\lambda_{\max}$ . Trap states are lower in

energy than band-edge emission, therefore a b/a ratio over 1 implies trap state emission, while a value of 1 is expected if no trap state emission occurs. For CdS-based shelling (figure 3.4a), b/a fluctuates but is centred around 1. For ZnSe-based shelling (figure 3.4b), b/a fluctuates much less, but is usually slightly higher than 1, suggesting that some trap state emission may be present.

How shelling with each material affects the sizes and shapes of QDs were further confirmed by TEM, as shown in figure 3.5 (for CdS-based shelling) and figure 3.6 (for ZnSe-based shelling).

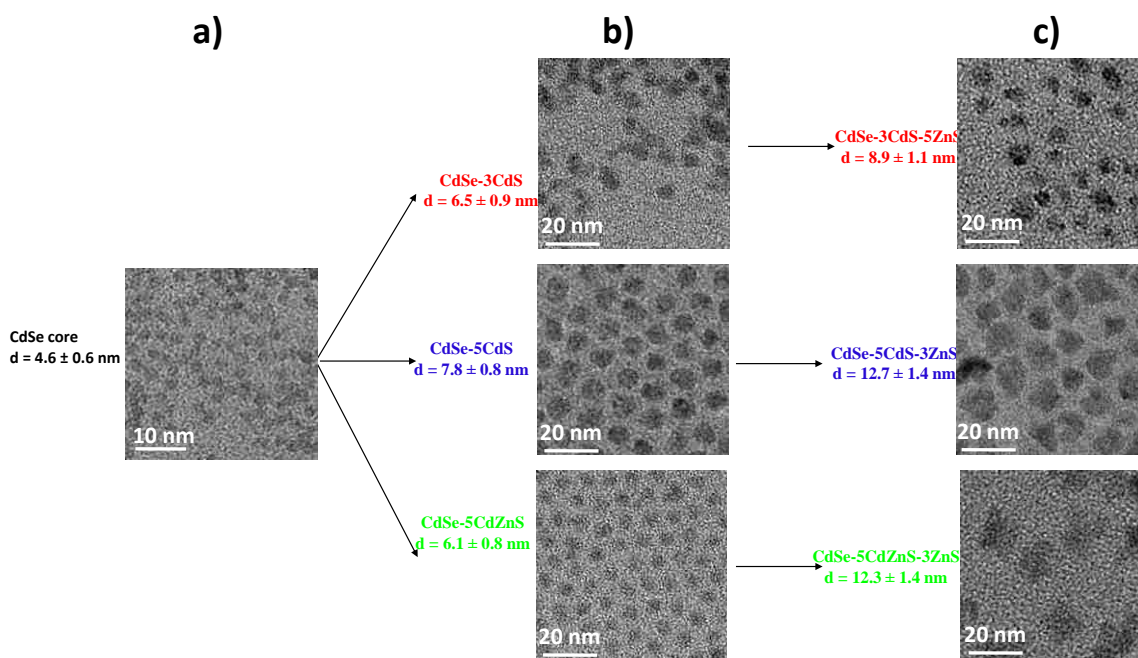


**Figure 3.5:** TEM images of a) core b) core-shell c) core-shell-shell QDs for QDs with CdS inner shell.



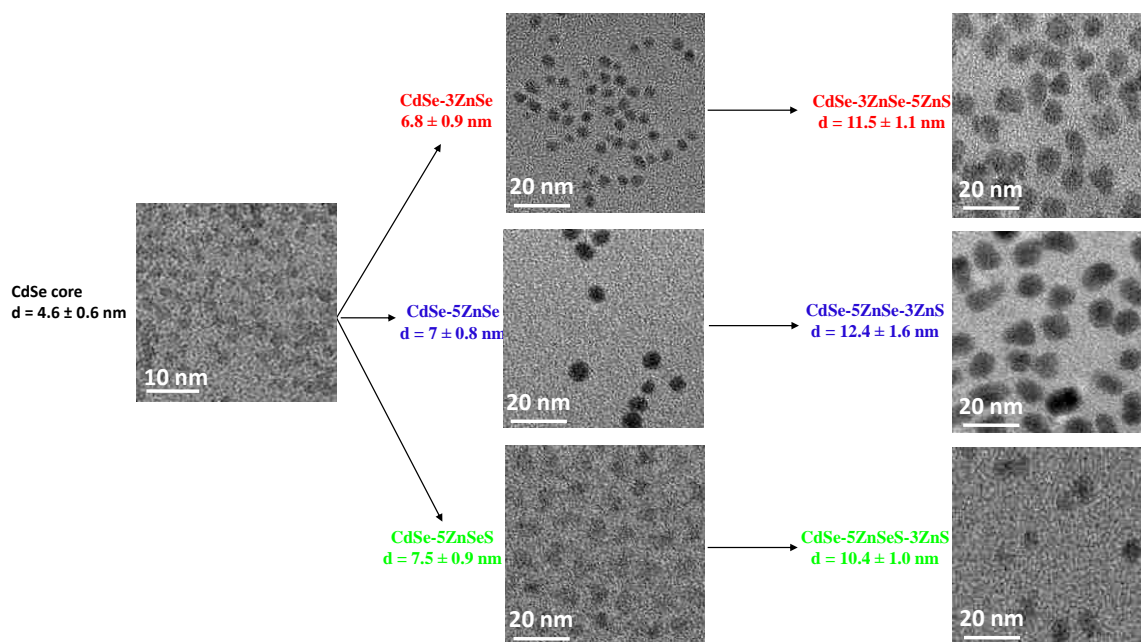


**Figure 3.6:** TEM images of a) core b) core-shell c) core-shell-shell QDs for QDs with ZnSe inner shell.

As shown in both the figures, the shape of QDs are spherical for CdSe core (Fig. 3.5a & 3.6a) and remain spherical in with 3 monolayers of CdS or ZnSe or 5 monolayers of CdS or  $\text{Cd}_{(1-x)}\text{Zn}_x\text{S}$  or ZnSe or  $\text{ZnSe}_{(1-x)}\text{S}_x$  (Fig. 3.5b & 3.6b). This means the higher lattice strain between CdSe and ZnSe-based shells still allows the shell to grow in a uniform manner. Adding the ZnS outer shell (Fig. 3.5c and 3.6c) does result in some non-uniformity in the shapes, although it is still close to being spherical in shape in most cases. CdSe/CdS-based/ZnS (Fig. 3.5c) are generally less spherical and have a higher size distribution than CdSe/ZnSe-based/ZnS (Fig 3.6c), which is likely to be the result of the higher lattice mismatch between CdS and ZnS than ZnSe and ZnS.

Photoluminescence QY trends (figure 3.7a and 3.7b) are quite complex. The lattice strain at the core/shell interface is expected to be more for ZnSe inner shells than with CdS inner shells due to a higher lattice mismatch of 7.2% for the former and smaller lattice mismatch of 3.8% for the latter relative to the CdSe core. However, for the outer shell, the case is reversed. The lattice

mismatch is higher (7.8%) for CdS/ZnS and lower (4.4%) for ZnSe/ZnS. In both cases (non-alloyed or gradient-alloyed) of adding CdS-based shells (figure 3.7a), addition of the 1<sup>st</sup> ML increased the PL QY, although the extent of the increase depended on whether it was alloyed or not. In both cases, there is a reduction in the number of surface traps available to the charge carriers compared to the bare core, but using Cd<sub>(1-x)</sub>Zn<sub>x</sub>S (with x = 0.2 in the first ML) likely results in more lattice strain than pure CdS. For the 2<sup>nd</sup> and 3<sup>rd</sup> MLs, in both cases of CdS-based shelling, the PL QY dropped. Then, with the 4<sup>th</sup> and 5<sup>th</sup> MLs of CdS (blue) or Cd<sub>(1-x)</sub>Zn<sub>x</sub>S (green), PL QY again rose, although the rise is less for the gradient-alloyed shell than the pure shell. If the 4<sup>th</sup> and 5<sup>th</sup> MLs are ZnS (red), the degree of rise in PL QY is less than pure CdS but more than the gradient alloyed Cd<sub>(1-x)</sub>Zn<sub>x</sub>S. Finally, adding 3 MLs of ZnS to 5 ML CdS or Cd<sub>(1-x)</sub>Zn<sub>x</sub>S causes a rapid decrease in PL QY, while adding 1 more ML of ZnS to the 3ML CdS/2ML ZnS increases it further before dropping slightly for the last 2 MLs ZnS. For the ZnSe-based shelling (figure 3.7b), the behavior is very different. For pure ZnSe shells, adding the first 3 MLs first caused an increase in PL QY followed by a decrease, although the degree of change was slightly different each time. Adding the 4<sup>th</sup> ML of ZnSe caused no further change, but adding the 5<sup>th</sup> ML of ZnSe caused a significant increase in PL QY. Adding ZnSe<sub>(1-x)</sub>S<sub>x</sub> instead of pure ZnSe resulted in very little change to the PL QY until the 5<sup>th</sup> ML was added, at which point the increase was quite significant. Clearly 5 ML of ZnSe-based shells is an important thickness to improve the PL QY; presumably at this thickness the competing effects of lattice strain and confinement potential are optimized. Adding a ZnS outer shell to CdSe/5 ML ZnSe or CdSe/ 5 ML ZnSe<sub>(1-x)</sub>S<sub>x</sub> resulted in a slight increase with the 1<sup>st</sup> ML, then a decrease with the next 2 MLs. Adding 3ML ZnS to CdSe/3 ML ZnSe to give CdSe/3ML ZnSe/3ML ZnS core/shell/shell QDs resulted in a significant increase in PL QY to the maximum of all our samples (almost 90%). The next 2 MLs of ZnS then resulted in a decrease to ~60% PL QY.

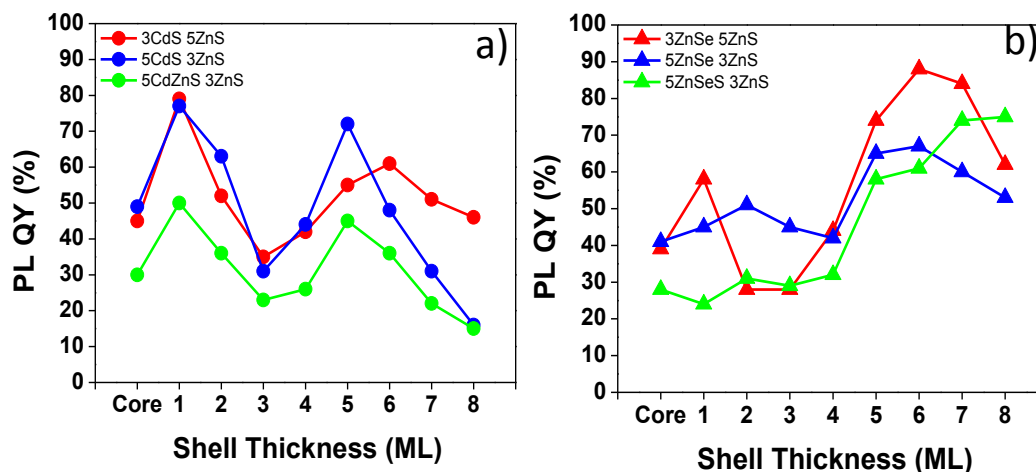


**Figure 3.7:** Photoluminescence quantum yield of a) QDs with CdS inner shell and b) QDs with ZnSe inner shell as a function of shell composition and thickness.

These complex changes in PL QY in each of these samples prompted us to try to quantify the physical chemical principles underlying them. Time-resolved fluorescence spectroscopy allows us to measure the fluorescence lifetime decay of each sample, which can then be fit to multi-exponential functions to extract out the various exciton decay dynamics. We found that a minimum of three exponentials was required to fit the data. Each fitting component for all the shell combinations and architectures were relatively consistent and, more importantly, well separated from each;  $\tau_1 = <1$  ns,  $\tau_2 = \sim 2-4$  ns and  $\tau_3 = \sim 20$  ns. Figure 3.8 (a-b) shows the fitted fluorescence lifetime results, where the fluorescence lifetimes are fit as a function of the shell thickness and architecture. The  $\sim 20$  ns component is due to band gap emission of the quantum dots, and therefore should be the high PL QY component. The  $<1$  ns and  $\sim 2-4$  ns components are likely to be due to quenched fluorescence states (lower PL QY). These quenched states have been proposed to originate from biexciton/surface trap ( $<1$  ns) and trion (2-4 ns) states, respectively,<sup>12, 31-34</sup> that occur due to the various trap states present in the QD.

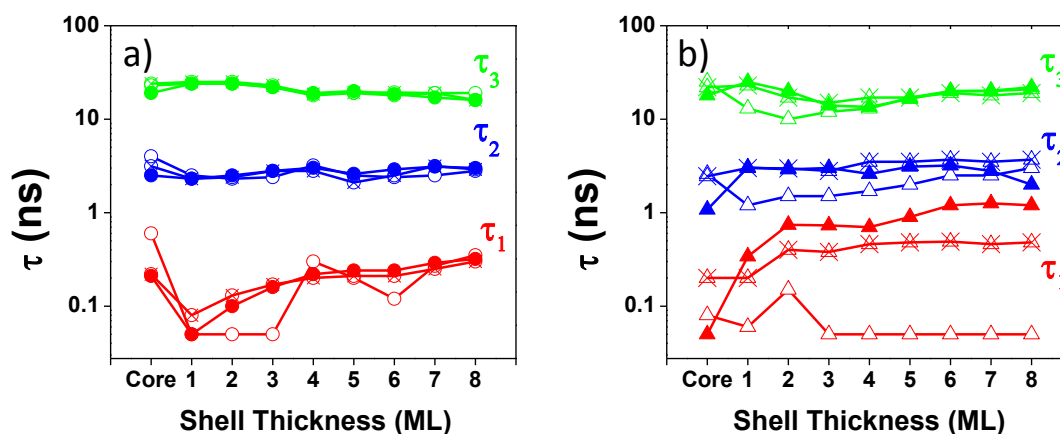


**Figure 3.8:** Fitted fluorescence lifetime components for a) CdS inner shell (empty circles for 3CdS/5ZnS, crossed circles for 5CdS/3ZnS and solid circles for 5CdZnS/3ZnS) QDs b) ZnSe inner shell (empty triangles for 3ZnSe/5ZnS, crossed triangles for 5ZnSe/3ZnS and solid triangles for 5ZnSeS/3ZnS) QDs

For both CdS-based and ZnSe-based inner shell QDs, the fitted lifetime components  $\tau_2$  and  $\tau_3$  remain very consistent on varying shell thickness or architecture, although there was a little more spread in them for ZnSe-based than CdS-based inner shells. However, the  $\tau_1$  component shows more variation with the shell thickness. For CdS-based inner shells, the  $\tau_1$  component drops first with the 1<sup>st</sup> ML. Then, after the 1<sup>st</sup> ML, there is a gradual increase in the  $\tau_1$  component. Small variations exist in the exact  $\tau_1$  values from sample to sample, which might be due to small differences in defects in the original core (although their PL QY for the core was always almost the same) being passivated differently with shelling. Then, from the 3<sup>rd</sup> or 4<sup>th</sup> ML onwards, the  $\tau_1$  component increases only very slightly for both additional CdS shells or adding ZnS outer shells. For ZnSe-based shelling, all the 3 fitted lifetime components show similar trends with shell thickness in the sense that all the 3 components show either an increase or a decrease (depending upon the architecture), but there is more spread in the exact values than for CdS-based shelling. The

trends for the  $\tau_2$  and  $\tau_3$  components show much less variation than  $\tau_1$ , although  $\tau_1$  does remain  $< 1$  ns in all cases. Adding 3ML or 5 ML of pure ZnSe shells caused only small changes in  $\tau_1$  compared to the CdSe core (crossed triangles and empty triangles, respectively). Differences in the exact  $\tau_1$  values were observed (as in CdS-based shelling), with might be again due to difference in the degree of coverage of surface defects of core QDs in the different cases. For gradient-alloyed ZnSeS (filled triangles), a consistent increase in the  $\tau_1$  value compared to the core was observed. In all cases, adding the ZnS outer shell to either 3 ML ZnSe, 5 ML ZnSe or 5 ML ZnSeS caused negligible changes in the  $\tau_1$  value, similar to that observed for CdS-based shells.

Figure 3.9 shows that the amplitudes of each of the fluorescence lifetime components. Clearly, the amplitudes change significantly with shell thickness for all the different architectures. In all types of architectures (whether CdS- or ZnSe-based QDs), the amplitudes of the  $<1$  ns ( $a_1$ ) and  $\sim 20$  ns ( $a_3$ ) components are anti-correlated; i.e. amplitudes for  $<1$  ns usually decrease while amplitudes for  $\sim 20$  ns components usually increase with shell thickness. However, the extent of the decrease or increase in  $a_1$  and  $a_3$  is different with different shell thicknesses and architectures. For gradient-alloyed CdZnS/ZnS (figure 3.9 c) QDs, the  $a_1$  component decreased significantly and the  $a_3$  component increased significantly with shell thickness up to 5 ML, with only a slight change in  $a_2$  – it decreased slightly with the 1<sup>st</sup> ML then increases slightly for ML 2-4. For non-alloyed CdS/ZnS QDs (figure 3.9 a-b), the  $a_1$  component decreased very slightly or remains almost the same from core up to the 3<sup>rd</sup> ML. In both cases, the  $a_2$  component decreased with the 1<sup>st</sup> ML then increased slightly from ML 2-4, just as with alloyed CdZnS. For shells thicker than 3 ML the decrease in  $a_1$  became more significant. The  $a_1$  component dropped further with shell thickness from 3 ML to 5 ML if these next 2 ML are additional CdS. The 1<sup>st</sup> ML of ZnS (for 3ML CdS) caused a drop in  $a_1$  as significant as the 2 additional ML (4<sup>th</sup> and 5<sup>th</sup> ML) of CdS. Adding more ZnS to 3ML CdS/1ML

ZnS caused no further change in  $a_1$  or  $a_2$ , while adding 3ML of ZnS onto both 5 ML non-alloyed CdS or alloyed CdZnS caused an increase in  $a_1$  and  $a_2$ . Interestingly, adding 1 ML ZnS onto 3 ML CdS (Figure 3.9 a) caused a significant increase in  $a_3$ , which then remained high from the next 4 ML ZnS, while adding 3 ML onto 5 ML CdS caused  $a_3$  to drop significantly. There was a similar decrease in  $a_3$  when adding to gradient-alloyed CdZnS, although it was not as strong as for ML non-alloyed CdS. So, there is a transition point in the exciton decay behavior between adding ZnS onto 3ML of CdS inner shell compared to adding it to 5 ML of CdS inner shell. Adding a thicker outer shell of ZnS onto a thinner inner CdS shell leads to a higher fraction of the longer lifetime/higher QY decay pathways ( $a_3$ ) than using a thinner outer shell of ZnS onto a thicker inner shell of CdS. This is reflected in the fact that the PL QY does not decrease as much with the ZnS outer shell using 3 ML CdS inner shell than using 5 ML CdS inner shell (Figure 3.7a).

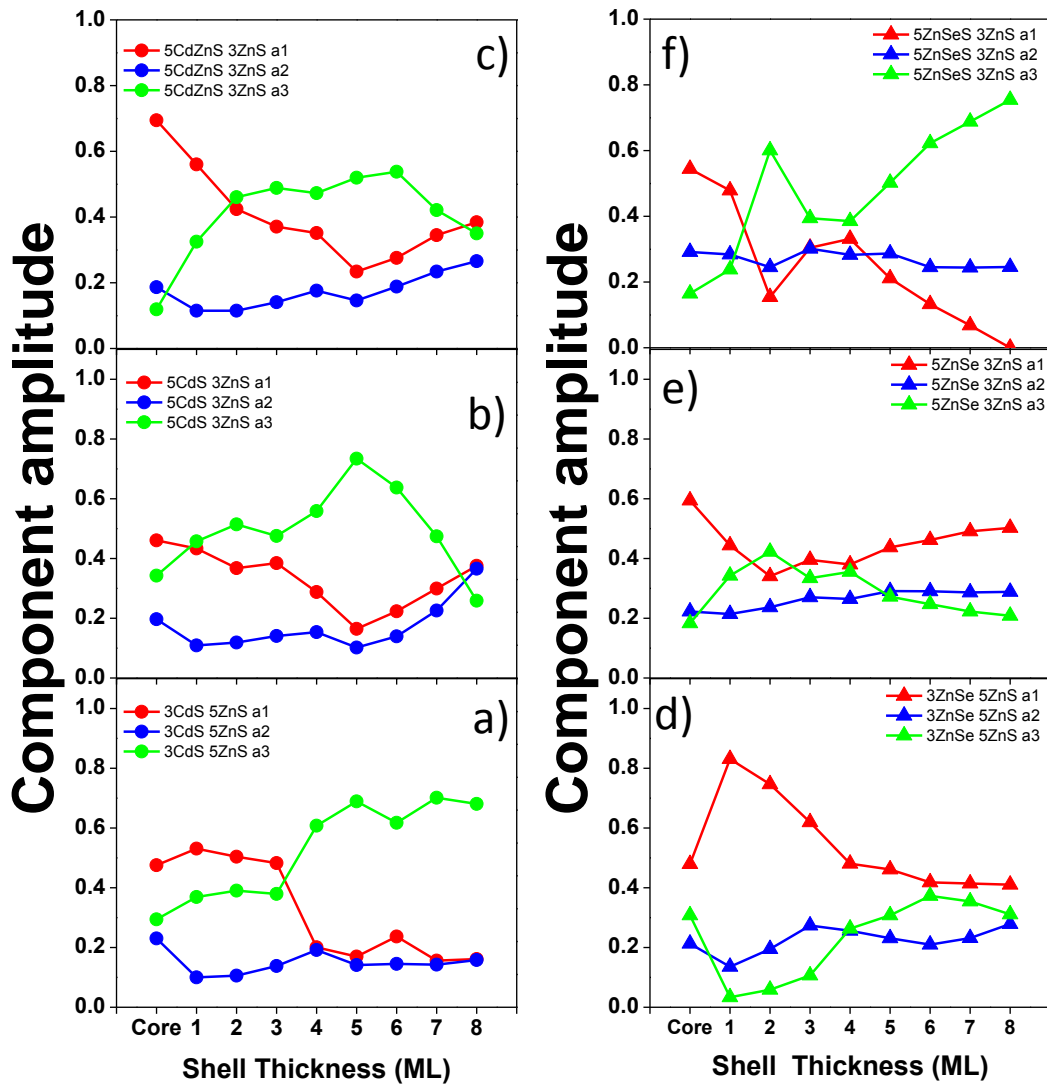


**Figure 3.9:** Component amplitudes as a function of shell thickness for (a-c) CdS inner shell and (d-f) ZnSe inner shell QDs

For ZnSe-based shelling, the a<sub>1</sub> and a<sub>3</sub> trends are also anti correlated in behavior, while a<sub>2</sub> does not show much variation figure 3.9 (d-f). The value of a<sub>2</sub> was generally higher for ZnSe-based shelling, but it varied less than CdS-based shelling. For the thinner non-alloyed inner shell QDs, a<sub>1</sub> increases sharply for 1<sup>st</sup> ML coating of ZnSe and later dropped gradually up to 8<sup>th</sup> ML, while the a<sub>3</sub> component for this set of QDs first dropped for 1<sup>st</sup> ML and then increased gradually up to 8<sup>th</sup> ML.

For the thicker non-alloyed ZnSe inner shell QDs,  $a_1$  dropped and  $a_3$  increased from the core to the 2<sup>nd</sup> ML. Then  $a_1$  increased slightly and  $a_3$  decreased slightly to the 8<sup>th</sup> MLs. For the gradient-alloyed ZnSeS inner shells,  $a_1$  decreased and  $a_3$  increased from the core up to the 2<sup>nd</sup> ML, became constant from the 3<sup>rd</sup> and 4<sup>th</sup> MLs, then  $a_1$  decreased and  $a_3$  increased significantly from the 4<sup>th</sup> up to the 8<sup>th</sup> MLs, with  $a_1$  dropping to effectively zero by the 8<sup>th</sup> ML. Adding an outer shell of ZnS onto alloyed ZnSeS inner shells allowed the high QY component ( $a_3$ ) to increase in amplitude significantly, while using non-alloyed ZnSe inner shells did not. Using a thinner ZnSe inner shell did allow  $a_3$  to recover from its low value at the 3<sup>rd</sup> ZnSe ML, but using the thicker ZnSe did not. However, even with the thin ZnSe inner shell,  $a_3$  did not reach the high value as using the alloyed ZnSeS. Clearly alloying ZnSe with ZnS is important to maintain the high QY decay pathways, that allows the QDs to reach the highest PL QYs of all our samples (Figure 3.7a). Interestingly, however, as we found in chapter 2 and published recently<sup>22</sup> this alloying did not decrease the blinking when compared to using non-alloyed ZnSe.

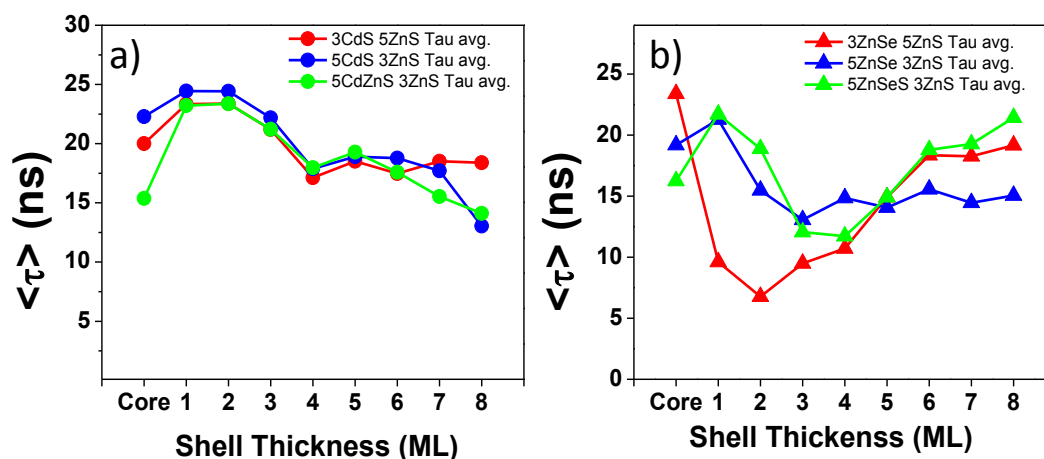


**Figure 3.10:** a) Average fluorescence lifetime for CdS inner shell QDs and b) Average fluorescence lifetime for ZnSe inner shell QDs



We plotted  $\tau_{av}$ , as a function of shell thickness and shell architecture in figure 3.10. For CdS-based shelling (fig. 3.10a), the trend for average fluorescence lifetime components for all the three samples is very similar. The average fluorescence lifetime of the starting cores were slightly different, as has been discussed above. However, for the 1<sup>st</sup> ML, the average fluorescence lifetime always shows a rise, followed by a gradual decrease up to the 4<sup>th</sup> ML. Then from the 4<sup>th</sup> to the 8<sup>th</sup> MLs, the average fluorescence lifetime remains almost constant, with the exception that adding ZnS to the gradient alloyed CdZnS caused the average fluorescence lifetime to continue to decrease. For ZnSe-based shelling (fig. 3.10b), the average lifetime varies a little more than CdS QDs with shell thickness. If the fluorescence lifetime is high, there is a significant decrease within the first 2 ML of adding pure ZnSe, but if the fluorescence lifetime of the core is low, the decrease is less significant upon adding either pure ZnSe or gradient-alloyed ZnSeS. In fact, there is a slight increase in the 1<sup>st</sup> ML, followed by a decrease between 1-3 ML. Then, once a minimum is reached at 2-3ML, the average fluorescence lifetime increases again up to 8ML, unless ZnS is added to CdSe/3 ML ZnSe; in that case the average fluorescence lifetime remains low

The average fluorescence lifetime can be calculated from the various components and amplitudes. Also, since PL QYs and fluorescence lifetimes are related to each other due to radiative and non-radiative decays of excitons, we also calculated the radiative and non-radiative rate constants from these two processes by applying the following equations.<sup>35</sup>



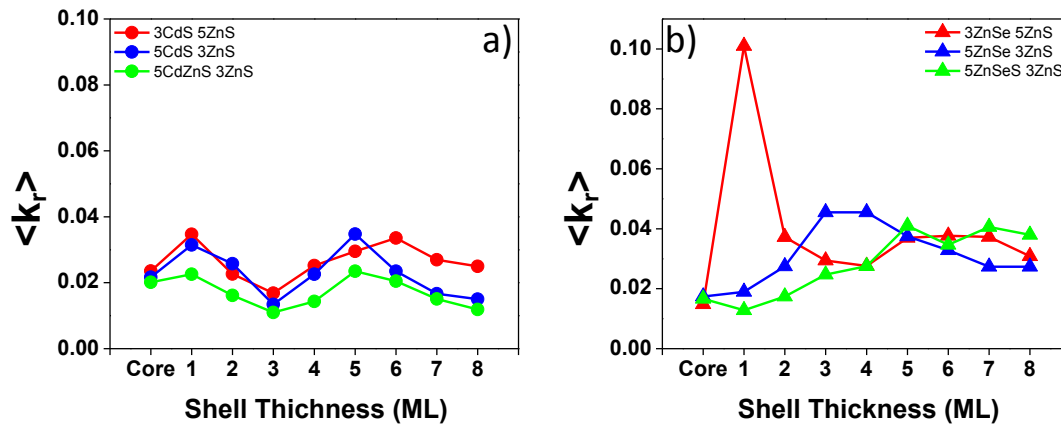


**Figure 3.11:** Radiative rate constant ( $k_r$ ) of a) QDs with CdS inner shell and b) QDs with ZnSe inner shell as a function of shell composition and thickness.

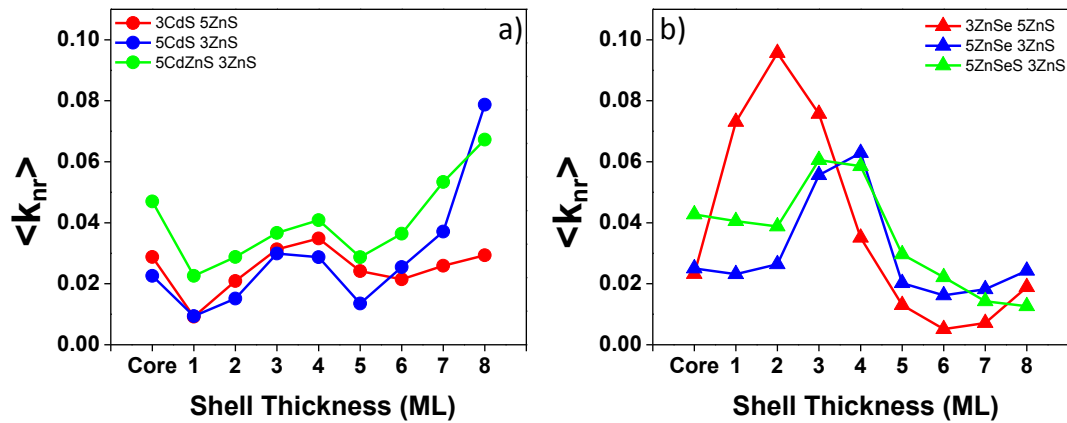


**Figure 3.12:** Average Non-radiative rate constant ( $\langle k_{nr} \rangle$ ) of a) QDs with CdS inner shell and b) QDs with ZnSe inner shell as a function of shell composition and thickness.

The average radiative rate  $\langle k_r \rangle$  and average non-radiative rate  $\langle k_{nr} \rangle$  are shown in figures 3.11 and 3.12 as a function of shell material and thickness. CdS based-shelling had very little effect on  $\langle k_r \rangle$ , but increased  $\langle k_{nr} \rangle$ , although only when the shells became thicker (5-8 ML). For ZnSe-based shelling,  $\langle k_r \rangle$  seemed to systematically increase with shell thickness more than CdS-based shelling. There is one outlier point at 1 ML for the 3ML ZnSe/5ML ZnS sample. At 1 ML, the 3ML ZnSe/5ML ZnS and the 5ML ZnSe/3ML ZnS are effectively the same sample at that point, so are

expected to behave the same way. Variation in passivating the number of trap states in the original CdSe core might be one reason for this, but this surprising outlier will need to be checked by repeating the synthesis of this sample at least 1-2 more times to check for reproducibility. For ZnSe-based shelling,  $\langle k_{nr} \rangle$  behavior is very different from the CdS-based shelling.  $\langle k_{nr} \rangle$  increases compared to the core for moderate shell thicknesses and then decreases for thicker shells, independent of the actual shell architecture (thin ZnSe/thick ZnS, thick ZnSe/thin ZnS or alloyed ZnSeS/ZnS). For ZnSe-based inner shelling, the lattice strain build up quicker than CdS-based inner shelling, which increases non-radiative decay pathways, before the increased confinement potential takes over and mitigates these lattice-strain induced non-radiative decay pathways, presumably by reducing the accessibility of the trap states to the delocalized excitons.

### 3.5. Conclusions:

We have successfully synthesized the different sets of CdSe/XX/ZnS core/multishell QDs by varying the architecture and thickness of inner shell in these QDs, with XX to be CdS, ZnSe,  $\text{Cd}_{(1-x)}\text{Zn}_x\text{S}$  or  $\text{ZnSe}_{(1-x)}\text{S}_x$ , where x increased from 0 to 1 by 0.2 increments in each sequential monolayer. The architecture of the inner shell material was chosen on the basis of the confinement potential and lattice mismatch parameters of the inner/outer shell materials. The monolayer by monolayer growth of these particles was monitored by the degree of red shift in the PL  $\lambda_{\text{max}}$ , which was larger for CdS-based QDs than in ZnSe-based QDs, and was reduced in the case of gradient-alloying in both cases. The shape of the particles at the core/shell or core/shell/shell level is very close to spherical in shape, indicating uniform shell growth. The main purpose of this work was to study how different inner/outer shell combinations affect the exciton decay dynamics of these QDs due to the competing effects of the confinement potential and lattice mismatch. PL QY trends for all

the shell combinations were quite complex, so to better understand the physical processes, we performed time-resolved fluorescence spectroscopy to measure the fluorescence lifetime decay of each component by fitting the data to multi-exponential functions to extract out the various exciton decay dynamics. Three lifetime fitting components for all the different shell combinations were found;  $\tau_1 = <1$  ns,  $\tau_2 = \sim 2-4$  ns and  $\tau_3 = \sim 20$  ns. For both CdS-based and ZnSe-based inner shell QDs, the fitted lifetime components  $\tau_2$  and  $\tau_3$  remained consistent upon varying shell thickness or architecture, although there was a little more spread in them for ZnSe-based than CdS-based inner shells. However, the  $\tau_1$  component showed more variation with the shell thickness, although still well-separated from the other two components. On the other hand, the amplitudes of these fluorescence lifetime components varied significantly with shell thickness for all the different architectures. In all types of architectures (whether CdS- or ZnSe-based QDs), the amplitudes of the  $<1$  ns ( $a_1$ ) and  $\sim 20$  ns ( $a_3$ ) components are anti-correlated; i.e. amplitudes for  $<1$  ns usually decreased while amplitudes for  $\sim 20$  ns components usually increased with shell thickness. However, the extent of the decrease or increase in  $a_1$  and  $a_3$  is different with different shell thicknesses and architectures.

We then calculated  $\langle k_r \rangle$  and  $\langle k_{nr} \rangle$  from the PL QY and average fluorescence lifetimes and studied how these varied with different interfaces influence. CdS-based shelling had very little effect on  $\langle k_r \rangle$  but increased  $\langle k_{nr} \rangle$ , although only when the shells became thicker (5-8 ML). This indicates that only when the ZnS outer shell is added did lattice strain built up to a significant amount to produce trap states. Being at the shell/shell interface, these trap states are close to the outer surface, which can lead to an increase in non-radiative decay processes. For ZnSe-based shelling,  $\langle k_r \rangle$  seemed to systematically increase with shell thickness more than CdS-based shelling, which should be due to high wavefunction confinement not allowing the electron access to the shell

surface trap states, however  $\langle k_{nr} \rangle$  behavior is very different from the CdS-based shelling.  $\langle k_{nr} \rangle$  increased compared to the core for moderate shell thicknesses and then decreases for thicker shells, independent of the actual shell architecture (thin ZnSe/thick ZnS, thick ZnSe/thin ZnS or alloyed ZnSeS/ZnS). For ZnSe-based inner shelling, the lattice strain builds up quicker than CdS-based inner shelling, which increases non-radiative decay pathways. When the shells become thicker, it is likely that the increased confinement potential takes over and mitigates non-radiative decay pathways, presumably by reducing the accessibility of the trap states to non-radiative pathways. This may be due to the fact that the interfacial trap states are closer to the core than to the outer shell surface, so that the main decay pathway for excitons trapped at the interface is to become detrapped and decay radiatively rather than non-radiatively via the QD surface (see Figure 3.1).

Also, we learned from our results that surface defects on the original core contribute significantly towards the overall optical properties of the QDs. We found that although the PL QY of the original core is similar for the original core, but still the shelling with same shell material behaves differently and gives the different trends of the exciton decay dynamics in terms of the fluorescence lifetime components or for average radiative and non-radiative decay components.

### 3.6. References

1. Dabbousi, B. O.; RodriguezViejo, J.; Mikulec, F. V.; Heine, J. R.; Mattoussi, H.; Ober, R.; Jensen, K. F.; Bawendi, M. G., (CdSe)ZnS core-shell quantum dots: Synthesis and characterization of a size series of highly luminescent nanocrystallites. *Journal of Physical Chemistry B* **1997**, *101* (46), 9463-9475.
2. Smith, A. M.; Ruan, G.; Rhyner, M. N.; Nie, S. M., Engineering luminescent quantum dots for In vivo molecular and cellular imaging. *Annals of Biomedical Engineering* **2006**, *34* (1), 3-14.
3. Drbohlavova, J.; Adam, V.; Kizek, R.; Hubalek, J., Quantum Dots - Characterization, Preparation and Usage in Biological Systems. *International Journal of Molecular Sciences* **2009**, *10* (2), 656-673.
4. McBride, J.; Treadway, J.; Feldman, L. C.; Pennycook, S. J.; Rosenthal, S. J., Structural basis for near unity quantum yield core/shell nanostructures. *Nano Letters* **2006**, *6* (7), 1496-1501.
5. Dooley, C. J.; Dimitrov, S. D.; Fiebig, T., Ultrafast electron transfer dynamics in CdSe/CdTe donor-acceptor nanorods. *Journal of Physical Chemistry C* **2008**, *112* (32), 12074-12076.
6. Hines, M. A.; Guyot-Sionnest, P., Synthesis and characterization of strongly luminescing ZnS-Capped CdSe nanocrystals. *Journal of Physical Chemistry* **1996**, *100* (2), 468-471.
7. Talapin, D. V.; Rogach, A. L.; Kornowski, A.; Haase, M.; Weller, H., Highly luminescent monodisperse CdSe and CdSe/ZnS nanocrystals synthesized in a hexadecylamine-trioctylphosphine oxide-trioctylphosphine mixture. *Nano Letters* **2001**, *1* (4), 207-211.
8. Medintz, I. L.; Uyeda, H. T.; Goldman, E. R.; Mattoussi, H., Quantum dot bioconjugates for imaging, labelling and sensing. *Nature Materials* **2005**, *4* (6), 435-446.
9. Snee, P. T.; Somers, R. C.; Nair, G.; Zimmer, J. P.; Bawendi, M. G.; Nocera, D. G., A ratiometric CdSe/ZnS nanocrystal pH sensor. *Journal of the American Chemical Society* **2006**, *128* (41), 13320-13321.

10. Yu, Z. H.; Guo, L.; Du, H.; Krauss, T.; Silcox, J., Shell distribution on colloidal CdSe/ZnS quantum dots. *Nano Letters* **2005**, *5* (4), 565-570.
11. Heyes, C. D.; Kobitski, A. Y.; Breus, V. V.; Nienhaus, G. U., Effect of the shell on the blinking statistics of core-shell quantum dots: A single-particle fluorescence study. *Physical Review B* **2007**, *75* (12).
12. Spinicelli, P.; Mahler, B.; Buil, S.; Quelin, X.; Dubertret, B.; Hermier, J. P., Non-Blinking Semiconductor Colloidal Quantum Dots for Biology, Optoelectronics and Quantum Optics. *Chemphyschem* **2009**, *10* (6), 879-882.
13. Zhu, H. M.; Song, N. H.; Lian, T. Q., Controlling Charge Separation and Recombination Rates in CdSe/ZnS Type I Core-Shell Quantum Dots by Shell Thicknesses. *Journal of the American Chemical Society* **2010**, *132* (42), 15038-15045.
14. Scotognella, F.; Miszta, K.; Dorfs, D.; Zavelani-Rossi, M.; Brescia, R.; Marras, S.; Manna, L.; Lanzani, G.; Tassone, F., Ultrafast Exciton Dynamics in Colloidal CdSe/CdS Octapod Shaped Nanocrystals. *Journal of Physical Chemistry C* **2011**, *115* (18), 9005-9011.
15. Rosenthal, S. J.; McBride, J.; Pennycook, S. J.; Feldman, L. C., Synthesis, surface studies, composition and structural characterization of CdSe, core/shell and biologically active nanocrystals. *Surface Science Reports* **2007**, *62* (4), 111-157.
16. Talapin, D. V.; Mekis, I.; Gotzinger, S.; Kornowski, A.; Benson, O.; Weller, H., CdSe/CdS/ZnS and CdSe/ZnSe/ZnS core-shell-shell nanocrystals. *Journal of Physical Chemistry B* **2004**, *108* (49), 18826-18831.
17. Lim, S. J.; Chon, B.; Joo, T.; Shin, S. K., Synthesis and characterization of zinc-blende CdSe-based core/shell nanocrystals and their luminescence in water. *Journal of Physical Chemistry C* **2008**, *112* (6), 1744-1747.
18. Liu, Y. S.; Sun, Y. H.; Vernier, P. T.; Liang, C. H.; Chong, S. Y. C.; Gundersen, M. A., pH-sensitive photoluminescence of CdSe/ZnSe/ZnS quantum dots in human ovarian cancer cells. *Journal of Physical Chemistry C* **2007**, *111* (7), 2872-2878.
19. Reiss, P.; Carayon, S.; Bleuse, J.; Pron, A., Low polydispersity core/shell nanocrystals of CdSe/ZnSe and CdSe/ZnSe/ZnS type: preparation and optical studies. *Synthetic Metals* **2003**, *139* (3), 649-652.

20. Jones, M.; Lo, S. S.; Scholes, G. D., Quantitative modeling of the role of surface traps in CdSe/CdS/ZnS nanocrystal photoluminescence decay dynamics. *Proceedings of the National Academy of Sciences of the United States of America* **2009**, *106* (9), 3011-3016.
21. Deka, S.; Quarta, A.; Lupo, M. G.; Falqui, A.; Boninelli, S.; Giannini, C.; Morello, G.; De Giorgi, M.; Lanzani, G.; Spinella, C.; Cingolani, R.; Pellegrino, T.; Manna, L., CdSe/CdS/ZnS Double Shell Nanorods with High Photoluminescence Efficiency and Their Exploitation As Biolabeling Probes. *Journal of the American Chemical Society* **2009**, *131* (8), 2948-2958.
22. Bajwa, P.; Gao, F.; Nguyen, A.; Omogo, B.; Heyes, C. D., Influence of the Inner-Shell Architecture on Quantum Yield and Blinking Dynamics in Core/Multishell Quantum Dots. *Chemphyschem* **2016**, *17* (5), 731-740.
23. Durisic, N.; Godin, A. G.; Walters, D.; Grätzer, P.; Wiseman, P. W.; Heyes, C. D., Probing the "Dark" Fraction of Core-Shell Quantum Dots by Ensemble and Single Particle pH-Dependent Spectroscopy. *ACS Nano* **2011**, *5* (11), 9062-9073.
24. Gao, F.; Kreidermacher, A.; Fritsch, I.; Heyes, C. D., 3D Imaging of Flow Patterns in an Internally-Pumped Microfluidic Device: Redox Magnetohydrodynamics and Electrochemically Generated Density Gradients. *Analytical Chemistry* **2013**, *85* (9), 4414-4422.
25. Omogo, B.; Gao, F.; Bajwa, P.; Kaneko, M.; Heyes, C. D., Reducing Blinking in Small Core-Multishell Quantum Dots by Carefully Balancing Confinement Potential and Induced Lattice Strain: The "Goldilocks" Effect. *ACS Nano* **2016**, *10* (4), 4072-4082.
26. Li, J. J.; Wang, Y. A.; Guo, W. Z.; Keay, J. C.; Mishima, T. D.; Johnson, M. B.; Peng, X. G., Large-scale synthesis of nearly monodisperse CdSe/CdS core/shell nanocrystals using air-stable reagents via successive ion layer adsorption and reaction. *Journal of the American Chemical Society* **2003**, *125* (41), 12567-12575.
27. Mahler, B.; Lequeux, N.; Dubertret, B., Ligand-Controlled Polytypism of Thick-Shell CdSe/CdS Nanocrystals. *Journal of the American Chemical Society* **2010**, *132* (3), 953-959.
29. Gong, K.; Kelley, D. F., A predictive model of shell morphology in CdSe/CdS core/shell quantum dots. *Journal of Chemical Physics* **2014**, *141* (19).



30. Acharya, K. P.; Nguyen, H. M.; Paulite, M.; Piryatinski, A.; Zhang, J.; Casson, J. L.; Xu, H. W.; Htoon, H.; Hollingsworth, J. A., Elucidation of Two Giants: Challenges to Thick-Shell Synthesis in CdSe/ZnSe and ZnSe/CdS Core/Shell Quantum Dots. *Journal of the American Chemical Society* **2015**, *137* (11), 3755-3758.
31. Gomez, D. E.; van Embden, J.; Mulvaney, P.; Fernee, M. J.; Rubinsztein-Dunlop, H., Exciton-Trion Transitions in Single CdSe-CdS Core-Shell Nanocrystals. *Acs Nano* **2009**, *3* (8), 2281-2287.
32. Qin, W.; Guyot-Sionnest, P., Evidence for the Role of Holes in Blinking: Negative and Oxidized CdSe/CdS Dots. *Acs Nano* **2012**, *6* (10), 9125-9132.
33. Rabouw, F. T.; Lunnemann, P.; van Dijk-Moes, R. J. A.; Frimmer, M.; Pietra, F.; Koenderink, A. F.; Vanmaekelbergh, D., Reduced Auger Recombination in Single CdSe/CdS Nanorods by One-Dimensional Electron Delocalization. *Nano Letters* **2013**, *13* (10), 4884-4892.
34. Park, Y. S.; Bae, W. K.; Pietryga, J. M.; Klimov, V. I., Auger Recombination of Biexcitons and Negative and Positive Trions in Individual Quantum Dots. *Acs Nano* **2014**, *8* (7), 7288-7296.
35. Omogo, B.; Aldana, J. F.; Heyes, C. D., Radiative and Nonradiative Lifetime Engineering of Quantum Dots in Multiple Solvents by Surface Atom Stoichiometry and Ligands. *Journal of Physical Chemistry C* **2013**, *117* (5), 2317-2327.

## **Chapter 4. Reducing Blinking in Small Core-Multishell Quantum Dots by Carefully Balancing Confinement Potential and Induced Lattice Strain: The “Goldilocks” Effect.**

Benard Omogo<sup>1</sup>, Feng Gao<sup>1</sup>, Pooja Bajwa, Mizuho Kaneko and Colin D. Heyes\*

Department of Chemistry and Biochemistry, University of Arkansas, Fayetteville, Arkansas 72701, United States of America

<sup>1</sup> These authors contributed equally to this work.

\*Corresponding author, Email: [cheyes@uark.edu](mailto:cheyes@uark.edu) Tel: 479-575-5607

Keywords: colloidal semiconductor, interfacial trap-states, lattice mismatch, single-particle fluorescence, fluorescence lifetime.

#### 4.1. Abstract

Currently, the most common way to reduce blinking in quantum dots (QDs) is accomplished by using very thick and/or perfectly crystalline CdS shells on CdSe cores. Ideally, a non-toxic material such as ZnS is preferred to be the outer material in order to reduce environmental and cytotoxic effects. Blinking suppression with multishell configurations of CdS and ZnS has only been reported for “giant” QDs of 15 nm or more. One of the main reasons for the limited progress is that the role that interfacial trap states play in blinking in these systems is not very well understood. Here, we show a “Goldilocks” effect to reduce blinking in small (~7nm) QDs by carefully controlling the thicknesses of the shells in multi-shell QDs. Furthermore, by correlating the fluorescence lifetime components with the fraction of time that a QD spends in the on state, both with and without applying a threshold, we found evidence for 2 types of blinking that separately affect the average fluorescence lifetime of a single QD. A thorough characterization of the time-resolved fluorescence at the ensemble and single particle level allowed us to propose a detailed physical model involving both short-lived interfacial trap states and long-lived surface trap states that are coupled. This model highlights a strategy of reducing QD blinking in small QDs by balancing the magnitude of the induced lattice strain, which results in the formation of interfacial trap states between the inner shell and the outer shell, and the confinement potential that determines how accessible the interfacial trap states are. The combination of reducing blinking while maintaining a small overall QD size, together with using a Cd-free outer-shell of ZnS will be useful in a wide array of applications, particularly for advanced bioimaging.

## 4.2. Introduction

Colloidal semiconductor nanocrystals, quantum dots (QDs), have unique optical and optoelectronic properties which, combined with ease of synthesis and processibility, have resulted in them becoming one of the most important class of nanomaterials. In particular, their photoluminescence (PL) and electroluminescence (EL) properties have led to their widespread development as biological fluorescent tags,<sup>1-3</sup> optical sensors<sup>4</sup> and tunable lighting/LEDs.<sup>5</sup> Improving the emission quantum yield (QY) of a fluorescent QD is usually accomplished by shelling the core with a higher band-gap material to reduce the accessibility of excitons to non-radiative surface trap-states.<sup>6,7</sup> The prototypical example of a core/shell colloidal QD is CdSe/ZnS but this material combination is not ideal due to the large mismatch in their lattice structures often resulting in non-uniform shells that generate defects at the interface.<sup>8,9</sup> QD blinking was discovered in 1996<sup>10</sup> and has become one of the greatest limitations in the applications of QDs, although the blinking process has been taken advantage of as a probe to study cation exchange reaction mechanisms within a single nanoparticle.<sup>11</sup> Debate still exists as to the exact details of the mechanism, but it is generally attributed to the existence of trap states either internal to or external to the QD. Several recent reviews<sup>12-15</sup> have summarized the extensive literature on the subject, but the problem is not yet adequately solved. It was found that adding ZnS shells onto CdSe cores had a negligible effect on blinking when up to 7 monolayers (ML) of the material was added.<sup>16</sup> Adding the more toxic CdS shell onto CdSe cores was reported to suppress blinking, but it was necessary to grow these CdS shells thick (~16 monolayers (MLs)), which is much easier to do than for ZnS due to the lower lattice mismatch of CdS with CdSe (~3.9%).<sup>17,18</sup> More recently, a slow shell-growth method was shown to generate exceptionally high crystalline shells that reduced the blinking of quantum dots with thinner CdS shells,<sup>19</sup> which have been further studied for potentially improving lasing applications<sup>20</sup> and hole transfer dynamics for solar cell applications.<sup>21</sup> The high-temperature

slow-growth shelling process was modified to form gradient-alloyed  $\text{Cd}_x\text{Zn}_{(1-x)}\text{S}$  core/shells with high PL QYs and reduced blinking dynamics that depended on the amount of CdS and ZnS added and the degree of alloying.<sup>22</sup> Many researchers still opt to use the lower-temperature SILAR shelling process, however, due to its high level of control over thickness and degree of alloying, as well as the versatility in material choice.<sup>23, 24</sup> For example, recently, Ren and coworkers recently used SILAR to produce CdSe/CdS QDs and then reduced blinking by adding a novel polymer coating that only modestly increased QD size.<sup>25</sup> While this is an effective way to reduce blinking, the presence of CdS on the outer shell surface is still a limitation, especially in biological applications.

To circumvent the challenges of high lattice strain core/shell CdSe/ZnS QDs, core-multishell systems are becoming a popular alternative.<sup>26, 27</sup> While this introduces more variables, these methods do allow for toxic cadmium to be completely eliminated from the outer surface of the QD. Fitzmorris *et al.*<sup>28</sup> recently used the wavelength-dependent fluorescence lifetimes of CdSe/ZnSe/ZnS QDs to show that the contributions from various decay pathways change upon adding the shells. Core/shell/shell QDs can also significantly reduce blinking, but, so far, only “giant” QDs with ~19 monolayers of shells have been reported to do so.<sup>18</sup>

We hypothesized that by systematically studying the exact roles of the core-shell and shell-shell interfaces of CdSe/CdS/ZnS core/shell/shell QDs on the exciton dynamics, an optimal combination of shell thicknesses could be found to reduce blinking in smaller-sized QDs. By quantifying the contributions of the various exciton decay pathways as a function of shell thickness, we report a “Goldilocks” effect in which we can balance the competing effects of induced lattice strain and confinement potential to reduce blinking in smaller-sized QDs than those that are currently available (~7 nm in diameter). Furthermore, by correlating the fluorescence lifetime

components of single QDs as a function of the fraction of time that they spend in the on state, both with and without applying a threshold, we found evidence for 2 types of blinking that separately affect the average fluorescence lifetime of a single QD. We propose a detailed physical model involving both short-lived interfacial trap states and long-lived surface trap states that explains both the two types of blinking as well as the “Goldilocks” effect. Due to the combination of reduced blinking while retaining a small size, together with the fact that the outer surface is composed of the low-toxicity ZnS material, these QDs should find utility in a wide range of applications, especially advanced bioimaging at the single molecule level.

### 4.3. Results and Discussion

Figure 4.1A shows that the PL QY for CdSe/CdS core/shells was at a maximum with 3ML of CdS and then decreased strongly as more MLs were added. Due to this QY maximum, we then synthesized CdSe/CdS/ZnS core/shell/shell QDs with a 3ML CdS inner shell for further study. The spectral properties of our CdSe/CdS/ZnS core/shell/shell QDs are provided in the supporting information (Figure 4.S1) and show narrow emission peaks that become slightly narrower upon adding shell MLs, well-resolved absorption peaks, and a steady red-shift in both absorption and emission peak maxima, which are all in agreement with previous reports on successful shelling.<sup>6, 7, 26, 27</sup> Transmission electron microscopy (TEM) was used to confirm the shape and size distribution of the QDs (Figure 4.2A-B) and showed well-controlled epitaxial shelling with multi-shells.<sup>29</sup> More importantly, annular dark field scanning transmission electron microscopy (ADF-STEM) coupled with electron energy loss spectroscopy (EELS) was used to confirm the multi-shell integrity (Figure 4,2C-H), which shows that the center of the QD is Cd-rich and the outer part of the QD is Zn-rich.

Taken together, the combination of spectral data and structural analysis strongly supports the formation and integrity of the core/shell/shell structure.

As can be seen in figure 4.1A, when ZnS is added to CdSe/3 ML CdS, the PL QY increased sharply with the first ML of ZnS, and then started to decrease. However, the decrease in PL QY upon adding more ML of the ZnS outer shell is less than the decrease upon adding thicker CdS shells. To investigate the underlying dynamics, we measured the PL lifetime decay curves (Figure 4.1B). Complex multi-exponential behavior was evident, suggesting multiple decay pathways for the excitons. It is expected that variations in the shapes of the fluorescence decays originate from variations in the relative contributions of each of these pathways.<sup>28</sup> Therefore, we analyzed each set of samples (core/shell and core/shell/shell) using a global fitting approach to the minimum number of decay components possible, which was found to be 3. Global fitting is plotted as the normalized amplitude of each component as a function of shell thickness in figures 4.1C (CdSe/CdS core/shell) and 4.1D (CdSe/CdS/ZnS core/shell/shell). The 3 components have characteristic lifetimes of ~0.7 ns, ~15-16 ns and ~40-50 ns for each sample. Based on previous QD literature,<sup>28, 30</sup> we assigned these components to trion emission, band-edge emission and shallow trap state emission respectively. Since the probability of trion emission is expected to increase with power at the expense of decreasing the contribution from band-edge emission, we further supported this assignment with power-dependent fluorescence lifetime measurements (Figure 4.1E), which indeed shows that the fast component increases with power, the medium component decreases with power and the slowest component shows very little power dependence, as would be expected from shallow trap state emission. For the CdSe/CdS core/shell QDs (figure 4.1C), there is slow decrease in the amplitude of the slowest (trap-state) component until it is no longer present above ~7ML CdS. On the other hand, there is a gradual increase in the relative contribution of the band-edge emission

between 1-4 ML CdS followed by a decrease for thicker CdS shells. For the fast (trion) emission, there is a slight decrease for thin shells until 4ML, but then rises sharply as the CdS shell thickness increases. For the CdSe/CdS/ZnS core/shell/shell QDs (figure 4.1D), there is the same steady decrease in the relative amplitude of the slowest (trap-state) component, although it never completely vanishes when additional ZnS MLs are added as it did when thicker CdS shells were used. The band-edge emission contribution rises as 1-3 ML CdS shells are added, but rises even more sharply when 1ML of ZnS is added to 3ML of CdS. The contribution of the band-edge emission also decreases as thicker ZnS shells are added, although it is a weaker decrease than observed when thicker CdS shells are used. The trion emission had a higher contribution in the CdSe cores that were used for the CdS/ZnS multishelling, highlighting a certain amount of variability in the contribution of the trion state for each CdSe core preparation, even when the QYs are very similar. However, the same trend of a decrease in the contribution of the fast component (trion state) and the slow component (trap state) as a thin shell is added, followed by an increase in the trion state contribution when thick shells are added is evident.

To obtain a deeper understanding of the exciton decay dynamics for the different core/shell and core/shell/shell samples, we calculated the average radiative and non-radiative rate ( $\langle k_r \rangle$  and  $\langle k_{nr} \rangle$ ) as follows:

$$\tau_{av} = \frac{\sum_i a_i \tau_i^2}{\sum_i a_i \tau_i} \quad (1)$$

$$\langle k_r \rangle = \frac{QY}{\tau_{av}} \quad (2)$$

$$\langle k_{nr} \rangle = \frac{1}{\tau_{av}} - \langle k_r \rangle \quad (3)$$



where  $\tau_{av}$  is the average lifetime of the excited state. The average radiative rate is shown in figure 4.1F and the average non-radiative rate is shown in figure 4.1G as a function of shell thickness for the CdSe/CdS core/shell and CdSe/CdS/ZnS core/shell/shell samples. Both samples show similarly qualitative trends of an initial rise in the average radiative rate for thin CdS shells which then decreases for thicker CdS shells but remains relatively high upon adding an outer ZnS shell instead of thickening the CdS shell. There is a negligible effect of the average non-radiative rate as up to 3 ML of a CdS shell is added. When more than 3MLs of a CdS shell is added, the average non-radiative rate increases significantly whereas if an outer ZnS shell is used instead of increasing the CdS shell thickness, the average non-radiative rate decreases with the first ZnS ML and then increases very slowly up until 5 MLs of ZnS are added. Rationalizing the changes in average radiative and non-radiative rates requires one to consider the multiple exciton decay pathways that result from the fact that both wavefunction overlap changes when shells are added, as do the number and localization of charge-carrier trap states. The conduction band offset between CdSe/CdS is fairly small with an upper value of  $\sim 0.3$  eV,<sup>31</sup> although the exact value depends on the relative core and shell diameters and is usually lower.<sup>32</sup> This enables the electron wavefunction to penetrate significantly into the CdS shell.<sup>32, 33</sup> The valence band offset is larger than the conduction band offset which, together with the heavier effective mass of the hole, confines the hole more strongly to the core. This effectively reduces the excitonic overlap integral when CdS shells are used. On the other hand, the lattice mismatch between CdSe/CdS is very small resulting in almost no lattice strain at the interface of CdSe/CdS compared to the more common CdSe/ZnS interface or, more specifically, the CdS/ZnS interface between the inner and outer shells used here. In other words, lattice strain determines how many interfacial trap states are formed whereas confinement potential determines the ability for the charge carriers to access these trap states. Furthermore, it is

expected that the blinking dynamics will depend strongly on both of the parameters. Therefore, before we further develop a model to explain the time-resolved fluorescence studies, we will first present the effect of the outer shell thickness on blinking of single CdSe/CdS/ZnS core/shell/shell QDs having 3ML of CdS inner shell while varying the ZnS outer shell thickness between 0 ML and 5 ML.

Diluted QDs were immobilized in a PMMA matrix and their fluorescence traces recorded under continuous wave (cw) and pulsed laser excitation, as shown in figure 4.3 and S3, respectively. Figure 4.3A shows a schematic depiction of the sample under study and figure 4.3B shows the corresponding blinking trace. Figure 4.3C shows photon counting histograms (PCHs) of each whole trace and figure 4.3D highlights 20-s zoomed-in regions of the blinking traces, showing clear on-off behavior. It is already evident from figures 4.3C and 4.3D that the CdSe/CdS/ZnS QD sample with a 3 ML ZnS outer shell thickness shows a significantly increased on-state compared to the other samples. Since the traces show clearly distinguishable on- and off- states, we applied a threshold (See supporting figure S2 for threshold details) to the fluorescence traces to quantify blinking in terms of on-time and off-time distribution functions ( $P_{on}$  and  $P_{off}$ , figure 4.4A,B), as well as to determine the fraction-on (the fraction of time that QDs spend in the on state over the 300-s measurement period, Figure 4.4C) and the relative on-state brightness (average fluorescence intensity of the on state, figure 4.4D) for individual QDs. The same data for blinking using pulsed laser excitation at the same average power is also given in the supporting information (Figure S4), which shows that, at this excitation power, there is no difference in blinking between the two excitation modes.

It is clear that CdSe cores with 3ML CdS inner-shell and 3ML ZnS outer-shell showed the slowest decrease in  $P_{on}$ , as shown in figure 4.4A (cw) and S4A (pulsed), meaning that longer on-

times are more probable for these QDs. The  $P_{off}$  distributions, as shown in figures 4.4B (cw) and 4.S4B (pulsed), are essentially identical for all of the QDs, appearing as straight lines in the log-log plots indicative of inverse power-law behavior. There is a slightly lower slope in  $P_{off}$  for CdSe/6CdS, *i.e.* slightly shorter off-times, although the effect is rather small. These results clearly demonstrate that varying the outer ZnS shell thickness significantly affects the on-times, with 3ML of ZnS outer-shell and 3ML CdS inner-shell showing the longest on-times. The fraction-on distributions are calculated by dividing the total time in which a quantum dots is “on” by the total collection time for each quantum dot, which is plotted as a histogram in figure 4.4C (cw) and S4C (pulsed). CdSe/3ML CdS core/shell QDs are on for an average of ~20% of the time. Adding 1ML of a ZnS outer shell has a negligible effect but, in agreement with the blinking statistics result, QDs with 3ML of a ZnS outer shell are on for an average of ~50% of the time with some QDs remaining on for 70-80% of the time. However, as the ZnS outer shell increases further to 5 ML, there is a significantly reduction in the amount of time QDs spent in the on state, with none being on for more than ~45% of the time. On the other hand, Figure 4.4D (cw) and S4D (pulsed) shows that the average brightness of single QDs in the on state effectively remains the same as the outer ZnS shell thickness becomes thicker, in agreement with a previous report on CdSe/ZnS core/shell QDs.<sup>16</sup>

One of the main reasons to verify that the blinking dynamics are the same under cw and pulsed illumination was to enable us to collect fluorescence lifetime decay curves for the single QDs using time-correlated single photon counting (TCSPC).<sup>34</sup> For the QDs that showed the widest distribution of fraction-on (CdSe/3ML CdS/3ML ZnS), we fitted each single QD to 3-exponentials, fixing the lifetime components according to those found from the global fitting of the ensemble data (figure 4.1) and varying the relative amplitudes of each component. We then plotted the amplitude of each component of each QD as a function of the fraction of time that QD spent in the on state

(fraction-on), as shown in figure 4.5a. While the slowest lifetime component ( $\sim 53$  ns, from trap state emission) shows only a minor contribution from single QDs with no dependence on fraction-on, there is a clear anti-correlation between the fast component ( $< 1$  ns from trion emission) and the 15 ns component (from band-edge emission). As the fraction-on increases, the fast trion emission decreases sharply while the slower band-edge emission increases sharply. However, the dependence becomes much weaker when the fraction-on increases, with an apparent change at about 35% fraction-on. Clearly, when the fraction-on increases, the trion emission contribution is lower and the band-edge emission contribution is higher, providing strong evidence that the trion state is complicit in blinking. This is true for all thicknesses of ZnS (Figure S5), although the other thicknesses of ZnS did not show as wide a distribution in fraction-on, and so the x-axis range is limited. It is important to highlight at this point that a significant contribution of the fast (trion) component remains even when the fraction-on is high. Furthermore, the average intensity of the on-state does not vary with fraction-on (Figure S6), suggesting that these changes in fluorescence lifetime components does not significantly affect the brightness of a QD in the on state.

In order to further examine this change in behavior of the fast lifetime component as a function of fraction on, we then performed the same single QD analysis after applying a threshold to include only photons from QDs that are considered on (above the threshold), as shown in figure 4.5b. This removes the strong dependence of  $\tau_1$  with fraction-on that was observed at low fraction-on ( $< \sim 35\%$ ), but still shows a weak dependence with fraction-on (approximately the same dependence as the fraction-on above 35% when the threshold was not applied, figure 4.5A). The results from Figures 4.5A and 4.5B strongly suggests that there are 2 types of trion formation that underlies the blinking behavior, one occurring faster than the binning time of 20 ms, and one occurring slower than the binning time (leading to off states longer than the 20-ms binning time).

Finally, we confirmed our assignment that this fast lifetime component at the single QD level was indeed due to trion formation by, again, performing a power-dependent experiment. A single QD was identified and then a blinking trace was acquired at low power (5  $\mu\text{W}$ ). Then, after allowing the QD to recover for a few minutes, a blinking trace from the *same* QD was taken at high power (50  $\mu\text{W}$ ). This was then repeated for multiple QDs. The on-times probability distribution in Figure 4.5C shows that blinking is increased at higher power compared to lower power. The fluorescence lifetime components for each QD was analyzed at each of the excitation powers. This allowed us to plot the change in each lifetime component for each QD as the power is increased as a function of its fraction of time spent on (at the lower power), as shown in figure 4.5D. Indeed, while there is some scatter in the data, it is clear that the QDs showed an  $\sim 40\%$  increase in the fast component at higher power than lower power at the expense of a decrease in the band-edge emission component. Furthermore, this power-dependence is independent of fraction-on. This result provides additional strong support to our assignment that this fast component at the single QD level is indeed from the trion state.

The ensemble and single particle fluorescence data can be collectively explained by the model presented in figure 4.6. This figure presents a schematic energy *vs.* distance diagram of the conduction and valence bands of CdSe core, CdSe/CdS core/shell and CdSe/CdS/ZnS core/shell/shell QDs, together with the relative number of trap states formed on the outer surface of the QD (due to incomplete passivation by the coordinating ligands), as well as at the core/shell and shell/shell interfaces (based on lattice strain). The approximate delocalized electron and hole wavefunctions are highlighted on the figure, together with the relative probability of being trapped at the surface and/or interface (red bands). Possible mechanistic connections between interfacial trap states and surface trap states, *e.g.* by electron or resonance energy transfer, is shown as a blue

arrow and between interfacial trap states and delocalization (trapping-detrapping) is shown by a double-headed green arrow. As will be described below, this relatively simple model can be used to explain several important observations reported in this study and, moreover, provides a strategic framework to fine tune both ensemble and single particle optical properties towards specific applications.

In CdSe cores, surface trap states are readily accessible for both electrons and holes. This leads to a high probability that one (or both) of the charge carriers will be trapped after excitation rather than emitting *via* band-edge emission. If a charge carrier is trapped, the following possibilities exist: 1) the energy is released non-radiatively, 2) the weak overlap between the wavefunctions of the trapped electron (or hole) with the delocalized hole (or electron) leads to trap-state emission with a relatively long decay time,<sup>28, 35</sup> or 3) the trapped electron (or hole) is still trapped when a subsequent photon excites the QD, forming a trion state, which can then emit with low QY but with a fast lifetime.<sup>30</sup> In cores, each of these possibilities are likely, leading to large contributions from all 3 decay components – trion emission, band-edge emission and trap-state emission (Figures 4.1C and D). The cores that were used to make the CdSe/CdS/ZnS core/shell/shell QDs had a larger contribution from trion emission than those that were used to make the CdSe/CdS core/shell QDs, even though they had approximately the same QY and average fluorescence lifetime. This suggests that subtle differences in the microscopic structure of core QDs has a dramatic effect on the decay pathways, even if their spectroscopic signatures (QY and average fluorescence lifetime) are very similar. In any case, adding thin CdS shells onto each of these cores had the same effect – to moderately increase the QY by increasing the contribution of the band-edge emission and decreasing the contribution of trap-state and/or trion emission – with the magnitude of decrease depending on how much was present to begin with (figure 4.1). By the point at which 3

ML of CdS shell was added, the contribution of the band-edge emission was ~50%, the contribution of trion emission was ~35% and the contribution of trap-state emission was ~15% for both sets of cores, independent of what the contributions of the pure cores were. If more than 3 ML CdS shell was added, the QY of the particles decreased sharply reaching the core QY level at 6-8 ML. Figure 1C shows that when CdS becomes thicker than 3ML for simple core-shell structures, the contribution from the trion emission increased while both the trap-state emission and the band-edge emission decreased. From figure 4.6, this can be explained as the number of accessible surface trap states decreasing weakly as the number of MLs of the CdS shell increases from 0 to 3ML to 6ML resulting in the electron having a lower probability of being trapped. The electron, once trapped can emit *via* trap-state emission, *via* trion emission, or become de-trapped. If the CdS shell becomes thicker than ~3ML, there is still a reasonable chance that the electron will be trapped at the surface. However, once trapped, there will be very little overlap with the delocalized hole wavefunction trap-state emission will become negligible. Also, with a thicker shell, de-trapping of the electron will be reduced and thus, once in this surface-trapped state, trions will become more probable. Furthermore, since the electron is localized on the outer surface, there will be a number of non-radiative decay pathways available, which depends on the exact microscopic environment of the QD, leading to an increase in the average non-radiative decay rate (figure 4.1G). Both the increased trion emission and non-radiative decay lead to a significant lowering of the ensemble PL QY (Figure 4.1A).

If a ZnS outer shell is added to 3 ML CdS rather than making the CdS shell thicker, different emission properties arise. The PL QY increases sharply for the first ML of ZnS then decreases as the number of MLs increase. However, the decrease in QY is much weaker than if more CdS MLs are added. From figure 4.1D, this is mainly because the rise in the trion component and the lowering

of the band-edge component is much weaker for the CdS/ZnS multi-shell system than the thick CdS single-shell system. From figure 4.6, due to the stronger wavefunction confinement by ZnS, there is a significantly reduced accessibility to surface trap states. This results in the trion emission and the average non-radiative rate remaining lower than with a thick CdS shell. As ZnS MLs are added, new trap states appear at the CdS/ZnS interface due to induced lattice strain between CdS and ZnS (~7.8% lattice mismatch). The increase in interfacial trap states is much slower than the reduction in the accessibility of the surface trap states up to 3ML ZnS, but becomes more significant for ZnS shells thicker than ~3ML. Notice also that, due to the presence of these interfacial trap states, the contribution from trap-state emission also decreases less for CdS/ZnS multi-shells than with using thick CdS single-shells (blue curves in Figures 4.1C and 4.1D). This is because there is now the possibility of overlap between the interfacial trap state electron (or hole) wavefunction and the delocalized hole (or electron) wavefunction.

The question arises as to how these trap states in core/shell/shell QDs are connected to blinking. The QD blinking dynamics have been extensively discussed in the framework of several models: an auger-assisting quenching model,<sup>36, 37</sup> external trap state model,<sup>38</sup> diffusion-controlled electron transfer,<sup>39, 40</sup> a diffusional resonance energy model<sup>41</sup> and a multiple recombination centers model.<sup>42-44</sup> Some features of these models are common, while others seem to be incompatible, suggesting multiple mechanisms may be responsible, as was hypothesized to explain the lack of a blinking effect on ZnS shell thickness dependence for CdSe/ZnS core/shells.<sup>16</sup> Subsequent spectroelectrochemical studies of QDs led to QD blinking dynamics being discussed in terms of “type A” blinking and “type B” blinking.<sup>14, 45</sup> Type A blinking was proposed to originate from trion states in which the fluorescence lifetime varies with intensity and “type B” blinking was proposed to be a result of activation of non-radiative recombination centers which can trap charge carriers



without leading to a charged QD and, thus, does not result in intensity-dependent fluorescence lifetime changes. Figure 4.4 shows that the on-times are not strongly affected by increasing the CdS shell thickness between 3ML and 6ML, but adding up to 3 ML ZnS MLs onto 3 ML CdS strongly increases the length of the on-times. Adding 2 ML more ZnS caused the on-time duration to decrease again. This manifests itself in the fact that QDs spend a larger fraction of their time, on average, in the on state (*i.e.* above the threshold) for CdSe/3MLCdS/3MLZnS compared to with thinner or thicker ZnS shells (Figure 4.4C), which we term a “Goldilocks Effect”. The result from figure 4.5 indicates that a significant contribution from the trion state is present, even when the long off events (>20 ms) are removed, and that this shows a weak dependence with fraction-on. This is consistent with fast blinking events that do not significantly change the average fluorescence lifetime of a single QD. On the other hand, when the long off events are included in the single QD lifetime analysis, the dependence of the trion component with fraction-on is much stronger when the low fraction-on is lower than ~35% (*i.e.* when the long off states contribute significantly to the time-averaged signal). This indicates the presence of slow blinking events that do change the average fluorescence lifetime. The relative contribution of each of these fast and slow blinking events determines the fraction of time a particular QD will spend above the threshold (fraction-on).

Figure 4.6 can be used to explain both these observations related to QD blinking - the “Goldilocks Effect” as well as the fast and slow blinking events. Induced lattice strain between CdS and ZnS causes the formation of interfacial trap states that allows charge carriers to become trapped. The thicker the ZnS outer shell, the more trap states are present. On the other hand, wavefunction confinement by the high band offset between CdS and ZnS reduces the accessibility for directly occupying the surface trap states from the delocalized state. The availability of shell/shell interfacial trap states in QDs that have a 3ML ZnS outer shell thickness is still relatively

small due to the fact that lattice strain has not built up significantly. Also, the accessibility to the surface trap states is significantly reduced due to its exponential decrease with shell thickness. As the shell increases by even a moderate 2ML more, lattice strain has built up to result in a significantly increased availability of shell/shell interfacial trap states.

Once the charge carrier is trapped in the interfacial trap states, it may either de-trap (green arrow, figure 4.6) or transfer to surface trap states (blue arrow, figure 4.6). While in a trapped state, absorption of another photon results in the formation of a trion state. The trapping-detrapping rate is proposed to be relatively fast ( $< \sim 20\text{ms}$ ), but slower than the fluorescence lifetime ( $> \sim 30\text{ ns}$ ), leading to a single time bin containing multiple events: excitonic emission, trion emission and trap emission. The trapping-detrapping rates, however, should have a characteristic timescale that is independent on the number of interfacial trap states since the average intensity of the on state does not vary significantly with either the ZnS shell thickness (figure 4.4D) or with the fraction of time a QD spends in the on state (Figure S6). Thus, there is an inherent limitation in the on-state brightness caused by this trapping-detrapping process.

The increase in the fraction of time that a QD spends on (fraction-on) as the ZnS outer-shell thickness is changed from 1 ML to 3 ML is primarily the result of increasing the average duration of the on state (Figure 4.4A) rather than decreasing the duration of the off-state (Figure 4.4B). The on-state duration then decreases again as the ZnS shell thickness increases to 5ML. Using, the schematic of figure 4.6, we can rationalize this result in terms of the connection between the interfacial-trap states and the surface-trap states, represented by the blue arrow, that leads to long-lived off states. When more interfacial trap states are present, there is a higher overlap between them and the surface trap states leading to an increased probability of transfer to these remote trap states, leading to long off times. Such a transfer could be controlled *via* a diffusive mechanism, such

as that predicted *via* diffusion controlled electron transfer (DCET)<sup>39, 40</sup> or a diffusive resonance energy model.<sup>41</sup> In other words, it is the increased number of interfacial trap states *coupled* with the unidirectionality of the transfer from interfacial trap state to surface trap state that leads to the slow blinking in thicker core/shell/shell QDs. This is why the window of opportunity for reducing blinking in small multishell QDs is so narrow.

Based on this model, increasing the CdS inner shell thickness should not significantly change the number of interfacial trap states, but should slightly reduce their accessibility, which is predicted to slightly reduce the blinking. Indeed, we found that increasing the inner shell thickness from 3ML CdS to 5ML CdS did have a small, but noticeable effect on reducing the blinking even more, as shown in figure 4.7, providing additional support to the model in figure 4.6.

As noted earlier, there is a wide distribution in fraction-on for the reduced-blinking QDs, even though their size distribution is no wider than the other samples. This suggests that the relative contribution of the fast and slow blinking processes is affected by the quality of the shell as well as its thickness. Only when the shells are of the optimal thickness and their quality is high, the QD will show a high fraction-on for the majority of the time. When this is the case, the trion decay component no longer reduces strongly with reduced blinking (Figure 4.5) due to fast blinking being the primary process over slow blinking.

Finally, to highlight the reproducibility in this observed “Goldilocks effect”, a new sample was synthesized using the same procedure but by a different student. This is shown in the supporting information as Figure S7. In this case, it was found that the least blinking core/shell/shell QD was CdSe/3ML CdS/4ML ZnS, followed by the blinking becoming worse for CdSe/3ML CdS/5ML ZnS. This data shows that the “Goldilocks effect” is reproducible within  $\pm 1$  ML of ZnS,

again highlighting the narrow window of opportunity for reducing blinking in core/shell/shell QDs when using SILAR and the CdSe/CdS/ZnS combination.

#### **4.4. Conclusion**

In conclusion, we have shown that by carefully balancing the confinement potential and the induced lattice strain by the thicknesses of the inner and outer shells in core/shell/shell QDs, it is possible to significantly reduce blinking while still maintaining their small size and having non-toxic ZnS as the outer shell. However the window of opportunity for doing so is rather narrow, leading to a “Goldilocks effect”. A model was proposed in which trap states at the shell/shell interface and at the shell-ligand interface at the outer surface of the quantum dots account for the various fluorescence properties, *i.e.* the quantum yield, fluorescence lifetime components and blinking. We found that increasing the duration of the on-times is caused by reducing slow blinking that is proposed to be the result of transfer from interfacial trap states to longer-lived surface trap states. However, fast blinking is still present in these samples that results in a significant trion state contribution caused by trapping-detrapping processes at the interfacial trap states that limits the QD brightness and ensemble PL QY. It can be expected that the strategy of balancing confinement potential and lattice mismatch at each interface will be useful for developing a range of QDs with finely tuned properties for a variety of applications. A significant advantage of these QDs is that using less toxic (*i.e.* Cd-free) outer shell surfaces combined with reduced blinking will be well-suited for bioimaging applications at the single molecule level.

## 4.5. Methods

**4.5.1. Chemicals.** Cadmium oxide (CdO, 90%, Sigma-Aldrich), selenium powder (Se, 99.99%, Alfa Aesar), zinc oxide (ZnO, 99%, Sigma-Aldrich), sulfur powder (S, 99.9%, Alfa Aesar), oleic acid (OA, tech. grade, Alfa Aesar), 1-octadecene (ODE, 90%, Alfa Aesar), octadecylamine (ODA, 95%, Acros Organics), tri-butylphosphine (TBP, 95%, Alfa Aesar), 5-carboxytetramethylrhodamine dye (5-CTMR dye, Invitrogen), poly(methyl methacrylate) (PMMA, Sigma-Aldrich) and tri-octylphosphine oxide (TOPO, Sigma-Aldrich) were used as purchased without further purification. Solvents: methanol, hexane, and acetone were of pure grade, except toluene which was of high purity grade for HPLC and were all bought from VWR international.

**4.5.2. CdSe Core Synthesis.** CdSe core samples were synthesized by modification of the literature methods.<sup>46-48</sup> Briefly, 0.04 M cadmium (Cd) precursor was prepared by degassing a mixture of 0.02565 g CdO, 0.4452 g OA and 2 g ODE under vacuum and then heating to 200°C under argon flow until the solution became clear. The temperature was then reduced to 50°C at which point 1.5092 g of ODA and 0.5026 g of TOPO was added, degassed and heated to 300°C under argon flow. At this temperature, a pre-made 0.04 M Se precursor solution (0.01579 g Se, 0.4653 g TBP and 1.37 g ODE) was swiftly injected and, after a few seconds, the heating mantle was removed to stop the growth of the particles. The solution was then allowed to cool to room temperature, and then purified by dissolving in approximately equal amounts of hexane and methanol. The mixture was centrifuged at 7,000 rpm for about 5 to 10 min. The process was repeated 3 times and the final, purified solution was kept in a refrigerator at 4°C for storage until the shelling process was performed.

**4.5.3. Shelling.** The shelling process was performed using a combination of thermal cycling (TC)<sup>23</sup> and successive ion layer adsorption and reaction (SILAR) methods.<sup>24</sup> Typically 0.04 M Cd or zinc (Zn) precursors were prepared in the same way as the Cd precursor described above, while 0.04 M S precursor followed the same method as that of Se. The starting CdSe core solution for shelling was prepared by mixing 1.5 mL of CdSe in hexane, 1.5 g ODA and 4 mL ODE in the reaction flask. Pre-calculated amounts of sulfur and either cadmium or zinc precursors, enough for the growth of a single monolayer (ML), were injected individually at a temperature of 180°C, allowed to equilibrate for 5 min each before raising the temperature to 210°C for an additional 20 min for the growth of a CdS shell ML and to 230°C for a ZnS shell ML. The S precursor was always injected first. Approximately 1 mL aliquots were taken out and dissolved in hexane for analysis prior to lowering the temperature for subsequent injection.

**4.5.4. Fluorescence and Absorption Spectroscopy.** Photoluminescence (PL) and absorbance spectra of the aliquots were measured with a Perkin Elmer LS 55 luminescence spectrometer and Hitachi U-3900H spectrophotometer, respectively. PL quantum yields (PL QYs) were measured by comparing the integrated area of each sample to that of 5-CTMR dye dissolved in methanol to the same optical density of 0.05 at the excitation wavelength of 500 nm.

**4.5.5. Transmission Electron Microscopy.** High resolution TEM (HRTEM) images were acquired on a Titan TEM (FEI) operating with an acceleration voltage of 300kV. Z-contrast scanning TEM (z-STEM) coupled with electron energy loss spectroscopy (EELS) were also obtained with the same Titan instrument, but in energy-filtered mode whereby a nanoscale probe of the beam is focused at one point as it is scanned across the survey region. TEM samples were prepared by depositing ~ 200  $\mu$ L of thoroughly purified sample on a thin film of carbon-coated copper grids.

The measurements of the QDs diameter was carried out using the Image J software and the EELS spectral analysis was performed using the digital micrograph software.

**4.5.6. Fluorescence Microscopy.** Fluorescence lifetimes and blinking measurements were measured using a MicroTime 200 fluorescence microscope (PicoQuant GmbH, Berlin, Germany), which is based on an Olympus IX71 microscope equipped with PicoHarp 300 TCSPC controller.<sup>34</sup>  
<sup>49</sup> It uses a 485 nm laser (PDL 485, Picoquant) operating at 10  $\mu$ W power to excite the QDs, using a dichroic mirror (500dxxr, Chroma) to send the laser through a water immersion objective (Olympus, Apochromat 60x, NA 1.3) to achieve a diffraction-limited laser focus. The fluorescence is collected by the same objective and passed through the same dichroic mirror and a 100  $\mu$ m diameter pinhole. A fluorescence filter (605/55, Chroma) is placed in front of Single Photon Avalanche Diode Detector (MPD SPAD, Microphotonic devices, Bolano, Italy) to reject background fluorescence and scattered laser light. The objective is positioned on a subnanometer precision 3D piezo scanning stage (PI, Berlin, Germany). SymPhoTime software is used to control all acquisition and exporting functions.

For ensemble fluorescence lifetime measurements, the pulsed laser was operated with a repetition rate of 2.5 MHz and focused into a  $\sim$ 10 nM solution of QDs. For fluorescence blinking experiments, 50  $\mu$ l of highly diluted QDs ( $\sim$ 200 pM) containing  $\sim$ 3% (W/V) Poly(methyl methacrylate) (PMMA) in toluene was spin coated onto a clean No.1 glass coverslip to result in a thin film of immobilized single QDs in the PMMA film. Fluorescence images of 20  $\mu$ m  $\times$  20  $\mu$ m were recorded and then the laser focus was sequentially directed onto the individual well-isolated bright spots in the recorded fluorescence images to record 5 minute long fluorescence traces. The data was subsequently binned at 20 ms resolution for blinking analysis or binned using the TCSPC card into 32ps channels for fluorescence lifetime analysis. The data were exported in ASCII format, which are then analyzed by

a home-written program using Igor (Wavemetrics) to obtain distributions of on-times, off-times, on-time fractions, and the average fluorescence intensity of the on state from individual QDs. The fluorescence lifetime decay curves were analyzed using the freely downloadable program DecayFit (Fluorescence Decay Analysis Software 1.3, FluorTools, [www.fluortools.com](http://www.fluortools.com)) using the instrument IRF for iterative reconvolution fitting.

#### **4.6. Acknowledgments**

We would like to thank Dr. Mourad Benamara for technical help with STEM-EELS measurements. We would like to acknowledge generous financial support from the National Science Foundation (CHE-1255440), NIH NCRR (COBRE grant P30 RR031154-01) and the Arkansas Biosciences Institute.

#### **4.7. Supporting Information**

Spectral data for core-multishell QDs, threshold analysis, blinking data under pulsed laser illumination and Relationship between QD fluorescence lifetime decay components, average On intensity and Fraction-On for all thicknesses of ZnS. This supporting information is available free of charge on the ACS Publications website.



#### 4.8. References

1. Bruchez, M.; Moronne, M.; Gin, P.; Weiss, S.; Alivisatos, A. P., Semiconductor Nanocrystals as Fluorescent Biological Labels. *Science* **1998**, *281*, 2013-2016.
2. Chan, W. C.; Nie, S., Quantum Dot Bioconjugates for Ultrasensitive Nonisotopic Detection. *Science* **1998**, *281*, 2016-2018.
3. Alivisatos, A. P.; Gu, W.; Larabell, C., Quantum Dots as Cellular Probes. *Ann.Rev. Biomed. Eng.* **2005**, *7*, 55-76.
4. Shamirian, A.; Ghai, A.; Snee, P., QD-Based FRET Probes at a Glance. *Sensors* **2015**, *15*, 13028-13051.
5. Anikeeva, P.; Halpert, J.; Bawendi, M.; Bulovic, V., Quantum Dot Light-Emitting Devices with Electroluminescence Tunable over the Entire Visible Spectrum. *Nano Lett.* **2009**, *9*, 2532-2536.
6. Hines, M. A.; Guyot-Sionnest, P., Synthesis and Characterization of Strongly Luminescing ZnS-Capped CdSe Nanocrystals. *J. Phys. Chem.* **1996**, *100*, 468-471.
7. Dabbousi, B. O.; Rodriguez-Viejo, J.; Mikulec, F. V.; Heine, J. R.; Mattoussi, H.; Ober, R.; Jensen, K. F.; Bawendi, M. G., (CdSe)ZnS Core-Shell Quantum Dots: Synthesis and Optical and Structural Characterization of a Size Series of Highly Luminescent Materials. *J. Phys. Chem. B* **1997**, *101*, 9463-9475.
8. Chen, X.; Lou, Y.; Samia, A. C.; Burda, C., Coherency Strain Effects on the Optical Response of Core/Shell Heteronanostructures. *Nano Lett.* **2003**, *3*, 799-803.
9. Yu, Z.; Guo, L.; Du, H.; Krauss, T.; Silcox, J., Shell Distribution on Colloidal CdSe/ZnS Quantum Dots. *Nano Lett.* **2005**, *5*, 565-570.
10. Nirmal, M.; Dabbousi, B. O.; Bawendi, M. G.; Maklin, J. J.; Trautman, J. K.; Harris, T. D.; Brus, L. E., Fluorescence Intermittency in Single Cadmium Selenide Nanocrystals. *Nature* **1996**, *383*, 802-804.
11. Routzahn, A. L.; Jain, P. K., Luminescence Blinking of a Reacting Quantum Dot. *Nano Lett.* **2015**, *15*, 2504-2509.
12. Mews, A. *Fluorescence Microscopy and Spectroscopy of Individual Semiconductor Nanocrystals*, In Nanoparticle Assemblies and Superstructures. CRC Press LLC. Boca Raton, FL. **2006**, pp 103-123.
13. Cordones, A. A.; Leone, S. R., Mechanisms for Charge Trapping in Single Semiconductor Nanocrystals Probed by Fluorescence Blinking. *Chem. Soc. Rev.* **2013**, *42*, 3209-3221.
14. Krauss, T. D.; Peterson, J. J., Quantum Dots: A Charge for Blinking. *Nat. Mater.* **2012**, *11*, 14-16.
15. Cichos, F.; von Borczyskowski, C.; Orrit, M., Power-Law Intermittency of Single Emitters. *Curr. Opin. Coll. Int. Sci.* **2010**, *12*, 272-284.

16. Heyes, C. D.; Kobitski, A. Y.; Breus, V. V.; Nienhaus, G. U., Effect of the Shell on the Blinking Statistics of Core-Shell Quantum Dots: A Single-Particle Fluorescence Study. *Phys. Rev. B* **2007**, *75*, 125431.
17. Mahler, B.; Spinicelli, P.; Buil, S.; Quelin, X.; Hermier, J. P.; Dubertret, B., Towards Non-Blinking Colloidal Quantum Dots. *Nat. Mater.* **2008**, *7*, 659-664.
18. Chen, Y.; Vela, J.; Htoon, H.; Casson, J. L.; Werder, D. J.; Bussian, D. A.; Klimov, V. I.; Hollingsworth, J. A., "Giant" Multishell CdSe Nanocrystal Quantum Dots with Suppressed Blinking. *J. Am. Chem. Soc.* **2008**, *130*, 5026-5027.
19. Chen, O.; Zhao, J.; Chauhan, V. P.; Cui, J.; Wong, C.; Harris, D. K.; Wei, H.; Han, H. S.; Fukumura, D.; Jain, R. K.; Bawendi, M. G., Compact High-Quality CdSe-CdS Core-Shell Nanocrystals with Narrow Emission Linewidths and Suppressed Blinking. *Nat. Mater.* **2013**, *12*, 445-451.
20. Adachi, M. M.; Fan, F.; Sellan, D. P.; Hoogland, S.; Voznyy, O.; Houtepen, A. J.; Parrish, K. D.; Kanjanaboos, P.; Malen, J. A.; Sargent, E. H., Microsecond-Sustained Lasing from Colloidal Quantum Dot Solids. *Nat. Commun.* **2015**, 8694.
21. Tarafder, K.; Surendranath, Y.; Olshansky, J. H.; Alivisatos, A. P.; Wang, L.-W., Hole Transfer Dynamics from a CdSe/CdS Quantum Rod to a Tethered Ferrocene Derivative. *J. Am. Chem. Soc.* **2014**, *136*, 5121-5131.
22. Boldt, K.; Kirkwood, N.; Beane, G. A.; Mulvaney, P., Synthesis of Highly Luminescent and Photo-Stable, Graded Shell CdSe/CdxZn1-xS Nanoparticles by *In Situ* Alloying. *Chem. Mater.* **2013**, *25*, 4731-4738.
23. Blackman, B.; Battaglia, D. M.; Mishima, T. D.; Johnson, M. B.; Peng, X., Control of the Morphology of Complex Semiconductor Nanocrystals with a Type II Heterojunction, Dots vs Peanuts, by Thermal Cycling. *Chem. Mater.* **2007**, *19*, 3815-3821.
24. Li, J. J.; Wang, Y. A.; Guo, W.; Keay, J. C.; Mishima, T. D.; Johnson, M. B.; Peng, X., Large-Scale Synthesis of Nearly Monodisperse CdSe/CdS Core/Shell Nanocrystals Using Air-Stable Reagents *via* Successive Ion Layer Adsorption and Reaction. *J. Am. Chem. Soc.* **2003**, *125*, 12567-12575.
25. Zhang, A.; Bian, Y.; Wang, J.; Chen, K.; Dong, C.; Ren, J., Suppressed Blinking Behavior of CdSe/CdS QDs by Polymer Coating. *Nanoscale* **2016**, *8*, 5006-5014.
26. Talapin, D. V.; Mekis, I.; Götzinger, S.; Kornowski, A.; Benson, O.; Weller, H., CdSe/CdS/ZnS and CdSe/ZnSe/ZnS Core-Shell-Shell Nanocrystals. *J. Phys. Chem. B* **2004**, *108*, 18826-18831.
27. Xie, R.; Kolb, U.; Li, J.; Basche, T.; Mews, A., Synthesis and Characterization of Highly Luminescent CdSe-Core CdS/Zn0.5Cd0.5S/ZnS Multishell Nanocrystals. *J. Am. Chem. Soc.* **2005**, *127*, 7480-7488.
28. Fitzmorris, B. C.; Cooper, J. K.; Edberg, J.; Gul, S.; Guo, J.; Zhang, J. Z., Synthesis and Structural, Optical, and Dynamic Properties of Core/Shell/Shell CdSe/ZnSe/ZnS Quantum Dots. *J. Phys. Chem. C* **2012**, *116*, 25065-25073.

29. Hai, L. B.; Nghia, N. X.; Nga, P. T.; Chinh, V. D.; Trang, N. T. T.; Hanh, V. T. H., Preparation and Spectroscopic Investigation of Colloidal CdSe/CdS/ZnS Core/Multishell Nanostructure. *J. Exp. Nanosci.* **2009**, *4*, 277-283.
30. Jha, P. P.; Guyot-Sionnest, P., Trion Decay in Colloidal Quantum Dots. *ACS Nano* **2009**, *3*, 1011-1015.
31. Wei, S.-H.; Zunger, A., Calculated Natural Band Offsets of all II–VI and III–V Semiconductors: Chemical Trends and the Role of Cation d Orbitals. *App. Phys. Lett.* **1998**, *72*, 2011-2013.
32. Zhou, S.; Dong, L.; Popov, S.; Friberg, A. T., Radiative Properties of Carriers in CdSe-CdS Core-Shell Heterostructured Nanocrystals of Various Geometries. *J. Eur. Opt. Soc. - Rapid Pub.;* **2013**, *8*, 13042.
33. Peng, X.; Schlamp, M. C.; Kadavanich, A. V.; Alivisatos, A. P., Epitaxial Growth of Highly Luminescent CdSe/CdS Core/Shell Nanocrystals with Photostability and Electronic Accessibility. *J. Am. Chem. Soc.* **1997**, *119*, 7019-7029.
34. Durisic, N.; Godin, A. G.; Walters, D.; Gruetter, P.; Wiseman, P. W.; Heyes, C. D., Probing the "Dark" Fraction of Core-Shell Quantum Dots by Ensemble and Single Particle pH-Dependent Spectroscopy. *ACS Nano* **2011**, *5*, 9062-9073.
35. Omogo, B.; Aldana, J. F.; Heyes, C. D., Radiative and Nonradiative Lifetime Engineering of Quantum Dots in Multiple Solvents by Surface Atom Stoichiometry and Ligands. *J. Phys. Chem. C* **2013**, *117*, 2317-2327.
36. Krauss, T. D.; Brus, L. E., Charge, Polarizability, and Photoionization of Single Semiconductor Nanocrystals. *Phys. Rev. Lett.* **1999**, *83*, 4840-4843.
37. Efros, A. L.; Rosen, M., Random Telegraph Signal in the Photoluminescence Intensity of a Single Quantum Dot. *Phys. Rev. Lett.* **1997**, *78*, 1110-1113.
38. Kuno, M.; Fromm, D. P.; Johnson, S. T.; Gallagher, A.; Nesbitt, D. J., Modeling Distributed Kinetics in Isolated Semiconductor Quantum Dots. *Phys. Rev. B* **2003**, *67*, 125304.
39. Tang, J.; Marcus, R. A., Diffusion-Controlled Electron Transfer Processes and Power-Law Statistics of Fluorescence Intermittency of Nanoparticles. *Phys. Rev. Lett.* **2005**, *95*, 107401.
40. Tang, J.; Marcus, R. A., Mechanisms of Fluorescence Blinking in Semiconductor Nanocrystal Quantum Dots. *J. Chem. Phys.* **2005**, *123*, 054704.
41. Frantsuzov, P. A.; Marcus, R. A., Explanation of Quantum Dot Blinking Without the Long-Lived Trap Hypothesis. *Phys. Rev. B* **2005**, *72*, 155321.
42. Frantsuzov, P. A.; Volkan-Kacso, S.; Janko, B., Model of Fluorescence Intermittency of Single Colloidal Semiconductor Quantum Dots Using Multiple Recombination Centers. *Phys. Rev. Lett.* **2009**, *103*, 207402.
43. Schmidt, R.; Krasselt, C.; Gohler, C.; von Borczyskowski, C., The Fluorescence Intermittency for Quantum Dots Is Not Power-Law Distributed: A Luminescence Intensity Resolved Approach. *ACS Nano* **2014**, *8*, 3506-3521.
44. Frantsuzov, P.; Kuno, M.; Janko, B.; Marcus, R. A., Universal Emission Intermittency in Quantum Dots, Nanorods and Nanowires. *Nat. Phys.* **2008**, *4*, 519-522.

45. Galland, C.; Ghosh, Y.; Steinbruck, A.; Sykora, M.; Hollingsworth, J. A.; Klimov, V. I.; Htoon, H., Two Types of Luminescence Blinking Revealed by Spectroelectrochemistry of Single Quantum Dots. *Nature* **2011**, *479*, 203-207.
46. Peng, Z. A.; Peng, X., Nearly Monodisperse and Shape-controlled CdSe Nanocrystals *via* Alternative Routes: Nucleation and Growth. *J. Am. Chem. Soc.* **2002**, *124*, 3343-3353.
47. Yu, W. W.; Peng, X., Formation of High-Quality CdS and Other II-VI Semiconductor Nanocrystals in Noncoordinating Solvents: Tunable Reactivity of Monomers. *Angew. Chem. Int. Ed.* **2002**, *41*, 2368-2371.
48. Peng, Z. A.; Peng, X., Formation of High-Quality CdTe, CdSe, and CdS Nanocrystals Using CdO as Precursor. *J. Am. Chem. Soc.* **2001**, *123*, 183-184.
49. Gao, F.; Kreidermacher, A.; Fritsch, I.; Heyes, C. D., 3D Imaging of Flow Patterns in an Internally-Pumped Microfluidic Device: Redox Magnetohydrodynamics and Electrochemically Generated Density Gradients. *Anal. Chem.* **2013**, *85*, 4414-4422.

## Figures

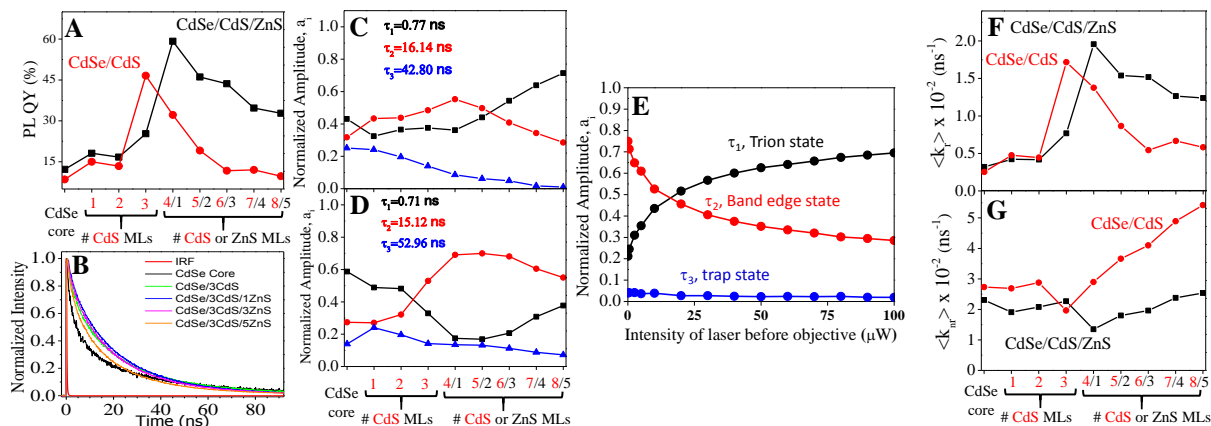


**Figure 4.1.** (A) PL quantum yields of CdSe/CdS core/shell QDs (red) and CdSe/CdS/ZnS core/shell/shell QDs (black) as a function of shell thickness. (B) Fluorescence lifetime decay curves of CdSe, CdSe/CdS core/shell and CdSe/CdS/ZnS core/shell/shell QDs with different shell thicknesses. (C) Relative amplitudes of decay components extracted from global fits to the set of decay curves for CdSe/CdS core/shell QDs. (D) Relative amplitudes of decay components extracted from global fits to the set of decay curves for CdSe/CdS/ZnS core/shell/shell QDs. (E) Relative amplitudes of decay components for CdSe/3ML CdS/3ML ZnS QDs as a function of power to support the assignments of each component to trion, band-edge and trap state emission, respectively. (F) Average radiative rate ( $\langle k_r \rangle$ ) for CdSe/CdS core/shell (red) and CdSe/CdS/ZnS core/shell/shell (black) QDs as a function of shell thickness. (G) Average non-radiative rate ( $\langle k_{nr} \rangle$ ) for CdSe/CdS core/shell (red) and CdSe/CdS/ZnS core/shell/shell (black) QDs as a function of shell thickness. [From Benard Omogo's thesis; Omogo, B.; Gao, F.; Bajwa, P.; Kaneko, M.; Heyes, C. D., Reducing Blinking in Small Core-Multishell Quantum Dots by Carefully Balancing Confinement Potential and Induced Lattice strain: The “Goldilocks” Effect. *ACS Nano* **2016**, *10* [4], 4072-4082]

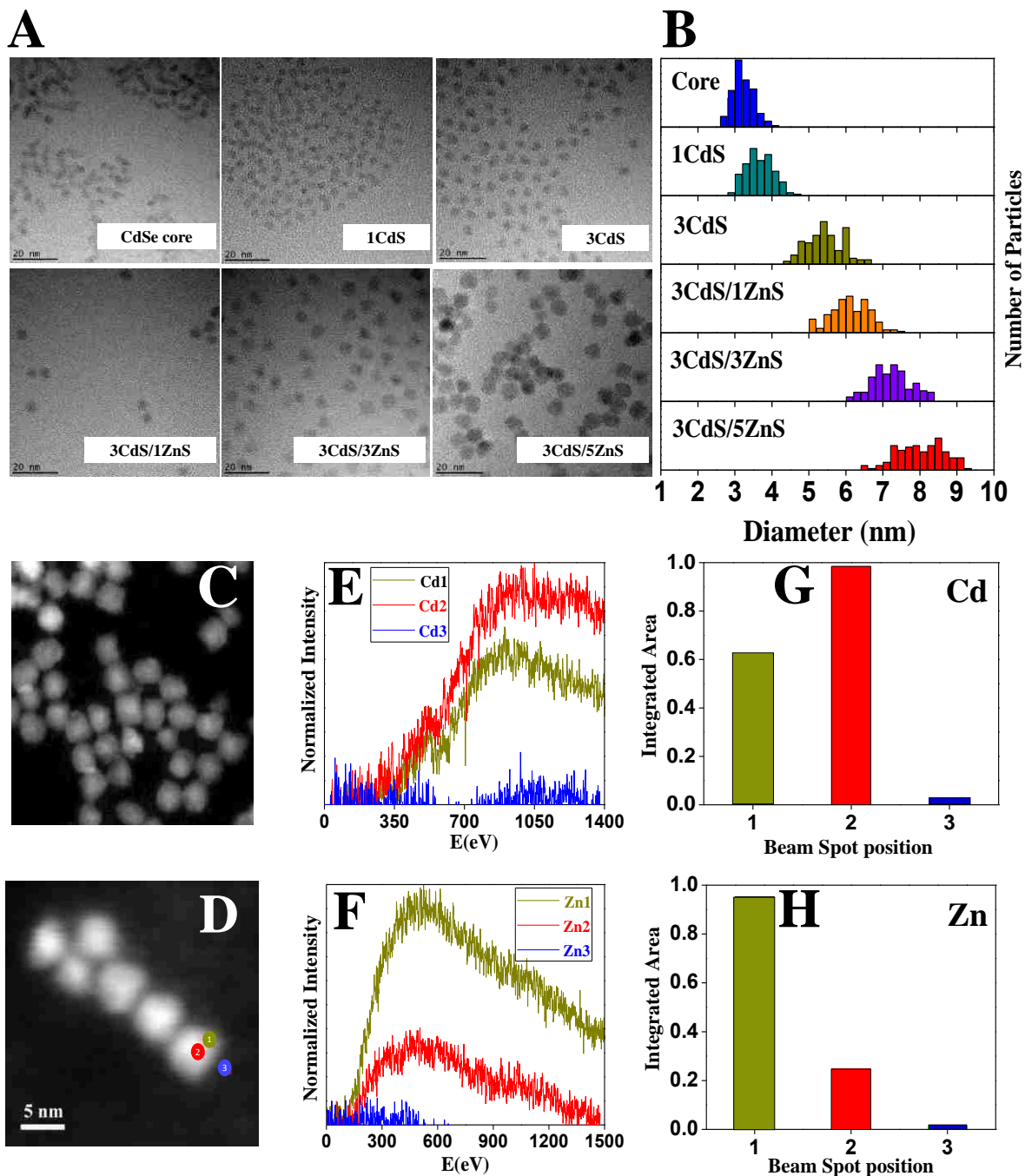


**Figure 4.2.** (A) TEM images of the selected samples together with their respective size distribution histogram (B). (C and D) Annular dark field (ADF)-STEM images of the CdSe/3CdS/5ZnS core/shell/shell sample. (E and F) are the electron energy loss spectra (EELS) of Cd and Zn signals, respectively, collected at positions indicated in figure D. (G and H) are the integrated area histograms calculated from the spectra in figures E (for Cd) and F (for Zn), respectively. [From Benard Omogo's thesis Omogo, B.; Gao, F.; Bajwa, P.; Kaneko, M.; Heyes, C. D., Reducing

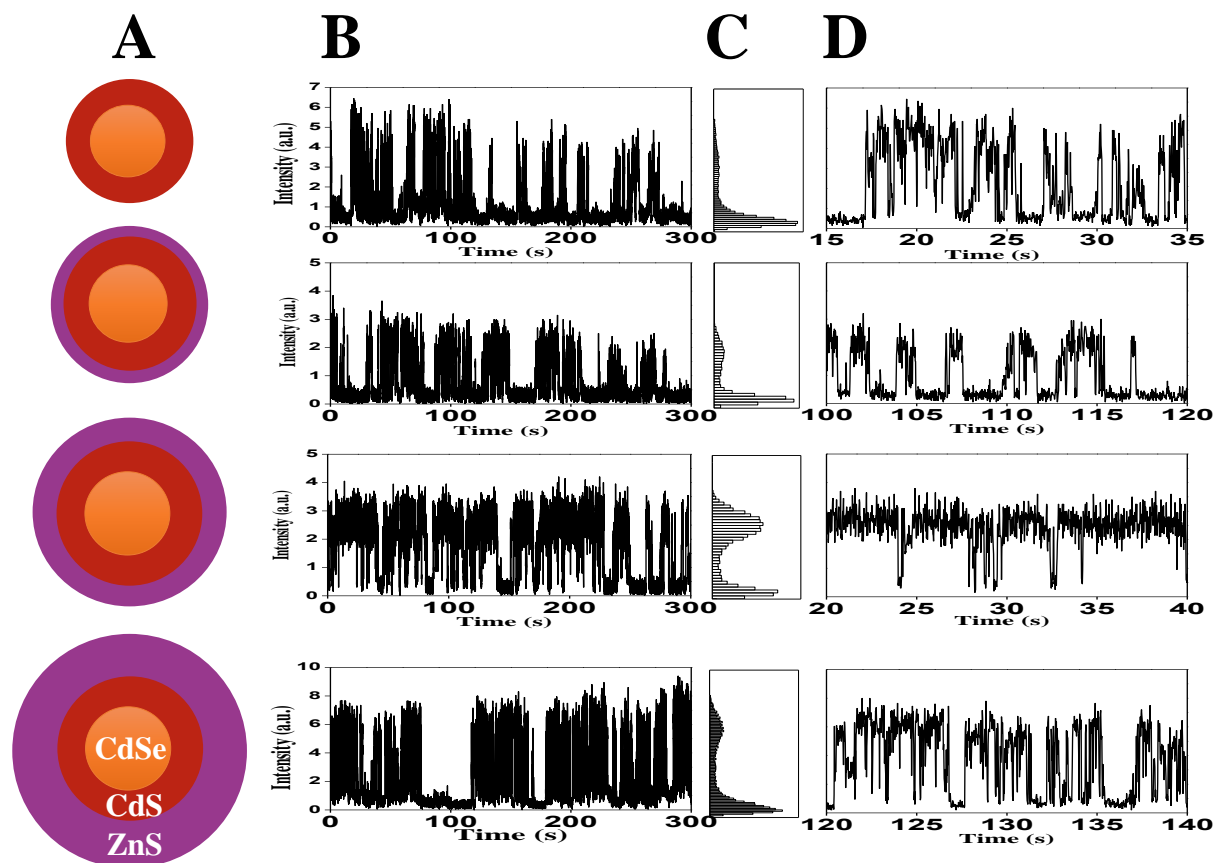


**Figure 4.3.** (A) Schematic structures of CdSe/CdS/ZnS core/shell/shell QDs with 0, 1, 3, and 5 ML ZnS outer shell. (B) The corresponding 300-s fluorescence traces of the synthesized CdSe/CdS/ZnS under cw laser excitation. (C) Photon counting histograms (PCHs) for the fluorescence traces shown in (B). (D) Zoomed in 20-s fluorescence traces showing the details of the fluorescence blinking behaviors of the QDs. [From Benard Omogo’s thesis; Omogo, B.; Gao, F.; Bajwa, P.; Kaneko, M.; Heyes, C. D., Reducing Blinking in Small Core-Multishell Quantum Dots by Carefully Balancing Confinement Potential and Induced Lattice strain: The “Goldilocks” Effect. *ACS Nano* **2016**, *10* [4], 4072-4082]

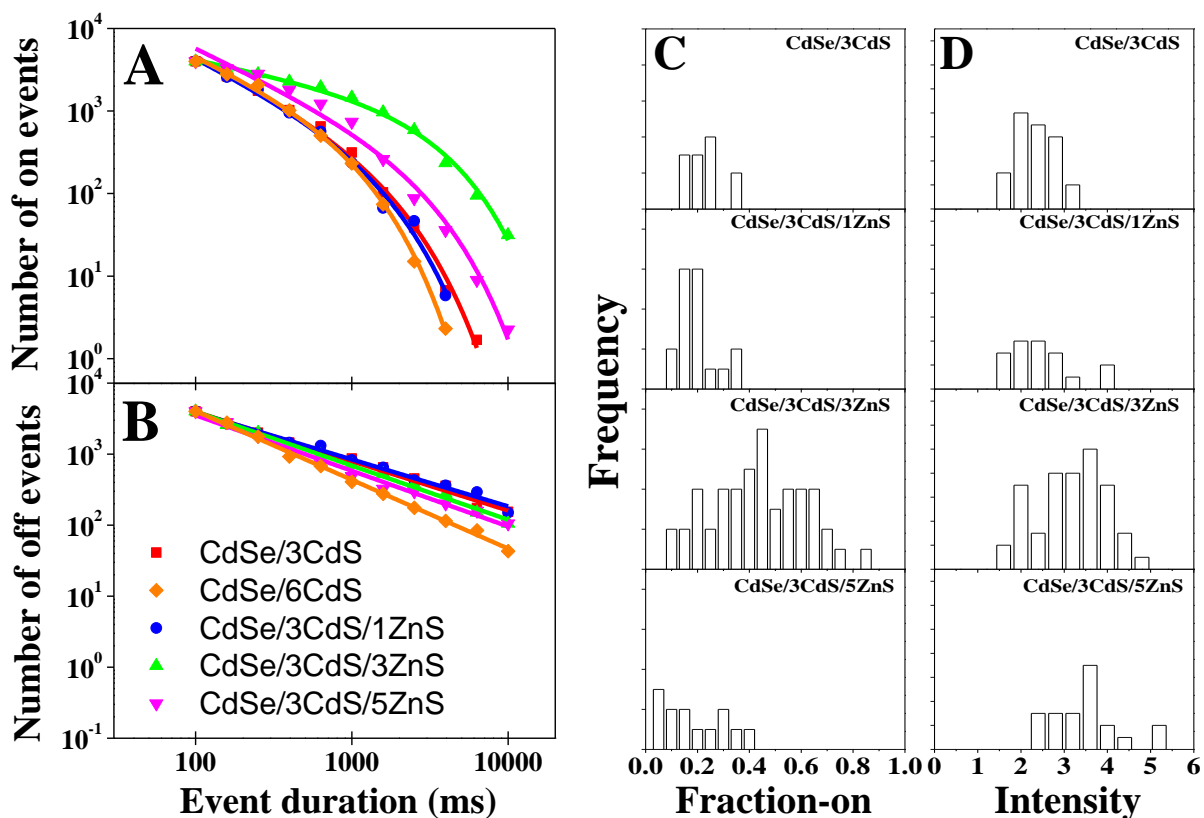


**Figure 4.4.** Log-log plots of  $P_{on}$  (A) and  $P_{off}$  (B) distributions for CdSe/CdS (red, orange) and CdSe/CdS/ZnS (blue, green, magenta) as a function of ZnS shell thickness under continuous wave laser excitation (pulsed laser excitation data is shown in supporting information). (C) Distributions of time spent by QDs in the on state (Fraction-on) for CdSe/CdS/ZnS QDs having 3 monolayers of CdS and different thickness of ZnS outer-shell under cw laser excitation. (D) Distributions of on state intensities for CdSe/CdS/ZnS QDs having 3 monolayers of CdS and different thickness of ZnS outer-shell under cw laser excitation. [From Benard Omogo's thesis; Omogo, B.; Gao, F.; Bajwa, P.; Kaneko, M.; Heyes, C. D., Reducing Blinking in Small Core-Multishell Quantum Dots by Carefully Balancing Confinement Potential and Induced Lattice strain: The “Goldilocks” Effect. *ACS Nano* **2016**, *10* [4], 4072-4082]



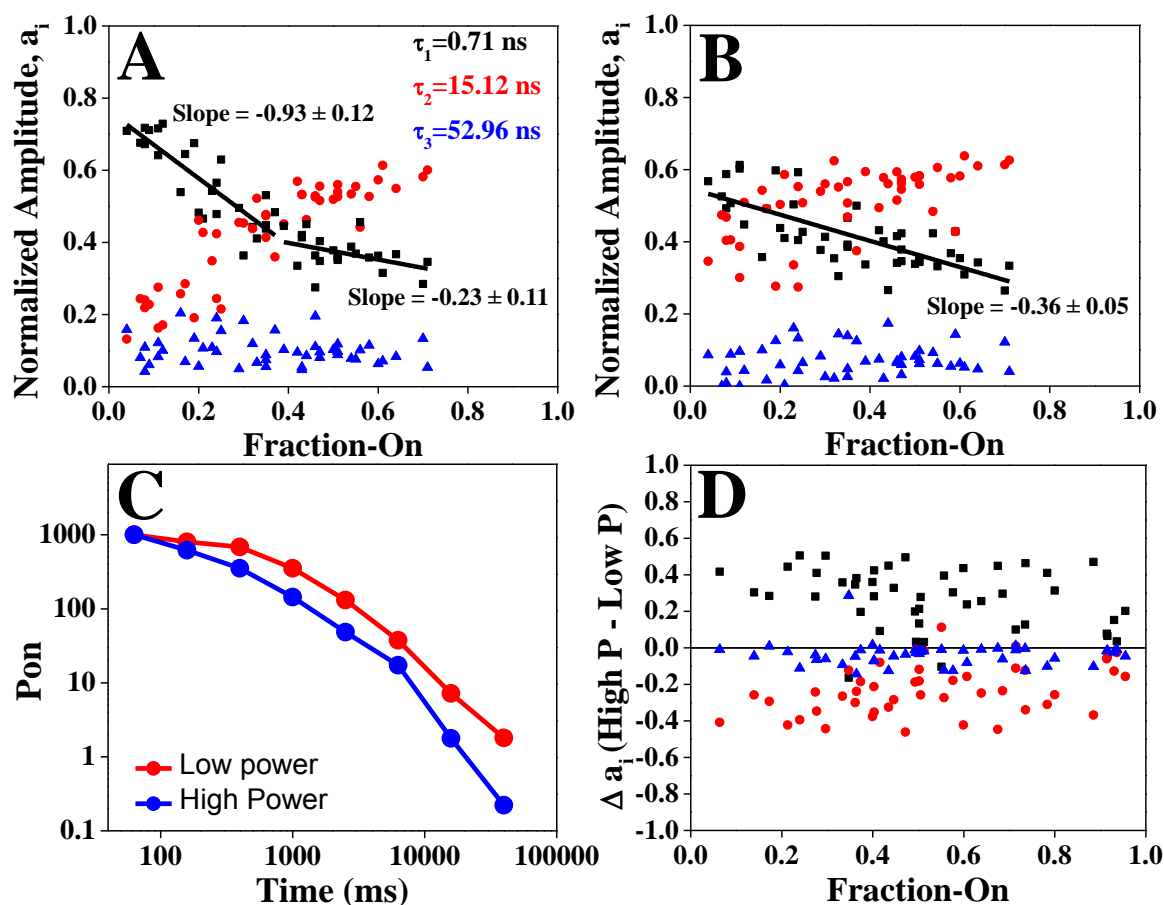


**Figure 4.5.** A) Relationship between QD fluorescence lifetime decay components of single CdSe/3ML CdS/3ML ZnS Core/Shell/Shell QDs and the fraction of time the QD spends in the “On” state during the blinking trace without applying threshold so that all on and off events are included. Linear fits to the fast lifetime (trion) component as a function of fraction-on in the low fraction-on and high fraction-on regions are overlaid B) Relationship between QD fluorescence lifetime decay components of single CdSe/3ML CdS/3ML ZnS Core/Shell/Shell QDs and the fraction of time the QD spends in the “On” state during the blinking trace after applying threshold to remove all off events. A linear fit to the fast lifetime (trion) component as a function of fraction-on is overlaid C) Probability distribution of on-times at low power and high power indicating that the on times are reduced at higher power. D) the change in the amplitude of fluorescence lifetime components of the *same* QD at high power – low power plotted as a function of that QDs Fraction-On at the lower power to support the assignment that the fast component observed in single QDs is the result of trion state formation. [Omogo, B.; Gao, F.; Bajwa, P.; Kaneko, M.; Heyes, C. D., Reducing Blinking in Small Core-Multishell Quantum Dots by Carefully Balancing Confinement Potential and Induced Lattice strain: The “Goldilocks” Effect. *ACS Nano* **2016**, *10* [4], 4072-4082]

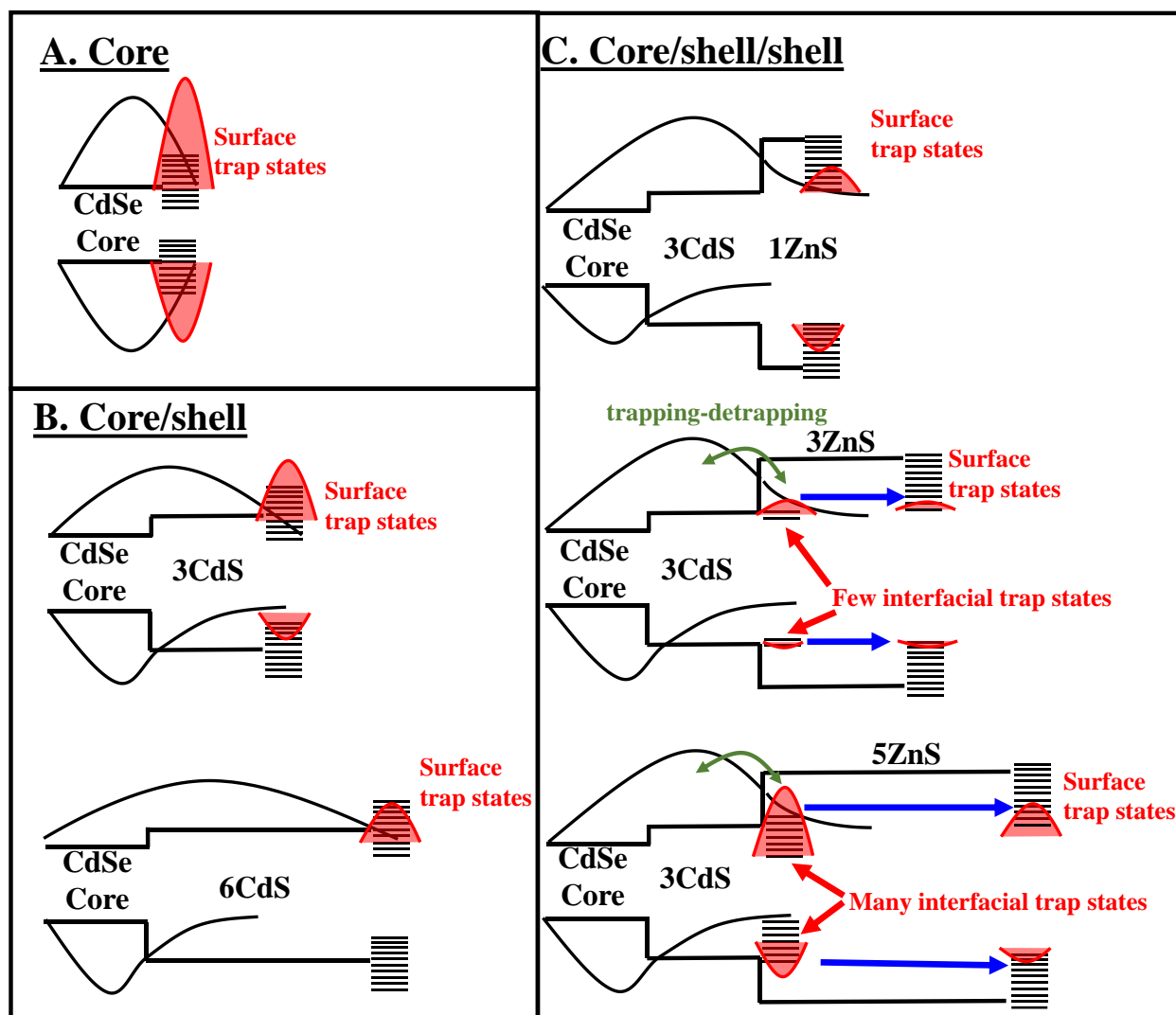


**Figure 4.6.** Proposed blinking model showing the conduction and valence bands of A) Core, B) CdSe/CdS core/shell and C) CdSe/CdS/ZnS core/shell/shell QDs, together with trap states at the surface and at the CdS/ZnS shell/shell interfaces. The black curves show the approximate wavefunctions of the delocalized electrons and holes. The red shaded area depicts the relative probability for charge carriers to be localized in these trap states based on both the relative number and accessibility. The green double-headed arrows represent fast trapping-detrapping processes at the interfacial trap states. The blue arrows represent possible transfer processes between the interfacial and long-lived surface trap states. The number of trap states at the CdSe/CdS interface is proposed to be negligible due to the much small lattice mismatch between CdSe and CdS (~3.8%). [Omogo, B.; Gao, F.; Bajwa, P.; Kaneko, M.; Heyes, C. D., Reducing Blinking in Small Core-Multishell Quantum Dots by Carefully Balancing Confinement Potential and Induced Lattice strain: The “Goldilocks” Effect. *ACS Nano* **2016**, *10* [4], 4072-408]

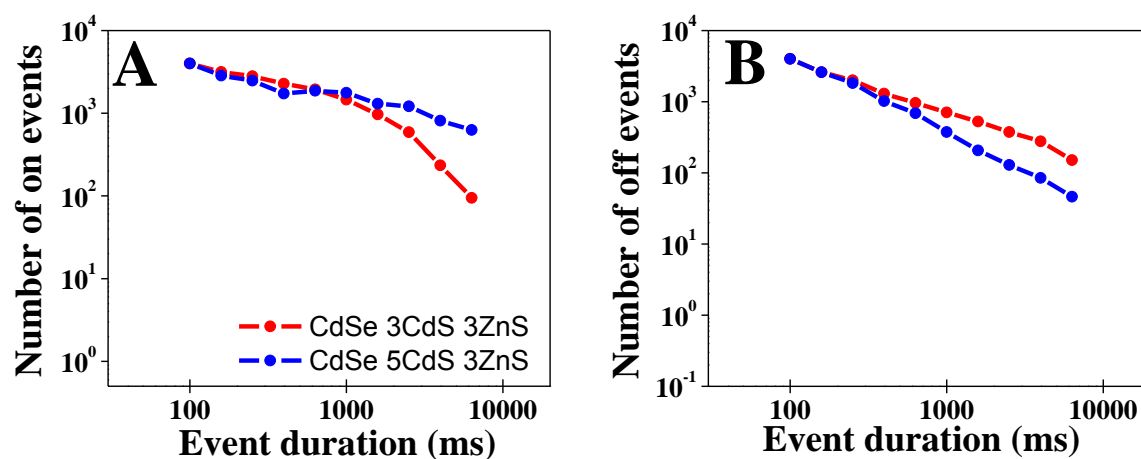
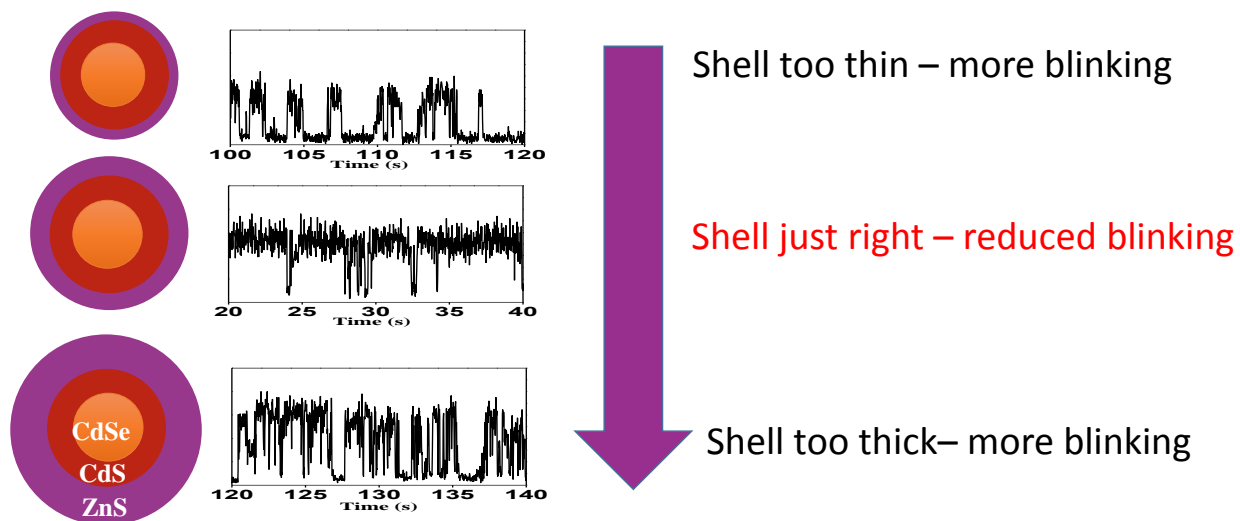


**Figure 4.7.** A) On-times probability distribution and B) Off-times probability distribution when the inner CdS is increased from 3ML to 5ML without changing the thickness of the outer shell. As predicted by the model shown in figure 6, QD blinking is slightly reduced when the inner CdS shell thickness is increased from 3ML to 5ML. [Omogo, B.; Gao, F.; Bajwa, P.; Kaneko, M.; Heyes, C. D., Reducing Blinking in Small Core-Multishell Quantum Dots by Carefully Balancing Confinement Potential and Induced Lattice strain: The “Goldilocks” Effect. *ACS Nano* **2016**, *10* [4], 4072-4082]

**Figure 4.8. TOC Graphic** [From Benard Omogo's thesis; Omogo, B.; Gao, F.; Bajwa, P.; Kaneko, M.; Heyes, C. D., Reducing Blinking in Small Core-Multishell Quantum Dots by Carefully Balancing Confinement Potential and Induced Lattice strain: The "Goldilocks" Effect. *ACS Nano* **2016**, *10* [4], 4072-4082]



## Chapter 5. Shell-Dependent Photoluminescence Studies Provide Mechanistic Insights into the Off-Grey-On Transitions of Blinking Quantum Dots

*Feng Gao, Pooja Bajwa, Anh Nguyen and Colin D. Heyes\**

*Department of Chemistry and Biochemistry, University of Arkansas, 345 N. Campus Drive,*

*Fayetteville, AR 72701*

*\*To whom correspondence should be addressed*

**5.1. Abstract:** The majority of quantum dot (QD) blinking studies have used a model of switching between two distinct fluorescence intensity levels, “on” and “off”. However, a distinct intermediate intensity level has been identified in some recent reports, a so-called “grey” or “dim” state, which has brought this binary model into question. While this grey state has been proposed to result from the formation of a trion, it is still unclear under which conditions it is present in a QD. By performing shell-dependent blinking studies on CdSe QDs, we report that the populations of the grey state and the on state are strongly dependent on both the shell material and its thickness. We found that adding up to 5 monolayers (ML) of a ZnS shell did not result in a significant population of the grey state. Using ZnSe as the shell material resulted in a slightly higher population of the grey state, although it was still poorly resolved. On the other hand, adding a CdS shell resulted in the population of a grey state, which depended strongly on its thickness between 1 and 5 ML. Interestingly, while the dwell time distribution and the brightness of the grey state did not change with CdS shell thickness, the frequency of transitions to and from the grey state had a very strong dependence. Moreover, we found that the grey state acts as an on-pathway intermediate state between on and off states, with the thickness of the shell determining the transition probability between them. Intensity-resolved single QD fluorescence lifetime analysis was used to identify the relationship between the various exciton decay pathways and the resulting intensity levels. We used this data to propose a model in which multiple states exist whose equilibrium populations vary with time that give rise to the various intensity levels of single QDs, and which depends on shell composition and thickness.

## 5.2. Introduction

Quantum dots (QDs) are semiconductor nanomaterials with applications in bioimaging<sup>1-4</sup>, sensors<sup>5,6</sup>, optoelectronics<sup>7-9</sup>, and renewable energy<sup>10-12</sup>. Their suitability in each of these applications requires control over the exciton decay pathways. Such control can be difficult due to the delocalized charge carriers entering trap states that can lead to fast non-radiative energy decay in the form of heat before more productive pathways such as radiative recombination (photonics) or charge separation (electronics) can occur. These trap states are strongly influenced by factors such as QD architecture<sup>13,14</sup>, structural defects<sup>15</sup>, surface ligands<sup>16,17</sup>, and the external environment<sup>18</sup>.<sup>19</sup> One way to better control radiative recombination or charge separation is to add one (or more) shells onto a core, and core/shell nanomaterials are more commonly used than core-only materials in most applications. Using type I core/shell materials, where both the electron and hole are confined to the core by the higher energy of the conduction and valence band states of the shell, increases photoluminescence (PL) quantum yield (QY), while charge separation is accomplished using type II core/shell materials, in which either the electron or hole has a lower energy in the shell. Quasi type I QDs results in one of the charge carriers to delocalize through the core and the shell, while the other charge carrier is localized to the core. However, in each case, trap states can also be introduced at the core/shell interface by induced lattice strain between the two materials, which affects the optical and electronic properties in complex ways.

It is known that single QDs show blinking behavior with fluorescence intensity fluctuations between on and off states, which is commonly interpreted in the framework of a two state model.<sup>20-27</sup> However, the existence of multiple-state blinking behaviors in some QDs have also been proposed.<sup>28-35</sup> Specifically, a distinct low-intensity level has been identified in some recent reports, the so-called “grey” or “dim” state. Other reports have postulated the fact that there is actually a

distribution of intensity levels that can be interpreted in the framework of a multiple recombination centers model<sup>36,37</sup> that fits blinking dynamics to a multi-exponential model rather than the commonly-used power-law dynamics model. If blinking is to be better controlled, it is imperative to relate how real physical states of the QD result in the different intensity levels. So far, reduced blinking has been reported in thick-shell (~16-19 monolayers (ML)) “giant” CdSe/CdS QDs<sup>25,38</sup>, in thinner-shell (~8 ML) highly-crystalline CdSe/CdS QDs<sup>39</sup>, in thin multi-shelled CdSe/CdS/ZnS QDs<sup>22</sup>, Zinc Blende structures<sup>40</sup> and in some reports of alloyed-shell QDs<sup>41</sup>. Some of these reports show the existence of the grey states and others have not. Although, the grey state has been postulated to result from either a positive trion<sup>29,30</sup> or a negative trion<sup>32,33,35,42</sup>, it is not yet clear under which conditions the grey state is formed, especially in how it relates to the shell architecture and to the suppression of blinking.

To address this question, we synthesized CdSe cores and systematically added either CdS, ZnSe or ZnS shells monolayer by monolayer using SILAR<sup>43</sup>. We found that the grey and on states are easily distinguishable when using CdS shells, but much less so when higher lattice mismatch shells (ZnSe and ZnS) are used. We found that, for CdSe cores, the fraction of time a QD spends in the grey state is negligible, but increases with each monolayer between 1 and 5 ML of CdS shell to ~30% of the time but does not change significantly if an extra 3 ML are added (8 ML total). The fraction of time spent in the on state rises in a similar way. We found that, although the probability of entering the grey state increases with shell thickness, its intensity or its dwell time does not. This is in contrast to the on state, which shows both an increase in intensity and dwell time with shell thickness. We found that the grey state is an on-pathway intermediate state between the off and on states, with the probability of entering the grey state from either the on or off state being higher than direct transitions for all shell thicknesses, but the extent of this ratio was very shell dependent.

Intensity-resolved fluorescence lifetime analysis was found to be multi-exponential in all intensity levels, with the amplitudes of each component depending on the intensity. We uncovered the existence of a very bright on state that had a very fast fluorescence lifetime component but was relatively short lived. A model was proposed to explain how a time-dependent equilibrium between various states led to the different intensity levels, and was used to explain how the transitions depended on the shell thickness and composition. It is expected that this model will be useful in developing strategies to better control blinking and to interpret exciton decay pathways in various core/shell QD architectures.

### 5.3. Results

Photoluminescence quantum yields (PL QY), PL  $\lambda_{\max}$  and TEM images of QDs as a function of the various shell materials and thicknesses are provided in the supporting information, and agree well with previous reports. TEM images show that the QD size increases as expected with shell thickness and that the shell grows isotropically.

#### *The grey state probability depends on the composition of the shell*

Figure 5.1 shows a typical CdSe/CdS QD blinking trace and photon counting histograms (PCHs) of representative QDs with different shells. It is already evident in the CdSe/CdS trace that there are three distinct fluorescence intensity levels, which the PCH quantifies. Clear peaks of Off, Grey and On states are present, which are well-resolved, highlighted by the boundaries at 8 counts/ms and 30 counts/ms, respectively. Using ZnS or ZnSe instead of CdS as the shell does not clearly resolve the grey state in the PCH or the blinking traces (example blinking traces of CdSe/ZnS and CdSe/ZnSe are shown in the supporting information), although there is a slightly



higher population of the grey and on states in CdSe/ZnSe than CdSe/ZnS. The population of the grey and on states thus appears to be anti-correlated with the lattice mismatch between the CdSe core and the shell (CdS<ZnSe<ZnS) suggesting that if a large number of defects at the core/shell interface induced by lattice mismatch are present, the grey state is poorly resolved. The fact that *more* interfacial trap states seems to result in *less* grey state formation initially seemed counterintuitive and prompted us to further investigate the details of grey state.

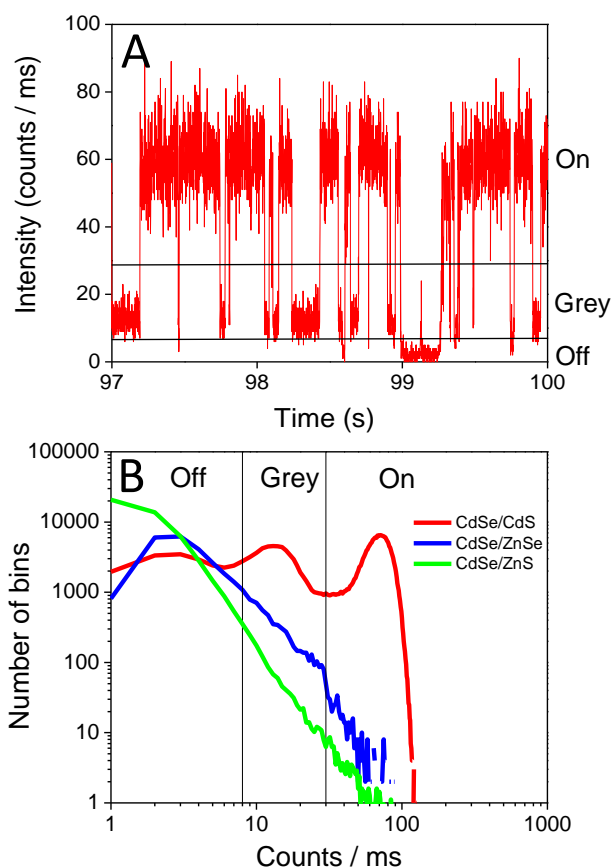


**Figure 5.1** – A) blinking trace of a single CdSe/5 ML CdS core/shell QD, highlighting the well-separated off, grey and on states. B) photon counting histograms (PCHs) of core/shell QDs of CdSe with either 5ML CdS (red), ZnSe (blue) or ZnS (green). The thresholds used to select the different states are highlighted.

***The thickness of the CdS shell increases the probability of the grey state formation, but not its intensity or its dwell time***

Figure 5.2 shows the probability distributions, intensity and fraction of time spent in the off, grey and on states as a function of CdS shell thickness. In general, from figures 5.2A-C, the on times become significantly longer from 0 to 5 ML CdS and then start to decrease slightly between 5 ML and 8 ML. The grey times show a similar trend to the on times, although the effect is much less. The off times become slightly longer with the first ML of CdS then become shorter as the shell thickness increases, saturating at about 5 ML CdS.

Figure 5.2D shows very interesting behavior in that, on average, the on state becomes brighter with increased CdS shell thickness (about two-fold brighter between 0 and 8 ML), but that the grey state intensity remains constant. This data is obtained by calculating the average intensity of each state in a given QD trace, with error bars representing the standard deviation in the average intensity from QD to QD. The upper and lower limits chosen for the grey state are 30 and 8 counts/ms, respectively, based on the photon counting histograms shown in figure 5.1. The average intensity of the grey state is 19 counts/ms with a standard deviation of ~1 counts/ms, highlighting that the limits are reasonably chosen. We obtain figure 5.2E by calculating the fraction of time a given QD trace spends in each of the off, grey and on states, with the error bars representing the standard deviation from QD to QD. For thin shells, the off state dominates, with only a small fraction of on and grey states. There is a continuous increase in the on and grey state fraction as the shell increases to 5ML. Between 5ML and 8 ML, there is a slight increase in the grey fraction and a slight decrease in the on fraction, although the changes are within the limits of the error bars suggesting that there is a saturating behavior in the blinking behavior with thicker shells.

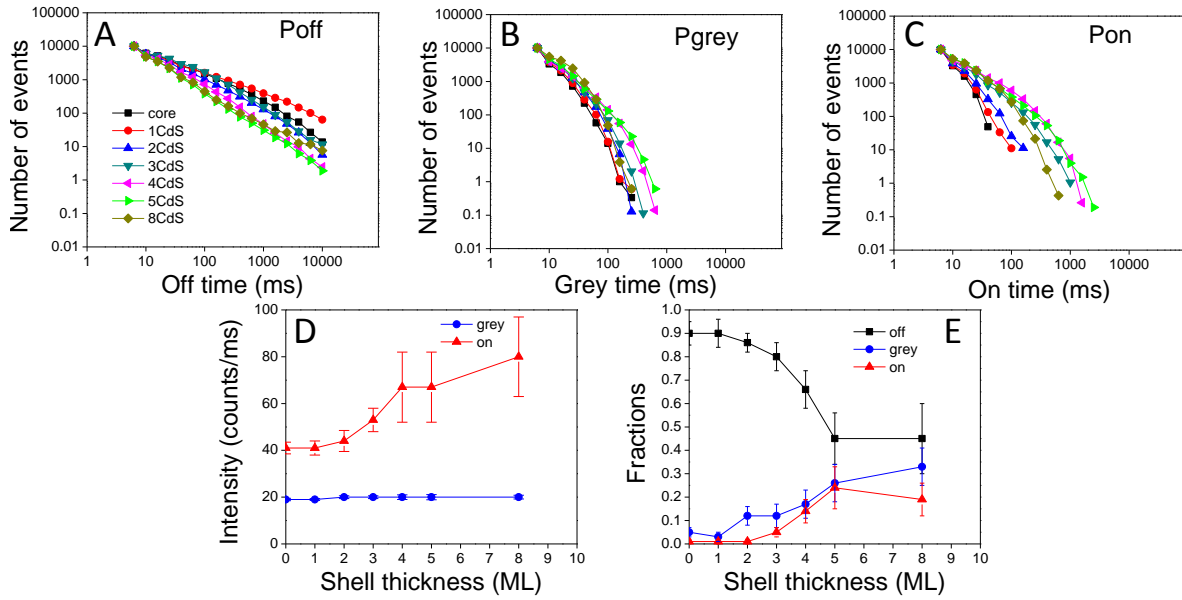


**Figure 5.2** – Probability distributions of A) Off, B) Grey and C) On dwell times (number of events normalized to the first time point to enable easy comparison). D) Average intensity of the grey (blue) and on (red) states as a function of CdS shell thickness. The error bars represent the standard deviation of the average intensity from QD-to-QD. E) The fraction of time a QD spends in the off (black), grey (blue) and on (red) states. The error bars represent the standard deviation of the average fraction of time from QD-to-QD.

*The QD shows stepwise blinking behavior with the grey state as an on-pathway intermediate between on and off transitions*

We calculated the ratios of transitions between the multiple states in Figure 5.3. The red and black curves demonstrate that there is a significant preference for transitions to the grey state from either the on state (red curve) or the off state (black curve) compared to direct transitions between the on and off states. The degree of preference for transitioning to the grey state depends strongly on shell thickness, showing a minimum around 3 ML, increasing with either thinner or thicker shells. However, even at the minimum, an off state is 5 times more likely to transition to a grey state than directly to the on state, and the on state is about 1.5 times more likely to transition to a grey state than directly to the off state. When the shell is thick (8ML), transitioning to the grey state is

30-40 times more likely that a direct transition from on-off or off-on. The blue curve shows that, once the QD is in the grey state, there is a preference to transition to the off state rather than the on state with thinner shells, but that they become equal in probability for shells thicker than 5 ML. This is consistent with the fact that coating thicker CdS shells onto CdSe core reduces the off state fraction to about 0.5 (Figure 5.2E).

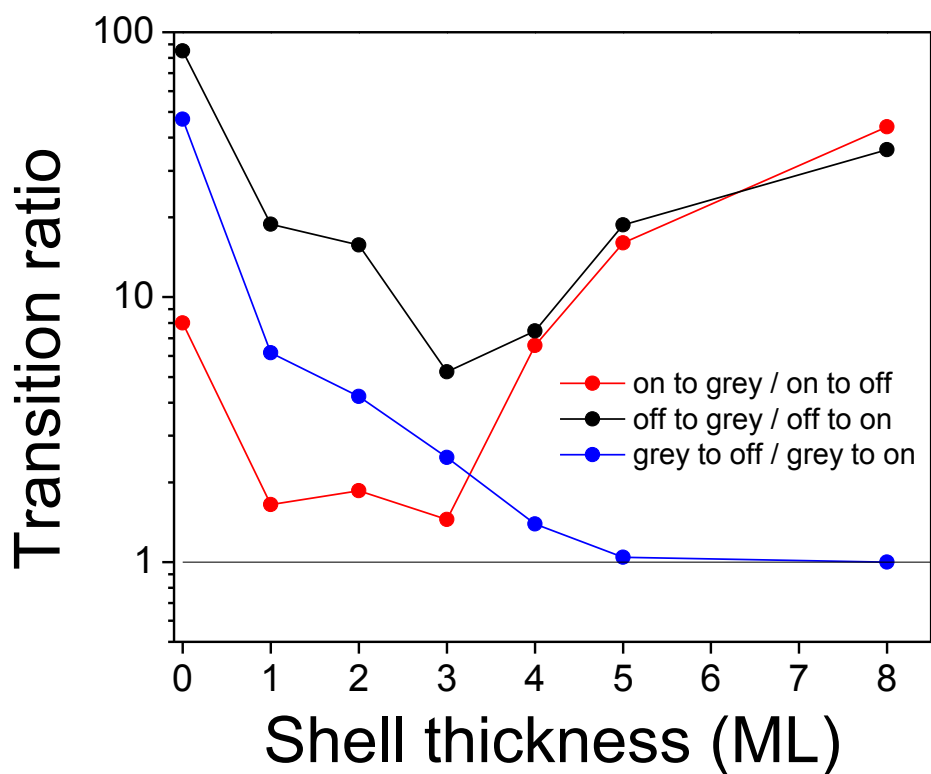


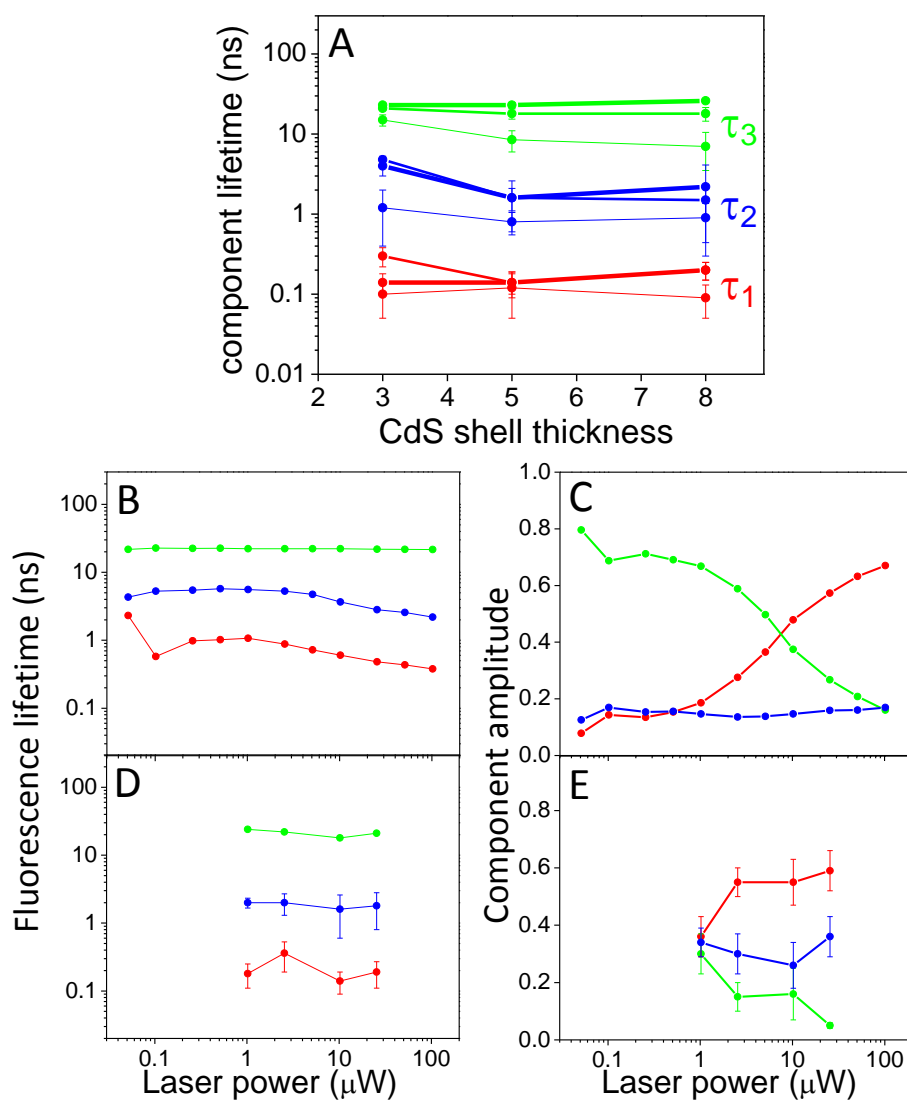
**Figure 5.3** – Ratio of transitions between the various states. Black - the ratio of times that, if the QD is in the off state, it will transition to the grey state rather than directly to the on state. Red - the ratio of times that, if the QD is in the on state, it will transition to the grey state rather than directly to the off state. Blue - the ratio of times that, if the QD is in the grey state, it will transition to the off state compared to the on state.

*Intensity-resolved fluorescence lifetime analysis of the grey and on states reveals multiple decay pathways*

To further gain mechanistic insights into what happens when a QD transitions between the grey and on states, we analyzed the single QD fluorescence lifetime data as a function of shell thickness, intensity level and dwell time in each state. Since the grey state fraction only becomes significant when the CdS shell thickness reaches 3ML CdS, we analyzed the fluorescence lifetime decay components for shell thicknesses of 3ML, 5ML and 8ML CdS (Figure 5.4A). Three exponentials were found to be the minimum number required to fit the data, as judged by the residuals and reduced chi-squared values, in agreement with previous reports on QD fluorescence lifetime analysis<sup>22, 44</sup>. All the fluorescence lifetime data are independently fitted with no constraints on the fitting parameters to enable as robust a fitting method as possible. In order to determine if changes in the average fluorescence lifetimes at different intensity levels result from changes to the characteristic lifetimes of the components or due to changes in their relative amplitudes (or both), we extracted only those photons from the blinking trace between the limits 8-30 kHz (Grey state), 30-150 kHz (low intensity on states) and >150 kHz (bright on states) and plotted them in figure 5.4A as thin, medium and thick lines, respectively. The error bars represent the standard deviation from QD-to-QD. Three distinct fluorescence lifetime components of  $\tau_1$  of ~0.1-0.2 ns,  $\tau_2$  of ~1-4 ns, and  $\tau_3$  of ~15-30 ns were found, with very little variation on either shell thickness or intensity level, suggesting that any changes in the average fluorescence lifetime results from changing the relative amplitudes of these distinct components, and not on fundamental changes in the decay pathways. Based on previously literature, we tentatively assigned the source of these components to be due to biexciton, trion and exciton processes<sup>29, 30, 32, 33, 35</sup>, respectively.

In order to verify these assignments, we performed a power-dependent study on one of the samples (CdSe/5 ML CdSe), expecting that amplitude of the bi-exciton (fastest) component should increase with laser power. This is shown in Figure 5.4B-E, at the ensemble (figure 5.4B-C) and

single QD level (Figure 5.4D-E). As observed for the different shell thicknesses and intensity levels, the fitted lifetime components are well-separated, and do not vary much over the range of excitation powers measured. However, the amplitude of the fast ( $\tau_1$ ) component increases with laser power, and that of the slowest ( $\tau_3$ ) component decreases. The  $\tau_2$  component has an approximately consistent amplitude at all laser powers. Due to the lower number of photons collected at the single QD level than the ensemble level, the lowest power that can be reached is  $\sim 1 \mu\text{W}$  in the single QD experiment, whereas the ensemble experiment can reach much lower excitation powers ( $< 0.1 \mu\text{W}$ ). Similarly, at very high excitation powers, blinking becomes significant that also reduces the collected number of photons in the single QD experiment. In the region that these two experiments overlap (1-20  $\mu\text{W}$ ) there are some similarities and some differences that are evident. Clearly, the 3 fitted lifetime components ( $\tau_1$ ,  $\tau_2$  and  $\tau_3$ ) are the same, and the trend of the amplitude of the fast component ( $a_1$ ) increasing and the amplitude of the slow component ( $a_3$ ) decreasing are similar. However, the exact amplitudes are different. At 1  $\mu\text{W}$ , the amplitudes of the fast component and the intermediate component are higher in the single QD experiment than in the ensemble experiment. The increase in the amplitude of the fast component saturates at about 2.5  $\mu\text{W}$  in the single QD experiment, whereas in the ensemble experiment it continues to increase up to  $\sim 100 \mu\text{W}$ . It is unclear at the moment as to the exact reason(s) for these differences, but it should be pointed out that differences between ensemble and single QD lifetimes have been observed previously and could be due to differences in the environment (embedded in PMMA for the single QDs vs in solution for the ensemble experiments) and/or due to the contribution of a “dark fraction” of QDs. Nevertheless, these experiments are consistent with our tentative assignment of the 3 lifetime components to be due to biexciton, trion and exciton processes.



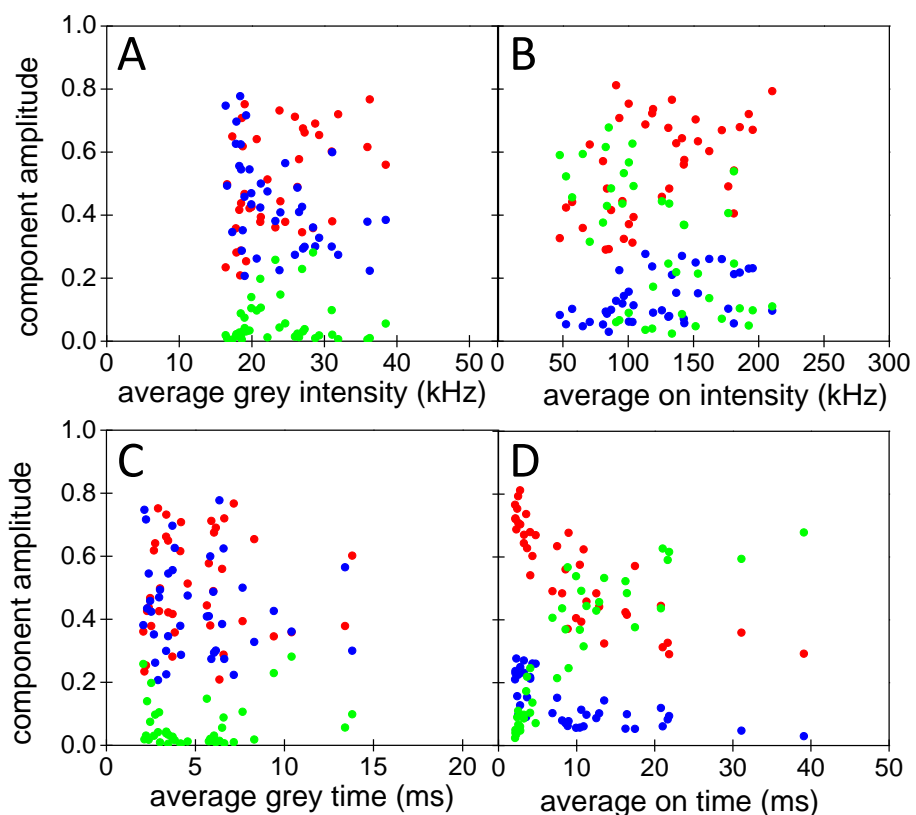
**Figure 5.4** – A) fitted fluorescence lifetime components from a multiexponential fitting of single QDs as a function of shell thickness. The thin lines only include photons between 8 and 30 counts/ms in the blinking trace, medium lines only include photons between 30 and 150 counts/ms and thick lines include only photons above 150 counts/ms. The fitted lifetime components are independent of both shell thickness and intensity level, suggesting that changes in intensity level are only due to differences in their relative amplitudes. Fitted fluorescence lifetime components and amplitudes as a function of laser excitation power at the ensemble (B, D) and single QD (C, E) level. For the single QD level, error bars represent the QD-to-QD standard deviation.

Figure 5.5 shows the fitted fluorescence lifetime component amplitudes for single QDs in the grey and on states as a function of the state intensity and its dwell time. This data is calculated

by extracting only photons from time bins that lie between the thresholds defining the grey and on states, respectively, and fitting them to three exponentials. Then, the component amplitudes is plotted against the average intensity of that state for each QD (Figure 5.5A-B) or against the average dwell time in each state for each QD (Figure 5.5C-D). In general, for the grey state (Figure 5.5A&C), the long timescale ( $\tau_3$ ) component is relatively low ( $<0.2$ ) for almost all the QDs and the two shorter lifetime components ( $\tau_1$  and  $\tau_2$ ) are approximately equal in amplitude. Although these components show a large amount of scatter from QD-to-QD, there is no specific dependence on either grey state intensity or its dwell time. On the other hand, for the on state (Figure 5.5B&D), the amplitudes of the three fluorescence lifetime components do appear to be dependent on both average intensity and average dwell time of the on state. Surprisingly, the amplitudes of the two fast ( $\tau_1$  and  $\tau_2$ ) components become larger and that of the slowest ( $\tau_3$ ) component becomes smaller as the average on state intensity becomes higher (Figure 5.5B). This seems to be in contradiction to the assignment that the slowest component is the highest quantum yield band-edge state and the faster components are due to low quantum yield biexciton and trion states. Figure 5.5D clearly shows that, as the average dwell time in the on state become longer, the amplitudes of the two fast ( $\tau_1$  and  $\tau_2$ ) components reduce and that of the slowest ( $\tau_3$ ) component increases. This result implies that there is an anti-correlation between the average intensity of the on state in a given QD and its average on time. This data is shown in Figure 5.6, and clearly shows that this is indeed the case.

Taken together, Figures 5.5 and 5.6 suggests that faster-blinking QDs (i.e. have shorter on times) are actually brighter when they are on and that they have higher amplitudes of the faster two components than slower-blinking QDs (i.e. have longer on times). This further suggests that a model of grey-to-on transitions as being simply due to transition from trion-to-exciton states is an incomplete picture.





**Figure 5.5** – fitted component amplitudes (same color scheme as in figure 4) for single QDs in the grey (A, C) and on (B, D) state as a function of the state intensity (A, B) and average state dwell time (C, D). Each colored dot represents the relative amplitude of that component in a single QD.

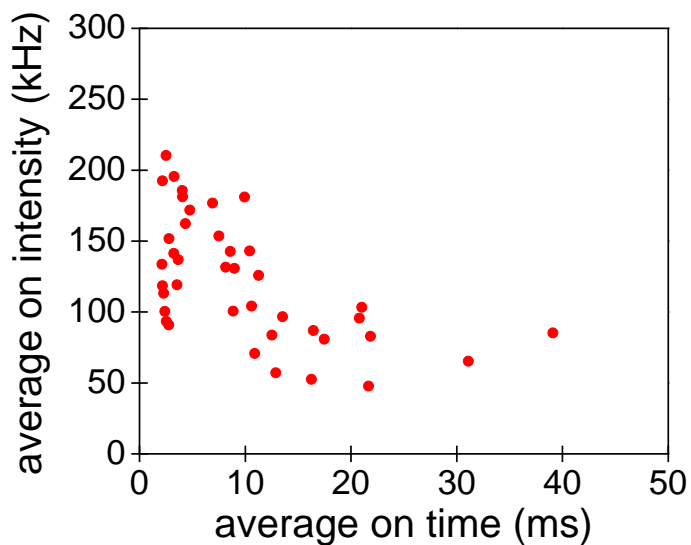


**Figure 5.6** – relationship between the average on intensity and the average on time of single QDs. Each dot represents a different QD.

## 5.4. Discussion

Developing a more complete model of grey-to-on transitions must incorporate the following key ideas based on the results discussed above:

- 1) The presence of the grey state depends on having a relatively low lattice strain at the core-shell interface. If the lattice strain becomes too high, the grey state probability is significantly reduced
- 2) The probability of forming the grey state increases with CdS shell thickness, saturating at ~5-8ML. However, once the QD is in the grey state, its intensity and dwell time does not depend on shell thickness.
- 3) Transitions between off and on states pass through the grey state in an on-pathway stepwise manner
- 4) Three distinct fluorescence decay components are present. The fastest (sub-ns) component is power dependent but is present in significant amplitudes in both the grey and the on states. The medium (~1-4 ns) component features heavily in the grey state but the slowest (~15-30 ns) component does not, while the opposite is true for the on state.
- 5) A sub-ns decay component contributes to a particularly bright on state, but that this state is short lived

It has been reported that a biexciton state has both a very low quantum yield and a fast (sub-ns) decay time<sup>35</sup>. The increase in the amplitude of the fast component with excitation power that we observe supports this fact. However, the correlation of the amplitude of this fast component with on-state intensity and anticorrelation with average on time seems to be in contradiction with this assignment. It is worth noting at this point that the relative amplitudes of the fluorescence lifetime components in the ensemble and single molecule experiments did not agree with each other, similar

to our previous reports, which may be due to a dark fraction not observable in single QD measurements<sup>13, 45-47</sup>. We had also previously postulated the existence of slow-blinking and fast-blinking events in core/multishell QDs<sup>22</sup>.

In order to explain all these observations, together with previous work that identified the role of trions in the grey state<sup>29, 30, 32, 33, 35</sup>, we postulated the model in figure 5.7 which build upon the idea of the multiple recombination centers model<sup>36</sup>. We rationalize the fact that there are multiple lifetime decay components in all fluorescence intensity levels that vary in relative amplitude but not in characteristic lifetime by proposing that there is an equilibrium set up between multiple states with certain characteristic lifetimes. The equilibrium is time-dependent, with the equilibrium position at any given time determining the fluorescence intensity level. In turn, the time-dependence of this changing equilibrium determines the dwell time in that particular level.

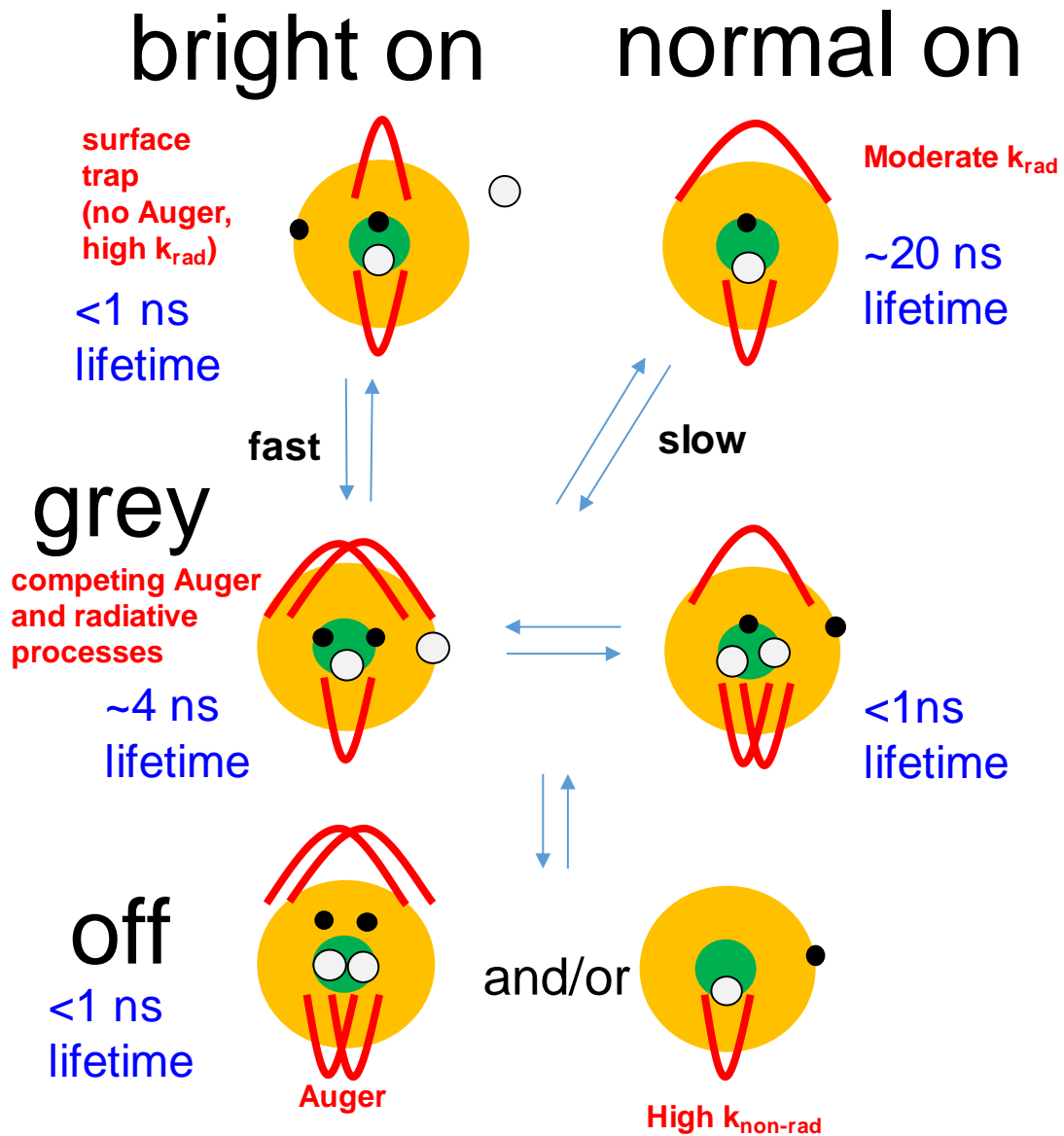


**Figure 5.7** – Model used to explain the blinking data. Black dots represent electrons and white circles represent holes. When the charge carrier is delocalized, the approximate wavefunction is shown in red above the electron or below the hole. The bright on state is proposed to be short lived, as represented by a fast-changing equilibrium while the normal on state is not as bright but longer lived, as represented by a more slowly hanging equilibrium. Proposed decay lifetimes for each state are given in blue with a description of the rationale in red.

The normal exciton emission is characterized by the fact that in CdSe/CdS QDs, being a quasi type-I QD, it is possible for the electron wavefunction to be distributed in both the core and the shell, but the hole wavefunction to be localized to only the core. This has the effect of lowering the overlap integral, leading to only a moderate radiative rate,  $k_{\text{rad}}$ . The exact  $k_{\text{rad}}$  will depend on the shell thickness but the  $k_{\text{non-rad}}$  will also vary with shell thickness since this will dictate the electron to lose its energy non-radiative at the shell surface. We reported the shell-dependent effect on the average  $k_{\text{rad}}$  and  $k_{\text{non-rad}}$  previously for core/shell vs core/shell/shell QDs<sup>22</sup>. Figure 5.3 shows that if the QD is on, before it turns off it will first pass through the grey state. In various reports, the grey state has been postulated to be either a positive trion<sup>29, 30</sup> or a negative trion<sup>32, 33, 35, 42</sup>. The study by Klimov and coworkers<sup>35</sup> found that for very thick-shell “giant” CdSe/CdS, the negative trion was brighter than the positive trion and had a longer lifetime while the positive trion was lower in intensity and had a faster lifetime. Fluorescence lifetime analysis of the grey state (figure 5.5A) shows both a <1ns and ~4ns component with widely varying amplitudes from QD to QD suggesting that both types of trion are possible, with the exact architecture of the single QD determining which is more likely. The details of this relationship between the grey state(s) and QD architecture and whether they can directly interconvert between each other or if they first pass through the off state will be the subject of future work.

As mentioned above, we observed a very bright but short-lived on-state in our CdSe/CdS QDs, similar to that recently observed by Schmidt et al for CdSe/ZnS QDs<sup>36</sup>. In our analysis of this state, we observed a correlation of the amplitude of a fast lifetime component with on state intensity and anti-correlation with on state time. This implies that there is a high quantum yield state with a very fast lifetime that can be accessed from the grey state but that this pathway is only available for a relatively short time. In our model, we propose that this bright on state is the result of trapping an

electron at the external trap state with the extra hole being ejected. If the shell is thick enough, trapping the electron at the surface would have the effect of repelling any excess delocalized electron so that its wavefunction is more in the core. This would effectively increase the overlap integral of the delocalized electron and hole wavefunctions, increasing  $k_{\text{rad}}$  and significantly reducing Auger processes. This would not be the case if the electron were ejected and a hole trapped at the surface, since the wavefunction of the second hole is already localized to the core, and the surface-trapped hole is not likely to increase the delocalized electron and hole overlap integral – in fact, the opposite is more likely. If our hypothesis of the very bright state is correct, this state is more likely to come from the negative trion grey state rather than the positive trion. Ejecting the hole when it is already trapped at the surface, followed by rapid electron trapping is a probably a more likely scenario than the extra hole from the core first becoming trapped followed by its subsequent ejection. However, technically, both possibilities are possible and more work is still needed to unambiguously make this assignment.

The off state can be the result of either biexciton processes or trapping of one of the charge carriers far from the other, as previously discussed. The increase in the fast lifetime component of either ensemble or single QDs with laser power (figure 5.4 C, E) agrees with the biexciton assignment, but it is known that blinking is still observed even at low laser power<sup>27, 48, 49</sup> suggesting that trapping is still responsible to some extent for off state. Different off states have been discussed in terms of two types of blinking<sup>50, 51</sup> and help explain why capping CdSe with ZnS does not reduce blinking<sup>21</sup> but using CdS does<sup>25, 38, 39</sup>.

This model proposed in figure 5.7 reasonably describes the various states underlying the multiexponential behavior in each state, but an important test of this model is whether it can be used explain the shell-dependent observations. Figure 5.7 describes the processes when the CdS shell is

thick (5.5-5.8 ML), specifically that the fraction of time a QD spends in the grey state is high and there is a 20-50 fold much higher probability of entering the grey state from either the on state or the off state compared to a direct transition between on and off. It is possible to redraw the model with a thinner shell (figure 5.8) to explain the processes that describe the following observations: as the shell becomes thinner (3ML), the population of the grey state decreases by about half (~30% to ~15%), the probability of an off-to-grey transition compared to an off-to-on transition decreases to ~5 fold, and the probability of an on-to-grey transition compared to an on-to-off transition decreases to ~1.5 fold. The on state intensity decreases by about 40% and the on state duration decreases slightly. These observations can be explained by adding an addition process that allows a direct transition between the trapped off state and the normal excitonic on state. This can be easily explained by the thinner shell allowing a rapid trapping-detrapping process. The fact that this new pathway does not pass through the bright on state also explains the average decrease in on state brightness. Furthermore, the fact that the on-to-off transition is more preferred over the off-to-on transition suggests that the trapping of the electron is faster than the detrapping, in line with the shorter on dwell time and longer off dwell time. Naturally, the presence of this pathway will decrease the probability of forming the grey state, but once it does form, the dwell time of the grey state will be unaffected, as we indeed observe.

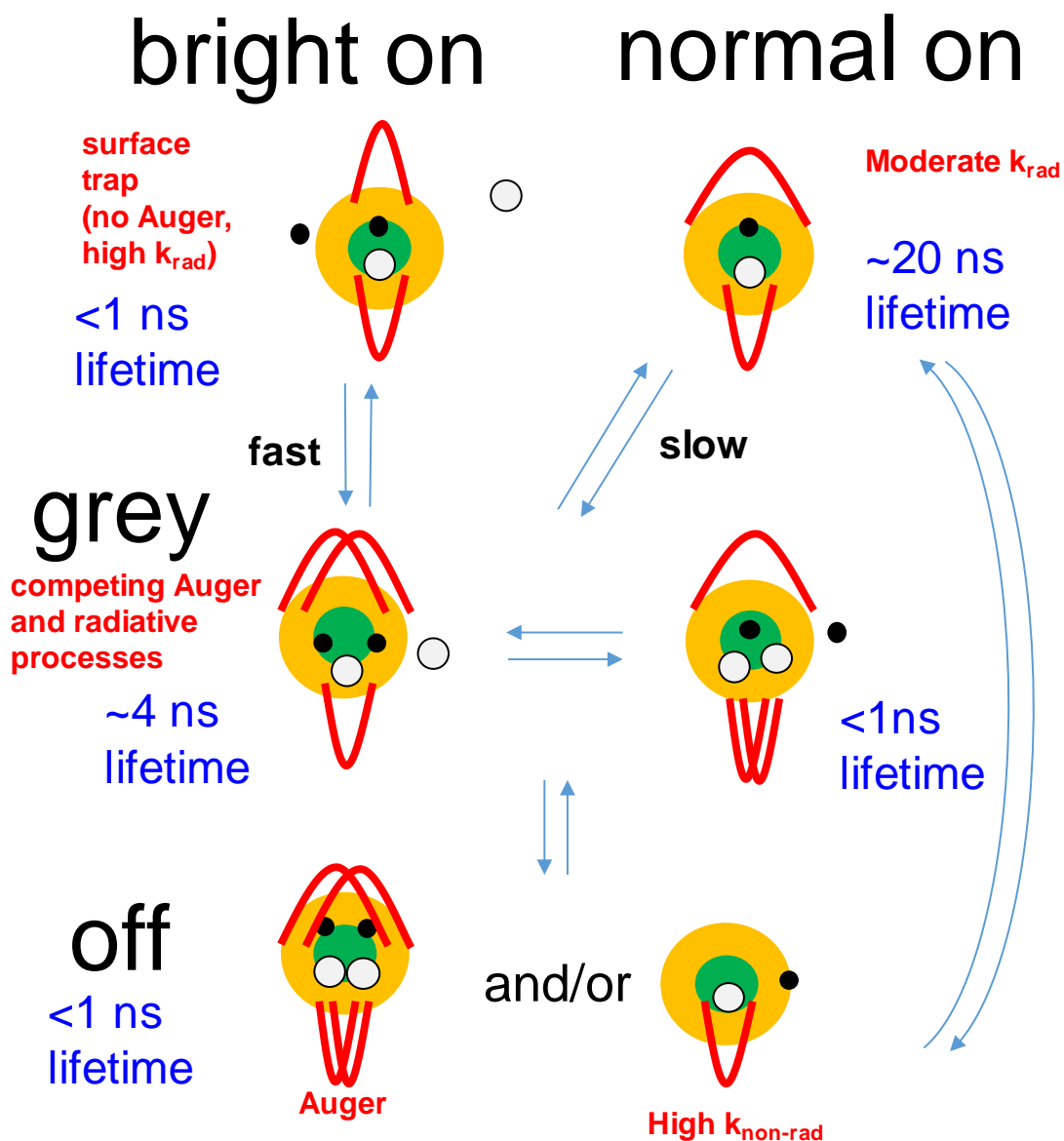


**Figure 5.8** – Redrawing of the model in figure 7 for thinner shells used to explain the faster blinking and the reduced grey state formation. A direct transition between off and on is now seen via a rapid trapping-detraping of the electron at the shell surface facilitated by the thinner shell.

When the shell becomes very thin ( $<2$  ML), it can be expected that the electron trapping rate from the excitonic on state to the trapped off state in this new pathway increases further due to the shorter distance through the shell that the electron has to go to become trapped, to the point that this



“shortcut” between on and off states now dominates over transitions to the grey state. This would explain why the fraction of time that the QD spends in the grey state is much lower, without affecting its dwell time when it does form a grey state. However, the transition ratio graph of figure 5.3 seems to suggest that the on-to-grey and off-to-grey transitions are more probable than the direct on-off or off-on transitions when the shell is  $<2$  ML. However, if a fast blinking process between the on and off states due to this new direct pathway now exists, this could show up as an average intensity between the on and off states (i.e. it would look like a grey state). Since this equilibrium is likely changing very rapidly, it would only show up within the grey state thresholds for 1-2 time bins before dropping either above or below it. In other words, with the rapid blinking behavior of thin-shelled QDs, it would be very difficult to now distinguish between the 3 different intensity levels unless the state was long-lived enough to reside in such a state for more than several consecutive time bins. This could be one reason why a wide distribution of intensity levels has sometimes been observed<sup>36, 52</sup>.

Similarly, the model can be used to explain the lower grey state population when there is a large amount of lattice strain at the interface, as is the case for ZnSe and ZnS shells. The large number of trap states at this interface caused by the lattice strain allows for a higher degree of trapping that leads to more direct on-to-off transitions. This interpretation may explain why ZnS shells are reported to not reduce blinking, even with up to  $\sim 7$  ML of ZnS<sup>21</sup>, and the fact that CdSe/ZnS QDs do not show a clear grey state. One recent report showed the presence of a small amount of grey state in CdSe/ZnS QDs under high excitation power<sup>34</sup>, which might be explained via our model as the result of the higher power forming more biexciton off-states that can then lead to trion grey states more readily. However, the QDs used in that study were commercial QDs and it is not clear if the core/shell interface is a sharp CdSe/ZnS interface or if the interface was made

smoother (either by alloying or adding a thin CdS shell) as QD commercial suppliers sometimes do to increase their PL QY.

## 5.5. Summary and Conclusions

We have systematically studied the role of the shell architecture on the off-grey-on transitions in blinking QDs. If a high lattice strain shell is used on CdSe, such as ZnSe and ZnS forming a type I core/shell QD with interfacial strain, the grey state is much less probable than using CdS, which forms a quasi type I QD with low lattice strain. We have quantified how the grey and on states evolve with increasing CdS shell thickness, in terms of the number of transitions to and from them as well as their intensity and dwell time. Our results show that QD blinking is stepwise with an on-pathway intermediate grey state linking the off and on states. Intensity-resolved fluorescence lifetime analysis shows that each intensity state contains multiple decay components, which is interpreted to result from various physical states with the equilibrium populations changing as a function of time. Interestingly, a fast decay component ( $<1$  ns) was found even in the on state, with its relative amplitude increasing with intensity but decreasing with average dwell time. We used this data to propose a model that contains multiple on and grey states. In particular, a very bright but short lived on state was proposed in which the extra electron from a negative trion is trapped in the shell that confines the other electron to increase its overlap integral with the hole. This model was used to explain the shell dependence with the opening up of a new pathway that directly connects the on and off states as the shell becomes thinner. This new “shortcut” pathway decreases the overall population of the grey state through decreasing the number of transitions to it, but not its dwell time once it does form. These results provide mechanistic insights into the shell dependence of QD blinking that may facilitate more efficient control of it to expand their various applications

in biology, particularly at the single molecule level, as well as in electro-optics and new energy materials.

## **5.6. Materials and Methods:**

**5.6.1. Chemicals:** Cadmium oxide (CdO, 90%, Sigma-Aldrich), selenium powder (Se, 99.99%, Alfa Aesar), zinc oxide (ZnO, 99%, Sigma-Aldrich), sulfur powder (S, 99.9%, Alfa Aesar), oleic acid (OA, tech. grade, Alfa Aesar), 1-octadecene (ODE, 90%, Alfa Aesar), octadecylamine (ODA, 95%, Acros Organics), tri-butylphosphine (TBP, 95%, Alfa Aesar), Sulforhodamine 101 dye (S 101 dye Invitrogen), poly(methyl methacrylate) (PMMA, Sigma Aldrich) and tri-octylphosphine oxide (TOPO, Sigma-Aldrich) were used as prepared without further purification. Solvents: All solvents were purchased from VWR international. Methanol, hexane and acetone were of pure grade. Toluene was of high purity HPLC grade.

**5.6.2. CdSe Core Synthesis:** CdSe core samples were synthesized by modification of the literature methods<sup>13, 53</sup>. Briefly, 0.04 M cadmium (Cd) precursor was prepared by degassing under vacuum and then heating a mixture of 0.02565 g CdO, 0.4452 g OA and 2 g ODE to 200°C under argon flow until the solution became clear. The temperature was then reduced to 50°C and then 1.5092 g ODA and 0.5026 g of TOPO was added. The reaction mixture was degassed again and heated to 300°C under argon flow. Once at this temperature, 0.4 M Se precursor solution (made from 0.1579 g Se, 0.4653 g TBP and 1.37 g ODE) was rapidly injected and, within a few seconds, the heating mantle was removed and reaction was quenched by adding hexane to avoid further growth of particles. After cooling the solution to room temperature, it was purified by washing with approximately equal amounts of hexane and methanol. The mixture was centrifuged for about 5 minutes at 7K rpm and process was repeated 2 more times.

**5.6.3. Core/shell/shell synthesis:** The shelling of CdSe core was accomplished by applying successive ion layer absorption and reaction (SILAR) with thermal cycling (TC).<sup>43</sup> Generally, 0.08 M Cd or Zn and 0.2 M Zn or Cd precursors (depending on the amount of precursor needed for each injection) were prepared by the same method as the Cd precursor while 0.08 M S or 0.08 M Se precursor were prepared in the same way as that of Se. The starting CdSe core solution for the shelling process was prepared by mixing together 3 mL of CdSe in hexane, 1.5 g ODA and 3 mL of ODE in a 3 necked reaction flask. Now, calculated amounts of Se or S and Zn or Cd were injected alternately one monolayer (ML) at a time at a temperature of 180°C, allowed to equilibrate for 5 minutes each, followed by crystallization of the shell by raising the temperature to 210°C for CdS or to 230°C for ZnSe or ZnS shell for 20 more minutes. The S or Se precursor was always injected first. Approximately 1 mL aliquots were taken out and dissolved in hexane after the growth of each ML before lowering the temperature and used for characterization. The first 5 ML injections were for either CdS or ZnSe shell while the last 3 ML injections were for the ZnS or CdS shell. All sample syntheses were performed at least twice to ensure reproducibility in the resulting optical and structural properties.

**5.6.4. Fluorescence and Absorption Spectroscopy:** Photoluminescence (PL) and absorbance of the aliquots for different monolayers were measured with a Perkin Elmer LS 55 luminescence spectrometer and Hitachi U-3900H spectrophotometer, respectively. PL percentage quantum yields (PL QYs) were measured by comparing the integrated areas of the PL spectra of QDs dissolved in hexane to that of the dye standard, Sulforhodamine 101 in ethanol, with the same optical density of 0.05 at the excitation wavelength of 530 nm.

**5.6.5. Transmission Electron Microscopy:** Transmission electron microscopy (TEM) and high resolution TEM (HRTEM) were performed using a Tecnai G2 F20-TWIN (TF20, FEI, Hillsboro,

OR). To prepare TEM samples, 200  $\mu\text{L}$  of thoroughly washed/purified samples were deposited on a thin film of carbon-coated grids. The QDs diameter was measured using the ImageJ software.

**5.6.6. Fluorescence Microscopy:** Fluorescence lifetimes and blinking measurements were measured using a MicroTime 200 scanning confocal fluorescence microscope (PicoQuant GmbH, Berlin, Germany), which is based on Olympus IX71 equipped with PicoHarp 300 TCSPC controller, was used.<sup>22, 45, 54</sup> It utilizes a 485 nm laser (PDL 485, Picoquant) operating in pulsed wave mode at a power of 10  $\mu\text{W}$  and repetition rate of 8 MHz for excitation of QD samples. A dichroic mirror (500dcxr, Chroma, McHenry, IL) sends the light through a water immersion objective (Olympus, Apochromat 60x, NA 1.3) to a diffraction-limited laser focus. The same objective collects the fluorescence and sends it through the same dichroic mirror and a 100  $\mu\text{m}$  pinhole. To reject background fluorescence and scattered laser light, a fluorescence filter that best matches the emission wavelength of the QDs (HQ560/40M for CdSe cores, HQ585/40M for CdSe/1CdS, HQ605/55M for CdSe/2CdS, HQ605/55M for CdSe/3CdS, HQ620/60M for CdSe/4CdS, HQ620/60M for CdSe/5CdS, HQ620/60M for CdSe/8CdS, HQ620/60M for CdSe/5CdS/3ZnS, HQ585/65M for CdSe/5ZnSe and HQ585/40M for CdSe/5ZnS, Chroma) is placed in front of Single Photon Avalanche Diode Detector (SPAD, MPI, Microphotonic devices, Bolano, Italy). For ensemble fluorescence lifetime measurements, the pulsed laser was operated with a repetition rate of 8 MHz and focused into a  $\sim 10$  nM solution of QDs. To perform blinking experiments, 50  $\mu\text{l}$  of a diluted quantum dot solution containing  $\sim 3\%$  (W/V) Poly(methyl methacrylate) (PMMA) in toluene was spin coated onto a clean No. 1 glass coverslip to make a thin film of immobilized single QDs in a PMMA matrix. The objective is positioned on a sub-nanometer precision 3D piezo scanning stage (PI, Berlin, Germany) and fluorescence images of 20 x 20  $\mu\text{m}$  were recorded. Then, from the recorded fluorescence images, the diffraction-limited focus was

focused onto the individually well-isolated bright spots to collect fluorescence time traces for up to 5 minutes. The collected photons were binned at 1 ms resolution for blinking analysis and the intensity-time data extracted for analysis of on and off time distributions using homemade analysis software written in Igor. All blinking data is the average of two separate preparations for each sample to ensure that the observed differences were reproducible. For fluorescence lifetime experiments, the photons are binned using the TCSPC card into 64ps channels for fluorescence lifetime analysis and the fluorescence lifetime decay curves were then analyzed using the freely downloadable program DecayFit (Fluorescence Decay Analysis Software 1.3, FluorTools, [www.fluortools.com](http://www.fluortools.com)) using the instrument IRF for iterative reconvolution fitting.

### **5.7. Acknowledgements**

Generous financial support by the NSF (CHE-1255440), the NIH (COBRE P30 GM103450), and the Arkansas Biosciences Institute is gratefully acknowledged. TEM instrumentation access is provided by the Arkansas Materials Characterization Facility (Funded in part by the NSF) and the Institute of Nanoscience and Engineering at the University of Arkansas.

## 5.8. References

1. Bruchez, M.; Moronne, M.; Gin, P.; Weiss, S.; Alivisatos, A. P., Semiconductor Nanocrystals as Fluorescent Biological Labels. *Science* **1998**, *281*, 2013-2016.
2. Chan, W. C. W.; Nie, S. M., Quantum dot bioconjugates for ultrasensitive nonisotopic detection. *Science* **1998**, *281* (5385), 2016-2018.
3. Alivisatos, A. P.; Gu, W. W.; Larabell, C., Quantum dots as cellular probes. In *Annual Review of Biomedical Engineering*, Annual Reviews: Palo Alto, 2005; Vol. 7, pp 55-76.
4. Mandal, G.; Darragh, M.; Wang, Y. A.; Heyes, C. D., Cadmium-free quantum dots as time-gated bioimaging probes in highly-autofluorescent human breast cancer cells. *Chemical Communications* **2013**, *49* (6), 624-626.
5. Shamirian, A.; Ghai, A.; Snee, P. T., QD-Based FRET Probes at a Glance. *Sensors* **2015**, *15* (6), 13028-13051.
6. Medintz, I. L.; Clapp, A. R.; Mattoussi, H.; Goldman, E. R.; Fisher, B.; Mauro, J. M., Self-assembled nanoscale biosensors based on quantum dot FRET donors. *Nat Mater* **2003**, *2* (9), 630-8.
7. Klimov, V. I.; Mikhailovsky, A. A.; Xu, S.; Malko, A.; Hollingsworth, J. A.; Leatherdale, C. A.; Eisler, H. J.; Bawendi, M. G., Optical gain and stimulated emission in nanocrystal quantum dots. *Science* **2000**, *290* (5490), 314-317.
8. Anikeeva, P. O.; Halpert, J. E.; Bawendi, M. G.; Bulovic, V., Quantum Dot Light-Emitting Devices with Electroluminescence Tunable over the Entire Visible Spectrum. *Nano Letters* **2009**, *9* (7), 2532-2536.
9. Ip, A.; Thon, S.; Hoogland, S.; Voznyy, O.; Zhitomirsky, D.; Debnath, R.; Levina, L.; Rollny, L.; Carey, G.; Fischer, A.; Kemp, K.; Kramer, I.; Ning, Z.; Labelle, A.; Chou, K.; Amassian, A.; Sargent, E., Hybrid passivated colloidal quantum dot solids. *Nature Nanotechnology* **2012**, *7* (9), 577-582.
10. Chuang, C.; Brown, P.; Bulovic, V.; Bawendi, M., Improved performance and stability in quantum dot solar cells through band alignment engineering. *Nature Materials* **2014**, *13* (8), 796-801.
11. Pattantyus-Abraham, A. G.; Kramer, I. J.; Barkhouse, A. R.; Wang, X.; Konstantatos, G.; Debnath, R.; Levina, L.; Raabe, I.; Nazeeruddin, M. K.; Gratzel, M.; Sargent, E. H., Depleted-Heterojunction Colloidal Quantum Dot Solar Cells. *ACS Nano* **2010**, *4* (6), 3374-3380.
12. Kamat, P. V., Boosting the Efficiency of Quantum Dot Sensitized Solar Cells through Modulation of Interfacial Charge Transfer. *Accounts of Chemical Research* **2012**, ASAP Article.
13. Bajwa, P.; Gao, F.; Nguyen, A.; Omogo, B.; Heyes, C. D., Influence of the Inner-Shell Architecture on Quantum Yield and Blinking Dynamics in Core/Multishell Quantum Dots. *ChemPhysChem* **2016**, *17* (5), 731-740.
14. Talapin, D. V.; Mekis, I.; Götzinger, S.; Kornowski, A.; Benson, O.; Weller, H., CdSe/CdS/ZnS and CdSe/ZnSe/ZnS Core-Shell-Shell Nanocrystals. *The Journal of Physical Chemistry B* **2004**, *108* (49), 18826-18831.

15. Chen, X.; Lou, Y.; Samia, A. C.; Burda, C., Coherency Strain Effects on the Optical Response of Core/Shell Heteronanostructures. *Nano Letters* **2003**, *3*, 799-803.
16. Talapin, D. V.; Rogach, A. L.; Kornowski, A.; Haase, M.; Weller, H., Highly Luminescent Monodisperse CdSe and CdSe/ZnS Nanocrystals Synthesized in a Hexadecylamine-Trioctylphosphine Oxide-Trioctylphosphine Mixture. *Nano Letters* **2001**, *1*, 204-211.
17. Breus, V. V.; Heyes, C. D.; Nienhaus, G. U., Quenching of CdSe-ZnS Core-Shell Quantum Dot Luminescence by Water-Soluble Thiolated Ligands. *Journal of Physical Chemistry C* **2007**, *111* (50), 18589-18594.
18. Lobo, A.; Borchert, H.; Talapin, D. V.; Weller, H.; Moeller, T., Surface oxidation of CdTe nanocrystals. A high resolution core-level photoelectron spectroscopy study. *Colloids Surf., A* **2006**, *286* (1-3), 1-7.
19. Adam, S.; Talapin, D. V.; Borchert, H.; Lobo, A.; McGinley, C.; De, C. A. R. B.; Haase, M.; Weller, H.; Moeller, T., The effect of nanocrystal surface structure on the luminescence properties: photoemission study of HF-etched InP nanocrystals. *Journal of Chemical Physics* **2005**, *123* (8), 084706/1-084706/10.
20. Nirmal, M.; Dabbousi, B. O.; Bawendi, M. G.; Macklin, J. J.; Trautman, J. K.; Harris, T. D.; Brus, L. E., Fluorescence intermittency in single cadmium selenide nanocrystals. *Nature* **1996**, *383* (6603), 802-804.
21. Heyes, C. D.; Kobitski, A. Y.; Breus, V. V.; Nienhaus, G. U., Effect of the Shell on Blinking Statistics in Single Core-Shell Quantum Dots - A Single Particle Fluorescence Study. *Phys Rev B* **2007**, *75*, 125431.
22. Omogo, B.; Gao, F.; Bajwa, P.; Kaneko, M.; Heyes, C. D., Reducing Blinking in Small Core-Multishell Quantum Dots by Carefully Balancing Confinement Potential and Induced Lattice Strain: The "Goldilocks" Effect. *ACS Nano* **2016**, *10*, 4072-4082.
23. Kuno, M.; Fromm, D. P.; Johnson, S. T.; Gallagher, A.; Nesbitt, D. J., Modeling distributed kinetics in isolated semiconductor quantum dots. *Physical Review B* **2003**, *67*, 125304.
24. Tang, J.; Marcus, R. A., Diffusion-Controlled Electron Transfer Processes and Power-Law Statistics of Fluorescence Intermittency of Nanoparticles. *Physical Review Letters* **2005**, *95* (10), 107401.
25. Mahler, B.; Spinicelli, P.; Buil, S.; Quelin, X.; Hermier, J. P.; Dubertret, B., Towards Non-Blinking Colloidal Quantum Dots. *Nature Materials* **2008**, *7* (8), 659-664.
26. Durisic, N.; Wiseman, P. W.; Grutter, P.; Heyes, C. D., A Common Mechanism Underlies the Dark Fraction Formation and Fluorescence Blinking of Quantum Dots. *Acs Nano* **2009**, *3* (5), 1167-1175.
27. Shimizu, K. T.; Neuhauser, R. G.; Leatherdale, C. A.; Empedocles, S. A.; Woo, W. K.; Bawendi, M. G., Blinking statistics in single semiconductor nanocrystal quantum dots. *Physical Review B* **2001**, *63*, 205316.
28. Zhang, K.; Chang, H.; Fu, A.; Alivisatos, A. P.; Yang, H., Continuous Distribution of Emission States from Single CdSe/ZnS Quantum Dots. *Nano Lett.* **2006**, *6*, 843-847.



29. Spinicelli, P.; Buil, S.; Quelin, X.; Mahler, B.; Dubertret, B.; Hermier, J. P., Bright and Grey States in CdSe-CdS Nanocrystals Exhibiting Strongly Reduced Blinking. *Physical Review Letters* **2009**, *102* (13), 4.
30. Gomez, D. E.; van Embden, J.; Mulvaney, P.; Fernee, M. J.; Rubinsztein-Dunlop, H., Exciton-Trion Transitions in Single CdSe-CdS Core-Shell Nanocrystals. *ACS Nano* **2009**, *3* (8), 2281-2287.
31. Amecke, N.; Cichos, F., Intermediate intensity levels during the emission intermittency of single CdSe/ZnS quantum dots. *Journal of Luminescence* **2011**, *131* (3), 375-378.
32. Qin, W.; Guyot-Sionnest, P., Evidence for the Role of Holes in Blinking: Negative and Oxidized CdSe/CdS Dots. *ACS Nano* **2012**, *6* (10), 9125-9132.
33. Rabouw, F. T.; Lunnemann, P.; van Dijk-Moes, R. J. A.; Frimmer, M.; Pietra, F.; Koenderink, A. F.; Vanmaekelbergh, D., Reduced Auger Recombination in Single CdSe/CdS Nanorods by One-Dimensional Electron Delocalization. *Nano Letters* **2013**, *13* (10), 4884-4892.
34. Hu, F. R.; Zhang, Q.; Zhang, C. F.; Wang, X. Y.; Xiao, M., Charged two-exciton emission from a single semiconductor nanocrystal. *Applied Physics Letters* **2015**, *106* (13), 4.
35. Park, Y. S.; Bae, W. K.; Pietryga, J. M.; Klimov, V. I., Auger Recombination of Biexcitons and Negative and Positive Trions in Individual Quantum Dots. *ACS Nano* **2014**, *8* (7), 7288-7296.
36. Schmidt, R.; Krasselt, C.; Gohler, C.; von Borczyskowski, C., The Fluorescence Intermittency for Quantum Dots Is Not Power-Law Distributed: A Luminescence Intensity Resolved Approach. *ACS Nano* **2014**, *8* (4), 3506-3521.
37. Frantsuzov, P. A.; Volkan-Kacso, S.; Janko, B., Model of Fluorescence Intermittency of Single Colloidal Semiconductor Quantum Dots Using Multiple Recombination Centers. *Phys. Rev. Lett.* **2009**, *103* (20), 207402/1-207402/4.
38. Chen, Y.; Vela, J.; Htoon, H.; Casson, J. L.; Werder, D. J.; Bussian, D. A.; Klimov, V. I.; Hollingsworth, J. A., "Giant" Multishell CdSe Nanocrystal Quantum Dots with Suppressed Blinking. *Journal of the American Chemical Society* **2008**, *130* (15), 5026-5027.
39. Chen, O.; Zhao, J.; Chauhan, V. P.; Cui, J.; Wong, C.; Harris, D. K.; Wei, H.; Han, H. S.; Fukumura, D.; Jain, R. K.; Bawendi, M. G., Compact high-quality CdSe-CdS core-shell nanocrystals with narrow emission linewidths and suppressed blinking. *Nat Mater* **2013**, *12* (5), 445-51.
40. Qin, H.; Niu, Y.; Meng, R.; Lin, X.; Lai, R.; Fang, W.; Peng, X., Single-Dot Spectroscopy of Zinc-Blende CdSe/CdS Core/Shell Nanocrystals: Nonblinking and Correlation with Ensemble Measurements. *Journal of the American Chemical Society* **2014**, *136* (1), 179-187.
41. Sonawane, K.; Agarwal, K.; Phadnis, C.; Sharma, D.; Layek, A.; Chowdhury, A.; Mahamuni, S., Manifestations of Varying Grading Level in CdSe/ZnSe Core-Shell Nanocrystals. *Journal of Physical Chemistry C* **2016**, *120* (9), 5257-5264.
42. Jha, P. P.; Guyot-Sionnest, P., Trion Decay in Colloidal Quantum Dots. *ACS Nano* **2009**, *3* (4), 1011-1015.
43. Li, J. J.; Wang, Y. A.; Guo, W.; Keay, J. C.; Mishima, T. D.; Johnson, M. B.; Peng, X., Large-Scale Synthesis of Nearly Monodisperse CdSe/CdS Core/Shell Nanocrystals Using Air-

- Stable Reagents via Successive Ion Layer Adsorption and Reaction. *J Am Chem Soc* **2003**, *125* (41), 12567-75.
44. Fitzmorris, B. C.; Cooper, J. K.; Edberg, J.; Gul, S.; Guo, J.; Zhang, J. Z., Synthesis and Structural, Optical, and Dynamic Properties of Core/Shell/Shell CdSe/ZnSe/ZnS Quantum Dots. *The Journal of Physical Chemistry C* **2012**, *116* (47), 25065-25073.
  45. Durisic, N.; Godin, A. G.; Walters, D.; Grutter, P.; Wiseman, P. W.; Heyes, C. D., Probing the "Dark" Fraction of Core-Shell Quantum Dots by Ensemble and Single Particle pH-Dependent Spectroscopy. *Acs Nano* **2011**, *5* (11), 9062-9073.
  46. Yao, J.; Larson, D. R.; Vishwasrao, H. D.; Zipfel, W. R.; Webb, W. W., Blinking and Nonradiant Dark Fraction of Water-Soluble Quantum Dots in Aqueous Solution. *Proceedings of the National Academy of Sciences of the United States of America* **2005**, *102*, 14284-14289.
  47. Owen, R. J.; Heyes, C. D.; Knebel, D.; Röcker, C.; Nienhaus, G. U., An Integrated Instrumental Setup for the Combination of Atomic Force Microscopy with Optical Spectroscopy. *Biopolymers* **2006**, *82*, 410-414.
  48. Kobitski, A. Y.; Heyes, C. D.; Nienhaus, G. U., Total internal reflection fluorescence microscopy - a powerful tool to study single quantum dots. *Applied Surface Science* **2004**, *234* (1-4), 86-92.
  49. Goushi, K.; Yamada, T.; Otomo, A., Excitation Intensity Dependence of Power-Law Blinking Statistics in Nanocrystal Quantum Dots. *J. Phys. Chem. C* **2009**, *113* (47), 20161-20168.
  50. Galland, C.; Ghosh, Y.; Steinbruck, A.; Sykora, M.; Hollingsworth, J. A.; Klimov, V. I.; Htoon, H., Two types of luminescence blinking revealed by spectroelectrochemistry of single quantum dots. *Nature* **2011**, *479* (7372), 203-U75.
  51. Krauss, T. D.; Peterson, J. J., QUANTUM DOTS: A charge for blinking. *Nature Materials* **2012**, *11* (1), 14-16.
  52. Zhang, K.; Chang, H. Y.; Fu, A. H.; Alivisatos, A. P.; Yang, H., Continuous distribution of emission states from single CdSe/ZnS quantum dots. *Nano Letters* **2006**, *6* (4), 843-847.
  53. Peng, Z. A.; Peng, X., Nearly Monodisperse and Shape-Controlled CdSe Nanocrystals via Alternative Routes: Nucleation and Growth. *Journal of the American Chemical Society* **2002**, *124* (13), 3343-3353.
  54. Gao, F.; Kreidermacher, A.; Fritsch, I.; Heyes, C. D., 3D Imaging of Flow Patterns in an Internally-Pumped Microfluidic Device: Redox Magnetohydrodynamics and Electrochemically Generated Density Gradients. *Analytical Chemistry* **2013**, *85* (9), 4414-4422.

## 5.9. Supporting Information for

### Shell-Dependent Photoluminescence Studies Provide Mechanistic Insights into the Off-Grey-On Transitions of Blinking Quantum Dots

Feng Gao, Pooja Bajwa, Anh Nguyen and Colin D. Heyes\*

Department of Chemistry and Biochemistry, University of Arkansas, 345 N. Campus Drive,

Fayetteville, AR 72701

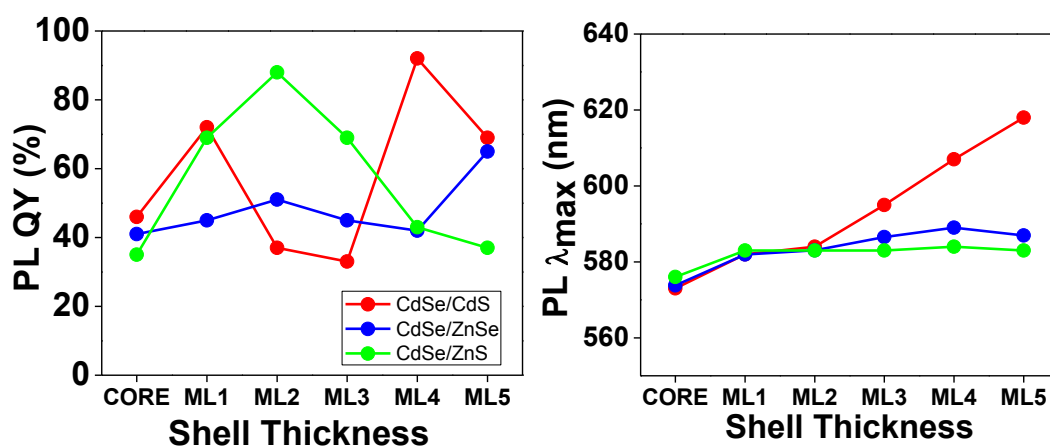


**Figure S1** – Photoluminescence quantum yield (PL QY) and PL maximum wavelength ( $\lambda_{max}$ ) as a function of shell material and thickness

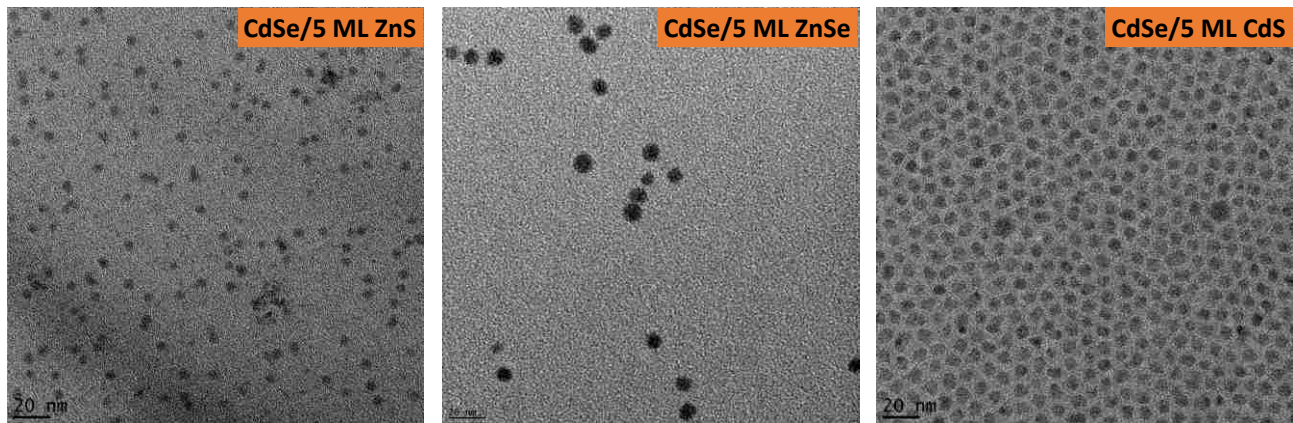


**Figure S2** – TEM images of CdSe QDs with 5 ML of ZnS, ZnSe or CdS shell

## Chapter 6. Conclusions and Outlook

This dissertation has been developed to understand the role of the inner shell architecture on the various blinking states and decay dynamics of core-shell and core-multishell quantum dots. In chapter 2, QDs with an inner CdS-shell and an outer ZnS shell were found to reduce blinking and so it is possible that these could be applied for tracking single biomolecules and other bioimaging applications at the single molecule level. QDs with an inner ZnSe-shell with an outer ZnS shell had a very high QY (~80%) and so, can be applied for the applications in LEDs, optoelectronics, sensors and in cellular bioimaging, where ensemble fluorescence properties are important. By investigating such different multi-shell combinations, we found that ensemble QY is not necessarily a good indicator of blinking behavior, highlighting that the relationship between ensemble behavior and single QDs is very complex. There might be two possible reasons for such uncorrelated behavior between QY and blinking. One possible factor might be the connection between blinking and dark fraction formation,<sup>1,2</sup> and the inner shell architecture could play a role in whether the worse blinking quantum dots are turned off or not. The other possible factor is that the inner shell architecture could lead to variations in the radiative and non-radiative rates of the on state(s). As part of this work, we used two different mathematical models to explain the on and off time distributions separately – truncated power law model and multi-exponential model. From these experiments, it was found that on-times are better explained by multi-exponential model while off-times can be better explained by truncated power law model, which possibly indicates that the mechanisms underlying switching on and switching off behaviors are different in origin. Future work can be extended further to investigate the relative contributions of these different possibilities. For example, these observations could be related to random static and/or dynamic heterogeneity in the environment of quantum dot such as ligand dynamics, surface reorganization or fluctuations in

the external, local environment. Therefore, the future work should be directed on systematically changing the environment to thoroughly investigate this mechanism.

In chapter 3, chapter 2 was extended to investigate whether the inner shell architecture leads to variations in the radiative and non-radiative rates by studying how different shell combinations affect the exciton decay dynamics due to the competing effects of the confinement potential and lattice mismatch. Using CdS-based inner shells, shelling had very little effect on  $\langle k_r \rangle$  but increased  $\langle k_{nr} \rangle$ , although only when the shells became thicker, and lattice strain built up to a significant amount to produce trap states. For ZnSe-based inner shelling, the lattice strain builds up quicker than CdS-based inner shelling, which increases non-radiative decay pathways with thinner shells. When the shells become thicker, it is likely that the increased confinement potential takes over and mitigates non-radiative decay pathways, presumably by reducing the accessibility of the trap states to non-radiative pathways, thus increasing ensemble PL QY. Also, one very interesting finding here was that the surface defects on the original core contributed significantly towards the overall optical properties of the final core/multishell QDs. Although the PL QY of the original core was similar for the original core, the exciton decay dynamics extracted from the fluorescence lifetime components varied, which affected the trends upon shelling. This observation encourages a more detailed study on the structural defects of the CdSe core by varying either the Cd:Se ratio or the ODA:TOPO ligands ratio while synthesizing the CdSe core QDs that will then be used for shelling.

In chapter 4, the effect of outer shell thickness (instead of the inner shell as studied in chapters 2 and 3) on ensemble fluorescence properties and blinking was investigated for CdSe/CdS/ZnS QDs. Here, it was found that the optimum shell thickness to reduce blinking the most was for 3ML of CdS and 3ML ZnS on CdSe core QDs. Thinner or thicker outer shells of ZnS increased blinking, leading to a “Goldilocks effect”.

Chapter 5 went deeper into the analysis of blinking by studying the presence of the grey state, and particularly how the off-grey-on transitions in core-shell QDs evolved with increasing shell thickness. We found that with more lattice strain, the lower the probability is of forming the grey state; CdSe/CdS shows the most obvious grey states and CdSe/ZnS QDs show negligible grey states. Our results showed that QD blinking is stepwise with the grey state as an on-pathway intermediate linking the on and off states. This kind of behavior is proposed to be due to the stepwise charge or discharge of QDs between trapped or delocalized exciton, trion, and biexciton states that have different quantum yields and fluorescence lifetimes. These results provided mechanistic insights into the shell dependence of QD blinking that may facilitate more efficient control to expand their various applications in biology, particularly at the single molecule level, as well as in electro-optics and new energy materials. A very interesting finding here was a very bright, but short-lived on-state, similar to that recently observed by Schmidt et al for CdSe/ZnS QDs.<sup>3</sup> The bright-on state was proposed to be due to a trapped trion state that might further depend upon how the surface defects of core are passivated by the ligands organization on surface of CdSe core or the Cd:Se atoms ratio.

It was discussed in the synthesis sections in chapters 2, 3 and 5 that the cores were all high quality (i.e. high quantum yield) QDs. One factor that we considered while synthesizing such high quantum yield QDs is the ratio of ODA:TOPO ligands ratio. It has been known<sup>4-7, 12</sup> that the higher the ratio of ODA ligands used compared to TOPO ligands, the higher the PL QYs that are usually obtained. One of the reasons behind this is as concluded by Ning et al<sup>6</sup> that although both the ligands are suitable for passivating the electron trap sites, TOPO tends to lead to a lower QY because the HOMO energy is closer to that of CdSe valence band, so it can extract the hole and thereby reduce the degree of overlap between electron and hole wave functions. This explanation is

true for the synthesis of our CdSe core QDs, where the QY range was 30% - 50%. However, in addition to ODA:TOPO ratio, we also maintained Cd:Se to be 1:10 that also contributes towards the high quantum yield of the QDs. One of the studies performed by Qu and Peng on the synthesis parameters for the organometallic synthesis of CdSe, using CdO and elemental Se as precursors.<sup>8,9</sup> According to them, higher Se:Cd ratios in the reaction mixture resulted in a higher QY for organic-soluble QDs. They proposed that this ratio becomes more important with respect to the organization of the passivating ligands on the surface rather than surface atomic stoichiometry. These results are opposite to those for the synthesis of high quantum yield CdTe QDs. As in recently published work by our lab, it has been found that Cd-rich surface shows higher quantum yield than a Te-rich surface.<sup>7</sup> The major reason behind this was proposed to be due to the higher radiative lifetime by uncoordinated Te atoms causing hole trapping processes. Also, it was found that co-ordinating ligands, primarily on the Cd-atoms, increases the non-radiative lifetime via a non-adiabatic coupling mechanism.

So, these contrasting results to our results encourage us to extend the work further toward synthesizing the CdSe core QDs with various ratios of Cd:Se and various ratios of ODA:TOPO ligands.. So, much work can be done to synthesize such QDs with different Cd:Se ratios or/and ODA:TOPO ratios. Then their various optical properties can be studied in future at ensemble level as well as at single molecule level with these QDs as it is done in chapters 2, 3 and 5 above. In chapter 4, the synthesis of QDs was also done by using 4:1 ratio of ODA:TOPO ligands and still the QDs obtained were low quantum yield QDs,<sup>9</sup> but this might also be due to the ratio of Cd:Se being 1:1. In addition to Cd:Se and ODA:TOPO ratios, there are several environmental factors such as the nature of ligands or pH of the solution that can affect the overall optical properties of the QDs.<sup>1,2</sup> Also, in the blinking studies of these QDs in this work, the fluorescence intensity of the blinking



traces was around 10 counts/ms only. However, for the QDs synthesized in chapters 2 and 3, the average fluorescence intensity of blinking traces is around 100 counts/ms. In addition to this, for the QDs (with Cd:Se ratio 1:1) used in chapter 4, no grey states were observed in the single molecule blinking traces. However, for the QDs studied in chapter 5 (with Cd:Se ratio 1:10), the grey states observed might be attributed towards the ratio of Cd:Se atoms since the origin of grey states in that chapter has been proposed to depend upon many factors and the structural defects in core is one of those factors. It is not only the ratio of ligands that matters here, the identity of ligands is also important. It is known, as from the work done in our lab<sup>7</sup> and in the literature<sup>10, 11</sup> shows, after ligand exchange of organic ligands with thiol-ligands such as MPA; mercaptopropionic acid (water soluble), the average radiative lifetime decreased, independent of the surface atom ratio. So, overall, the ligands need to be optimized qualitatively as well as quantitatively.

Another factor to influence fluorescence properties of the CdSe core QDs is the pH of the environment around QD. Durisic et al<sup>1</sup> performed a detailed study of the dependence of the ensemble and single molecule fluorescence properties on pH was carried out. They found that as the PH decreased from pH 9 to 6, the ensemble fluorescence intensity decreased along with a decrease in the “on” fraction due to the effect of pH on blinking dynamics. They proposed the diffusion-controlled model in which they showed that H<sup>+</sup> ions interact with QDs, changing the number and/or energies of trap states, which affect the blinking dynamics as well as dark fraction and thereby, PL QY of the QDs.

So, the study of Cd:Se ratio and different TOPO:ODA ratios, with other external environmental factors influencing the optical properties of CdSe core in core/shell QDs can be further extended to find the optimum factors with which the blinking can be maximum reduced and also, for which how fluorescence QY and excitons decay dynamics vary. In terms of Cd:Se ratio,

the different Cd:Se ratios can be varied from 1:1 upto 1:10 and it will be possible to obtain the best ratio of Cd:Se atoms, for which the blinking of QDs can be maximum reduced. Also, this should help further to investigate as how this ratio is correlated to the probability of grey state formation in QDs. The same correlation can be found for the ratio of ODA:TOPO ligands. These ratios can help to give the random measure of surface defects on the core. So, depending upon how much surface defects are there at the core surface, the passivation happens by the shelling and contributes accordingly for the enhancement of the optical properties of QDs.

## 6.1. References

1. Durisic, N.; Wiseman, P. W.; Grutter, P.; Heyes, C. D., A Common Mechanism Underlies the Dark Fraction Formation and Fluorescence Blinking of Quantum Dots. *Acs Nano* **2009**, *3* (5), 1167-1175.
2. Durisic, N.; Godin, A. G.; Walters, D.; Grutter, P.; Wiseman, P. W.; Heyes, C. D., Probing the "Dark" Fraction of Core-Shell Quantum Dots by Ensemble and Single Particle pH-Dependent Spectroscopy. *Acs Nano* **2011**, *5* (11), 9062-9073.
3. Schmidt, R.; Krasselt, C.; Gohler, C.; von Borczyskowski, C., The Fluorescence Intermittency for Quantum Dots Is Not Power-Law Distributed: A Luminescence Intensity Resolved Approach. *Acs Nano* **2014**, *8* (4), 3506-3521.
4. Qu, L. H.; Peng, X. G., Control of photoluminescence properties of CdSe nanocrystals in growth. *Journal of the American Chemical Society* **2002**, *124* (9), 2049-2055.
5. Green, M., The nature of quantum dot capping ligands. *Journal of Materials Chemistry* **2010**, *20* (28), 5797-5809.
6. Ning, Z. J.; Molnar, M.; Chen, Y.; Friberg, P.; Gan, L. M.; Agren, H.; Fu, Y., Role of surface ligands in optical properties of colloidal CdSe/CdS quantum dots. *Physical Chemistry Chemical Physics* **2011**, *13* (13), 5848-5854.
7. Omogo, B.; Aldana, J. F.; Heyes, C. D., Radiative and Nonradiative Lifetime Engineering of Quantum Dots in Multiple Solvents by Surface Atom Stoichiometry and Ligands. *Journal of Physical Chemistry C* **2013**, *117* (5), 2317-2327.
8. Mews, A.; Eychmuller, A.; Giersig, M.; Schooss, D.; Weller, H., PREPARATION, CHARACTERIZATION, AND PHOTOPHYSICS OF THE QUANTUM-DOT QUANTUM-WELL SYSTEM CDS/HGS/CDS. *Journal of Physical Chemistry* **1994**, *98* (3), 934-941.
9. Omogo, B.; Gao, F.; Bajwa, P.; Kaneko, M.; Heyes, C. D., Reducing Blinking in Small Core-Multishell Quantum Dots by Carefully Balancing Confinement Potential and Induced Lattice Strain: The "Goldilocks" Effect. *Acs Nano* **2016**, *10* (4), 4072-4082.
10. Wuister, S. F.; Swart, I.; van Driel, F.; Hickey, S. G.; Donega, C. D., Highly luminescent water-soluble CdTe quantum dots. *Nano Letters* **2003**, *3* (4), 503-507.
11. Wuister, S. F.; Donega, C. D.; Meijerink, A., Influence of thiol capping on the exciton luminescence and decay kinetics of CdTe and CdSe quantum. *Journal of Physical Chemistry B* **2004**, *108* (45), 17393-17397.
12. Omogo, B. Understanding the Influence of Interfacial Chemistry in Core, Core/Shell and Core/Shell/Shell Quantum Dots on their Fluorescence Properties. *Ph.D. dissertation* **2014**.